University of Crete
Department of Physics

Bachelor Diploma Thesis

Application of fluorescence spectroscopy combined with multivariate statistical analysis methods for the rapid detection of adulterants and contaminants in olive oil

Eleni Charitoudi

Supervisor:

- **Michalis Velegrakis**, Research Director Institute of Electronic Structure and Lasers, Foundation for Research and Technology - Hellas, IESL FORTH

Committee member:

- **T. Peter Rakitzis**, Professor of Atomic, Molecular, and Optical Physics at the Department of Physics of the Univ. of Crete, leader of the Polarization Spectroscopy group at IESL-FORTH.

- **Peter C. Samartzis**, Principal Researcher at Institute of Electronic Structure and Laser, Foundation for Research and Technology - Hellas, IESL FORTH

Heraklion 2024

Acknowledgments

In expressing my deepest gratitude, I acknowledge the outstanding individuals whose unwavering support and contributions have been pivotal to the successful completion of this work. First and foremost, I express my most profound appreciation to my supervisor, Michalis Velegrakis, for allowing me to work in his lab and entrusting me with the preparation of my thesis. His guidance, support, and willingness to address my queries have been invaluable throughout our collaboration. Furthermore, I want to acknowledge Dr. Petros Samartzis for his valuable contribution as a member of the three-member examination committee. I am grateful for his time and effort in thoroughly reviewing this text. Special thanks to Professor Peter Rakitzis for graciously agreeing to serve as the liaison with the Physics department at my university.

My heartfelt thanks go to Dr. Zoumi Katerina for her insightful guidelines and advice, which played a pivotal role in shaping this thesis. I am also indebted to the laboratory technician, Stamataki Katerina, for her warm welcome into the Lab and for generously sharing her expertise on the lab's instruments. Furthermore, appreciation is extended to the Ph.D. student, Orfanaki Mano, whose extensive support included explaining the theoretical and technical background crucial for this thesis. His ongoing communication and valuable advice at every step were instrumental to the success of this work, and I am particularly grateful for the thoughtful guidance he provided in various aspects of my academic journey. I want to thank all the laboratory members for fostering a culture of open communication and collaboration. Your collective efforts have contributed significantly to the positive environment in which this research thrived.

In conclusion, I am deeply thankful to my parents for their unwavering support throughout my life and to my big brother, whose belief in me has been a constant source of encouragement. I am grateful to my extended family and friends for your steadfast presence and encouragement as I pursued my academic goals.

Table of content

Abstract

Olive oil is an essential daily commercial product in people's lives, attributing its popularity to its rich taste and high nutritional value, making it one of the vital elements of the Mediterranean diet. Olive oil's impact extends to consumer health and the industry's economic landscape. This research focuses on the application of optical methods, in particular fluorescence spectroscopy, to verify the authenticity and safety of olive oil. The main objective is the comprehensive detection of seed and mineral oils in olive oil. The study includes the analysis of 23 samples of pure olive oil, 260 samples of adulterated olive oil with seed and pomace oil, and 144 contaminated olive oil samples with ten different mineral oils from three companies. These samples were analyzed by fluorescence spectroscopy, and the results were processed by multivariate analysis techniques such as Partial Least Squares (PLS) and Partial Least Squares Discriminant Analysis (PLS-DA). A consequence of this research is the successful prediction of adulteration rate and the detection of contaminants in olive oil. This research was conducted in the Photonics for AgroFood and Environment Laboratory at the Institute of Electronic Structure and Lasers of the Foundation for Research and Technology, Hellas.

Περίληψη

Το ελαιόλαδο είναι ένα σημαντικό καθημερινό εμπορικό προϊόν στη ζωή των ανθρώπων, αποδίδοντας τη δημοτικότητά του στην πλούσια γεύση και τη υψηλή διατροφική του αξία, καθιστώντας το ένα από τα βασικά στοιχεία της μεσογειακής διατροφής. Ο αντίκτυπος του ελαιόλαδου επεκτείνεται τόσο στην υγεία των καταναλωτών όσο και στο οικονομικό τοπίο του κλάδου. Η παρούσα έρευνα επικεντρώνεται στην εφαρμογή οπτικών μεθόδων, ειδικότερα της φασματοσκοπίας φθορισμού, για την εξακρίβωση της γνησιότητας και της ασφάλειας του ελαιόλαδου. Ο κύριος στόχος είναι η ολοκληρωμένη ανίχνευση σπορέλαιων και ορυκτελαίων στο ελαιόλαδο. Η μελέτη περιλαμβάνει την ανάλυση 23 δειγμάτων καθαρού ελαιόλαδου, 260 δειγμάτων νοθευμένου ελαιόλαδου με σπορέλαια και πυρηνέλαιο και 144 επιμολυσμένων δειγμάτων ελαιόλαδου με δέκα διαφορετικά ορυκτέλαια από τρεις εταιρείες. Αυτά τα δείγματα αναλύθηκαν με φασματοσκοπία φθορισμού και τα αποτελέσματα επεξεργάστηκαν με τεχνικές πολυπαραγωντικής ανάλυσης όπως τα Μερικά ελάχιστα τετράγωνα (PLS) και η ανάλυση διάκρισης μερικών ελαχίστων τετραγώνων (PLS-DA). Ως αποτέλεσμα αυτής της έρευνας είναι η επιτυχημένη πρόβλεψη του ποσοστού της νοθείας καθώς και η ανίχνευση επιμολυντών μέσα στο ελαιόλαδο. Η παρούσα έρευνα πραγματοποιήθηκε στο εργαστήριο Εφαρμογών Φωτονικής για την Αγροδιατροφή και το Περιβάλλον στο Ινστιτούτο Ηλεκτρονικής Δομής και Λέιζερ του Ιδρύματος Έρευνας και Τεχνολογίας.

Chapter 1: Introduction

This research focuses on olive oil because there are cases of adulteration and contamination. This situation has an impact on health and the economy because olive oil is a daily consumption product, and the industry produces large amounts of olive oil daily. The most common techniques for the analysis of olive oil are analytical techniques such as Gas Chromatography-Mass Spectrometry (GC–MS), High-Performance Liquid Chromatography (HPLC), and Inductively Coupled Plasma Mass Spectrometry (ICP-MS). Furthermore, Nuclear Magnetic Resonance (NMR) spectroscopy has successfully classified, assessed quality, and detected adulteration in edible oils. Even though these analytical techniques are quantitative and accurate, they are time-consuming, using expensive instrumentation while sample pre-treatment is necessary. Therefore, using optical spectroscopic methods becomes crucial for detecting adulterants in EVOO, as they are faster, cost-effective, and do not require extensive sample preparation. One of those methods is vibrational spectroscopic techniques such as Raman and Fourier transform infrared (FTIR). Furthermore, the Ultraviolet–Ultraviolet-visible-near infrared (UV–vis–Nir) absorption spectroscopy is a prevalent optical technique for detecting adulterants[1]. The final method that is commonly used for this purpose is fluorescence spectroscopy[2]. This project uses fluorescence spectroscopy and statistical analysis to efficiently determine the presence of seeds or pomace oils in EVOO.

1.1 Theoretical Background

This chapter presents theoretical knowledge about electromagnetic radiation, focusing mainly on the properties of light. Understanding these theoretical principles is critical to monitoring various phenomena when light reacts with the molecules of observed samples. As a result, to characterize their structure and chemical composition.

1.1.1 Electromagnetic Radiation

Electromagnetic radiation indicates the energy that travels through space in the form of electromagnetic waves, which include a broad spectrum of waves. The wavelengths used in those experiments range from approximately 200 to 700 nanometres (nm) along the electromagnetic radiation corresponding to visible light, often described by optical radiation. Also, the above range encompasses part of ultraviolet. Beyond this region, the electromagnetic spectrum includes X-rays and gamma rays, which have even shorter wavelengths, measuring less than 1nm. Conversely, infrared electromagnetic radiation, microwaves, and radio waves belong to the more extended wavelength of the electromagnetic spectrum than visible light[3].

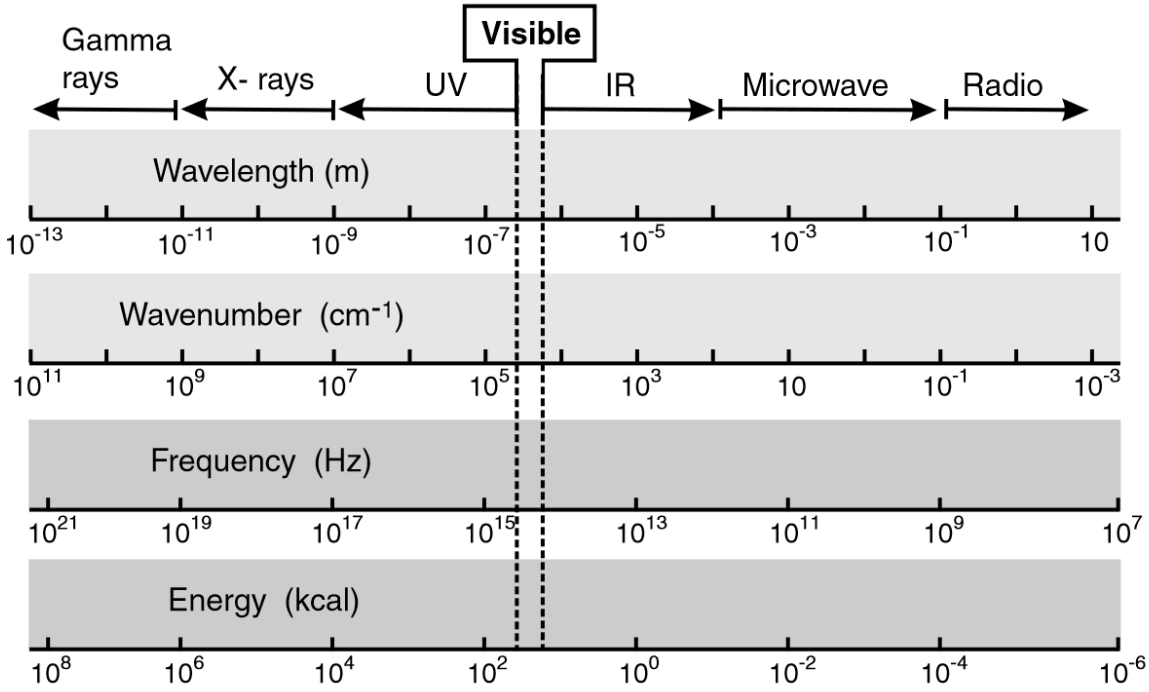

Figure 1.1: The electromagnetic spectrum[4]

Furthermore, light behaves as both wave and particle. When light exhibits wave properties, such as wavelength, frequency, and speed, it travels through space, and phenomena such as diffraction and interference appear. In vacuum space, light travels at the constant speed of c (the speed of light), which is equal to

$$c = \lambda \cdot v = 3 \cdot 10^8 \text{ m/s}$$

, where λ and v represent the wavelength and frequency of electromagnetic radiation, respectively.
When light behaves as a particle, it's referred to as a photon, which is characterized by one wavelength or frequency (monochromatic radiation)[5], and each photon has energy:

$$E = h \cdot v$$

, where h is the Planck constant which equals $6.626 \cdot 10^{-34} m^2 kg/s$ and v is frequency[6]. Light, with particle properties such as momentum, can interact with matter through collisions with the particles that constitute matter. Due to particle-wave duality, light can be reflected, refracted, transmitted, absorbed, or scattered.

1.1.2 Absorption Spectroscopy

The absorption in the infrared (IR) region is due to rotations and vibrations between molecules. IR spectroscopy is used to define the bonds of molecules, in contrast to the absorption of light in the ultraviolet (UV) or visible (Vis) region of the electromagnetic spectrum, which specifies the electronic structure of molecules.

The formation of a molecule happens with the interaction of two atomic orbitals. This process creates two energy states constituting the molecule, called molecular orbitals.

One has a lower energy than the two original atomic orbitals and is called a bonding orbital. The electrons in this state are located in opposite directions of their spins. On the other hand, the second energy state is higher and is called an antibonding orbital. During the creation of bonding between the atoms for the forming of molecules, the orbitals overlap each other, and depending on the geometry of their overlap, the orbitals are divided into σ and π. The σ is obtained by overlapping atomic orbitals along the axis connecting the centers of the two atomic orbitals, and the resulting bond is called a sigma bond. The π's arise by lateral overlapping of atomic orbitals. The resulting corresponding bond is called a π bond. The σ bond is more potent than a π bond because the electron prefers the lowest energy state. Therefore, bands of energy states are created when more than two atoms are combined to form molecules[4].

Figure 1.2 depicts the bands of energy states of a molecule. In more detail, the black lines indicate the ground S_0 and the first excited electronic state S_1, and the blue and red lines present vibration and rotation energy states, respectively. It is observed that the energy differences between the vibrational energy levels are considerably minor compared to those of the electronic energy states, and the energy differences between the rotational levels are even more insignificant than those of the vibrational ones.

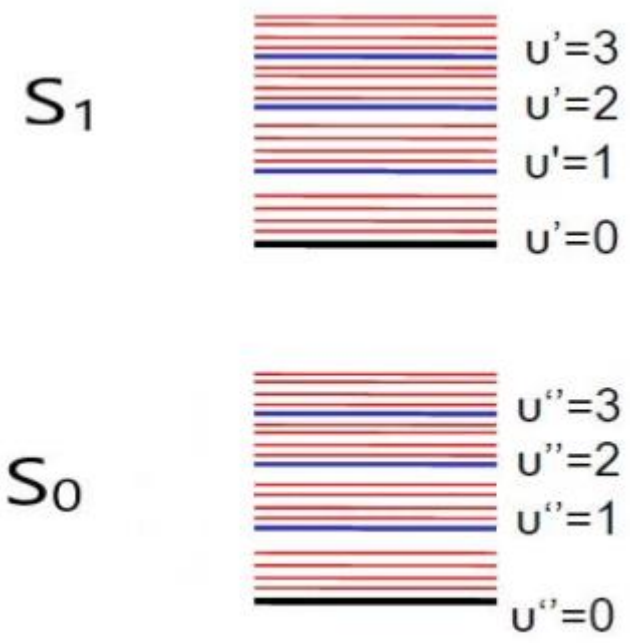

Figure 1.2: Energies states of a molecule [7]

The UV and Vis absorption is due to electron stimulation from the ground electronic state to an excited single state, and the IR absorption is affected by electron transitions between rotations and vibrations energy states produce. Therefore, the absorption process starts with the light source that emits radiation with an intensity of I_0 and illuminates a sample. The matter absorbs radiation, and the transmitted light with an I intensity will be measured. When the initial intensity (I_0) of light is incident perpendicularly on the walls of a cell containing a liquid sample, then the final intensity (I) that the light has after it passes through the sample depends on the initial intensity and the molar absorptivity (ε) in units of $M^{-1}cm^{-1}$, which is the characteristic number of the substance that indicates the amount of light it can absorb at a specific wavelength. Furthermore, the final intensity also depends on the concentration of the molecular

species in the solution (C) in units of mol/L (M) and the optical path length (L) in units of cm or mm.

The absorbed or transmitted radiation is described by Lambert-Beer law[3,2]:

$$I = I_0 \cdot e^{(-\varepsilon \cdot C \cdot L)}$$

$$T = \frac{I}{I_0} = e^{(-\varepsilon \cdot C \cdot L)}$$

$$A = log\frac{I}{I_0} = \varepsilon \cdot C \cdot L$$

, where A and T are the numbers of absorbance and transmittance, respectively, and they are both without units of measurement. The absorption theory is depicted in **Figure 1.3**

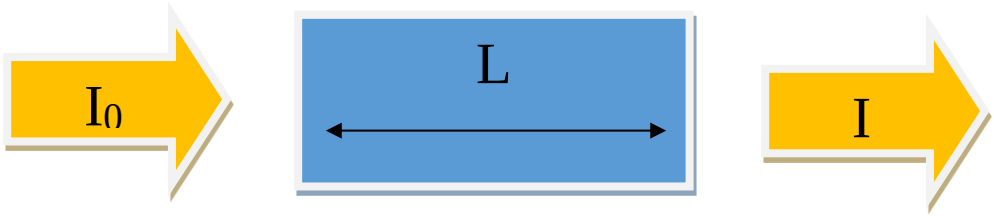

Figure 1.3: The Lambert-Berr law that describes the Optical absorption spectroscopy

1.1.3 Fluorescence Spectroscopy

Fluorescence is the emission of light after the absorption of ultraviolet or visible light of a fluorescent molecule[8]. The general principle of the fluorescence phenomenon is illustrated by the Jablonski diagram, as shown in **Figure 1.4**. This diagram depicts a molecule's electronic and vibrational energy states, where electrons are generally located in the state with the lowest energy, indicated by S_0, which is called the ground state.

The blue line entering from the left indicates the interaction of an electron with appropriate energy with a molecule. When this happens, the photon may be absorbed, causing an electron to transmit from the ground state to an excited state (S_1, S_2). The energy difference between the ground and excited states is the appropriate energy that the photon can be absorbed. Thus, not all incident photons are equally likely to be absorbed. This transition process is very fast, on the order of 10^{-15} seconds.

An excited-state electron rapidly (on the order of 10^{-12} seconds) loses its energy and is de-stimulated to the lowest level of the first (S_1) excited state, which can occur without the emission of radiation. This loss of energy happens through collisions, resulting in vibrational relaxation. This process is called internal conversion, described by the wavy black line in the diagram below. From there, the electron may fall to the ground (S_0) state, emitting a photon with energy equivalent to the energy difference of

the transition. This happens on a time scale of nanoseconds (10^{-9} – 10^{-8} seconds) after the initial photon is absorbed[9]. Since the emitted photon has less energy than the absorbed photon, it is at a longer wavelength. During electron de-excitation, the electrons transferred from an excited state to many vibrational sub-levels of the ground states, creating broader peaks in fluorescence spectra[4].

The probability that a photon will be absorbed varies with wavelength (energy). Even for those photons that are absorbed, there are other processes that compete with fluorescence for de-excitation of the excited-state electrons. The number of photons fluoresced relative to the number absorbed is the quantum efficiency. The higher the absorption and quantum efficiency, the brighter the fluorescence[9].

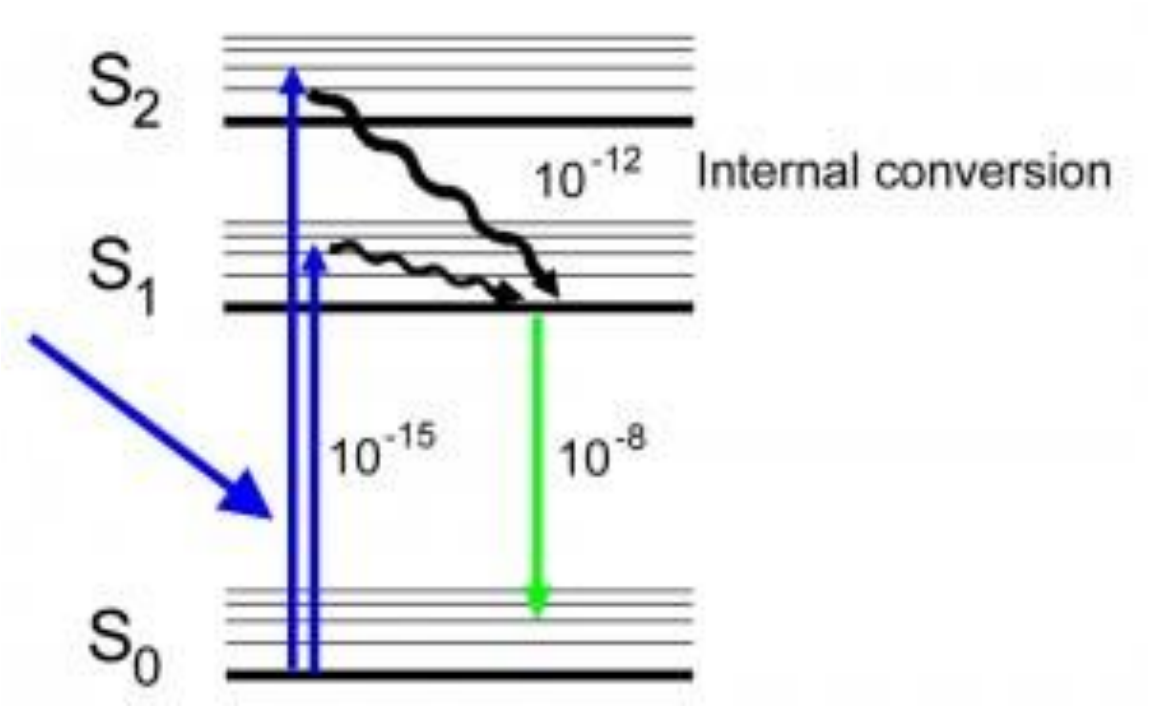

Figure 1.4: The Jablonski diagram for fluorescence[9]

1.2 Instrument of Fluorescence Spectroscopy

The best way to document the fluorescence properties of a particular specimen is to measure excitation and emission spectra with a fluorometer. The excitation spectrum is a plot of the relative efficiency of different wavelengths of light to excite fluorescence in the subject. In contrast, the emission spectrum is a plot of the relative distribution of energy released in fluorescence[9]. Therefore, the instrument fluorometer is designed to detect the proportion of a fluorescent molecule, called a fluorophore, in the observed sample. Fluorophores are chemical molecules capable of absorbing energy at a specific wavelength and then emitting energy at different wavelength ranges. The emission energy depends on the fluorophore's presence and chemical environment. Usually, only aromatic or highly polyunsaturated organic compounds fluoresce. The advantage of fluorescence spectroscopy is its multidimensional character, distinguishing it from other spectroscopic techniques[10].

1.2.1 Organology of Fluorometer

Fluorometers are instruments used for measuring fluorescence spectroscopy, polarization, and lifetime. This instrumentation typically consists of a light source, a specimen chamber equipped with integrated optical components, two monochromators, and a high-sensitivity detector, such as photomultipliers or charge-coupled device cameras.

The optical excitation and detection light paths run along the orthogonal axis. This geometry helps minimize the excitation light leakage into the detection side and beam to avoid the reflection effects. Also, the excitation and emission light signals don't overlap in this way. Additionally, the samples are not subjected to chemical pre-treatment because they are placed in the front face geometry at 35^{o} to the incident, and the fluorescence signal comes from the sample's surface, not from its volume. Therefore, there are no self-absorption phenomena. Finally, this instrument includes two monochromators that select a specific wavelength for the excited and emitted light.

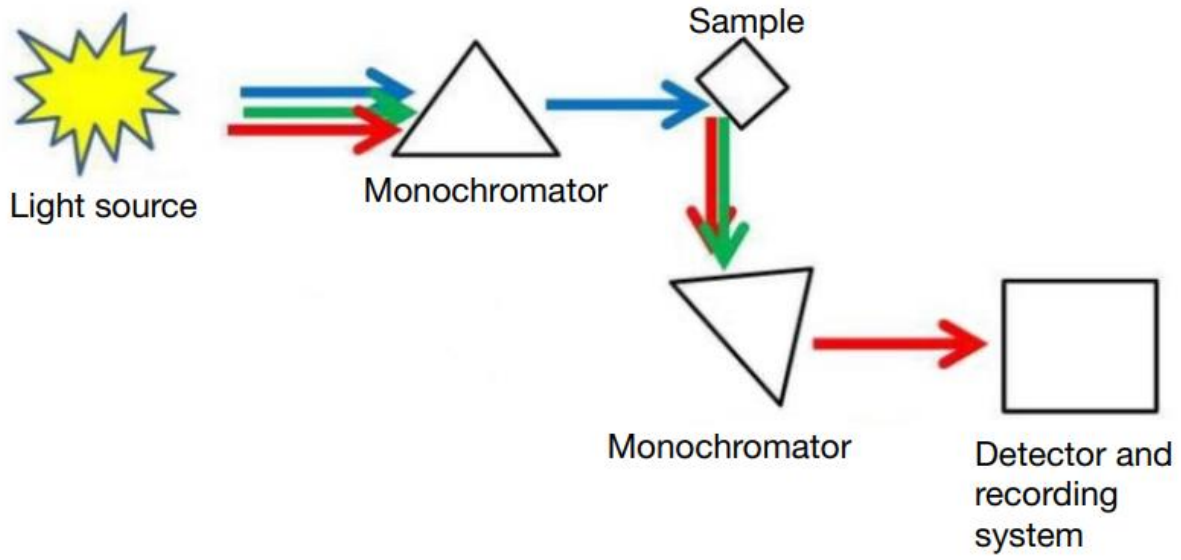

Figure 1.5: The organology of elements that constitute the equipment of the fluorometer [5]

For the fluorescence measurement in the experiments conducted for this project, a Fluoromax-P fluorometer by Horiba was utilized, illustrated in **Figure 1.6**. This instrument features a 150W ozone-free xenon-arc lamp as the source, emitting light within a range of wavelengths corresponding to the UV and visible regions of the electromagnetic radiation spectrum. It includes one excitation monochromator with an aperture range of 220 to 600 nm and one emission monochromator ranging from 290 nm to 850 nm. Each monochromator is followed by slits that control the amount of emission and excitation light that passes through them. Additionally, the fluorometer incorporates lenses and mirrors to manage the light path. It employs a photomultiplier of the R928P type, capable of detecting light within 180-850 nm of electromagnetic radiation.

Figure 1.6: Fluorometer Fluoromax-P, Horiba

1.2.2 The Different Types of Fluorescence Spectra

Different types of fluorescence spectra result from the organology mentioned above. Those types of spectra are illustrated in **Figure 1.7**. The kind of spectrum required depends on the sample's fluorescence region and the type of data needed. The most common type of spectra for fluorescence observation is a diagram of the fluorescent intensity measured as a function of wavelength at a constant, chosen emission or excitation wavelength, which are called excitation or emission spectrum, respectively. Furthermore, if we need data from both excitation and emission wavelength simultaneously, the most comprehensive fluorescence characterization is obtained by measuring an excitation-emission matrix. This matrix can be represented as a three-dimensional plot, with fluorescent intensity illustrated on the z-axis as a function of excitation and emission wavelength on the x and y axes. It can also be presented as a contour map, where the colors in the map indicate the amount of intensity. Those two different representations of the excitation-emission matrices are illustrated in **Figure 1.8**, which shows that after the completion of all the scans, the 3-D plot is created, and this plot is transformed into a contour map for better visualization. Alternatively, a way to visualize the fluorescence phenomenon is by using synchronous spectroscopy. This technique involves simultaneous scanning of excitation and emission wavelengths, with the difference in wavelengths being constant or following a function. In such spectra, the fluorescence intensity is plotted as a function of excitation and emission wavelength for specific differences between them[11].

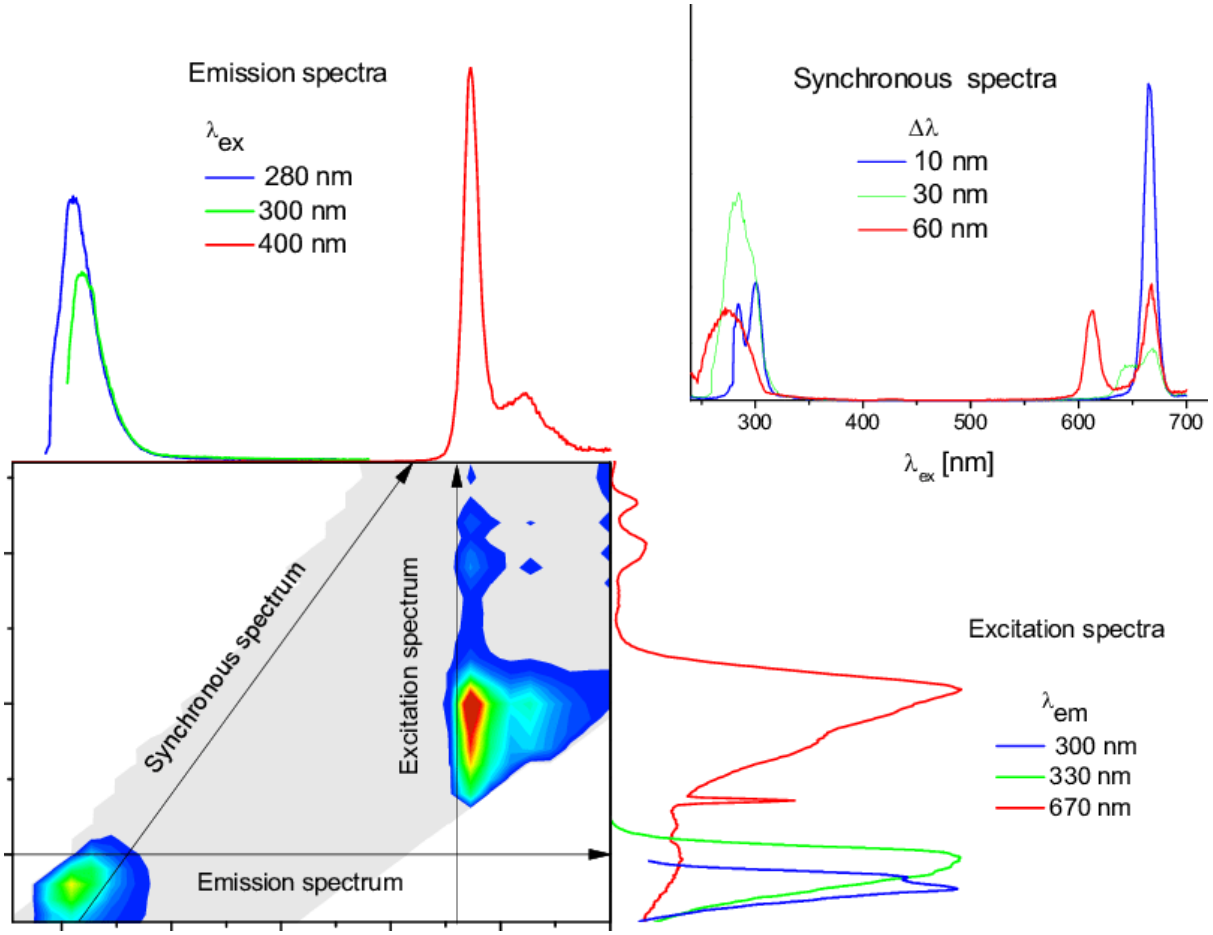

Figure 1.7: Type of fluorescence spectroscopy of extra virgin olive oil sample diluted with hexane on concentration at 1% v/v [11]

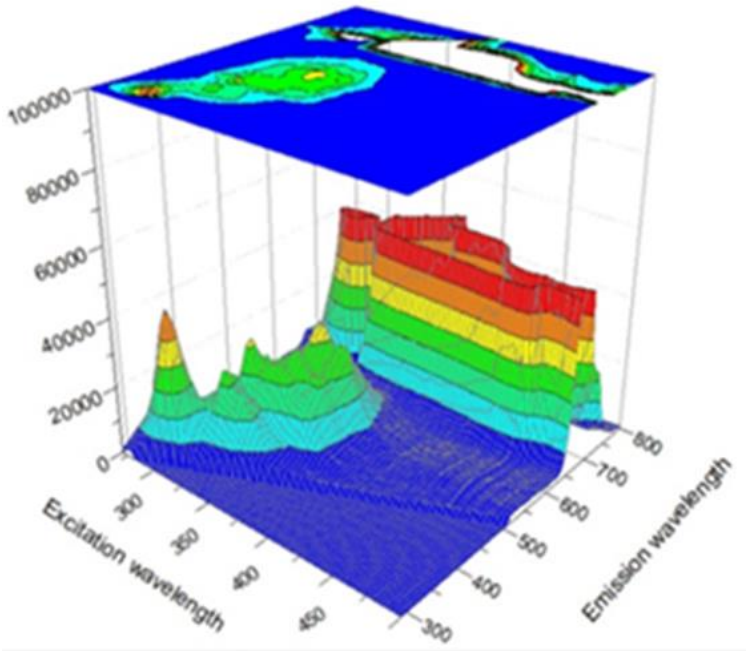

Figure 1.8: The transformation of olive oil's excitation-emission matrix formed as a 3-D plot to a contour map

1.3. Statistical analysis

In numerous fields, the imperative need to process a vast amount of data has given rise to methodologies for analyzing data, such as a matrix framework. Statistical analysis is an intersection of mathematics and computer science, and it is used as a tool for summarizing, interpreting, and extracting insights from data. This method facilitates drawing conclusions, making inferences, and testing hypotheses. Statistical analysis consists of two categories. The first is univariate, which focuses on examining one variable at a time, and the second type of statistical analysis is called multivariate analysis. This method involves the simultaneous measurement and analysis of two or more variables, providing a more comprehensive perspective on the relationships and patterns within the dataset[12] and investigating the dependence structure between the involved variables[13].

1.3.1 Definition and Categories of Multivariate Analysis

In this project, multivariate statistical analysis was applied, contributing to the optimal utilization of experimental data. This technique facilitated the collection of a large amount of data extracted by measuring several variables for each specimen. Consequently, multivariate analysis was employed for discriminating and classifying data, considering all simulated variables rather than comparing one variable at a time. The two variables can be represented graphically using a data vector, but the visualization of three or more variables is complicated. Therefore, the need arises for computer analysis to correlate the variables that matrix algebra describes. There are two main categories of multivariate analysis methods. The first is unsupervised pattern recognition, which describes a method where prior knowledge of the groups is not expected. On the other hand, the second category is represented by the supervised method that involves situations where the group origin of many objects is known. This method aims to create a function that all objects follow, allowing the correct allocation of the membership group for a new object from an unknown group[14].

1.3.2 The Partial Least Squares and Partial Least Squares Discriminant Analysis

Partial Least Squares (PLS) is a multivariate technique used when there is a need to establish a connection between two sets of data. These data sets are represented as two matrices: the first matrix (X) comprises quantified predictors (independent), and the second matrix (Y) consists of responses (dependent) variables. PLS is a predictive model that utilizes a linear combination of predictor variables to establish the connection between the two matrices. This happened because, in PLS, variables that show a high correlation with the response variables are given extra weight. Thus, they will be more effective at prediction[14]. Initially, observation values are developed for a training set and form in the X matrix, which is used to determine new observations. The standard multivariate approach involves a calibration model. In this project, the square root of the standard deviation was employed as the calibration model instead of the auto-scaling model. According to this approach, each variable measurement is divided by the square root of the mean of that variable. This modification increases the importance of high values in the contribution. The performance of the PLS model is

evaluated using two fundamental values: the R^2 (coefficient of determination) and RMSECV (root mean square error of cross-validation). These values indicate how well the model predicts actual values. For optimal performance, R^2 should be close to 1, indicating a strong correlation, and RMSECV should be minimized to zero, reflecting accurate predictions during cross-validation[15].

The Partial Least Squares Discriminant Analysis (PLS-DA) is a multivariate classification method. It can recognize the matching of each sample to its appropriate class based on a set of measurements. So, after the calibration of this model, the origin class of an unknown sample can be determined. PLS-DA is a linear classification method that combines the properties of partial least squares regression with the discrimination power of a classification technique. In PLS-DA, the linear combination of the original variables is modeled by Latent Variables (LVs), which indicate the data variability. This model is presented by graphical visualization, resulting in a better understanding of the different data patterns and relations by LV score and loading plots. More specifically, loadings plots are the coefficients of variables in the linear combinations that determine the LVs. Therefore, they represent which range of data influences the formation of each LV, while score plots represent the coordinates of samples in the LV projection hyperspace. Furthermore, the extension of the PLS-DA algorithm is the Orthogonal Partial Least Squares-Discriminant Analysis (O-PLS-DA). O-PLS-DA separates the latent variables that are related from those that are unrelated to a variable with the most significant influence weight. In conclusion, both methods can effectively predict differences by providing a matrix, which quantitatively indicates the classification's success rate of the classification achieved[16]. Still, the second method is more easily interpretable when there is a need to determine differences between the groups[17].

However, before applying PLS or PLS-DA in the context of fluorescence spectroscopy data, those data need to pass through preprocessing by using an algorithm. This process transforms the format of the fluorescence data into a suitable structure for analysis. The transformations involve the separation of emission spectra collections and their combination into a single line of data for each sample. This transformation is necessary to perform PLS or PLS-DA in EEM measurements. A loading plot is created once the statistical analysis model is applied and the results are obtained. The loading plots are used as a visualization tool that helps understand the relationships between the variables and the class separation in the data. However, presenting the loading plot in the initial EEM format is desirable for better visualization and explanation.

To achieve this, another algorithm was employed to reverse the initial transformation. This algorithm reconstructs the data to resemble the latent variables produced by the above analysis methods in its initial EEM form, and then a new contour plot is generated. These contour plots correspond to loading plots and visually represent the relationship between the variables and the class separation in the EEM data. In summary, the first step of the statistical analysis process involves transforming EEM data into a single-line format suitable for the PLS-DA analysis. After that, another algorithm is used to revert the PLS-DA loading plot to a format that resembles the initial EEM data. This allows for better visualization and interpretation of the results in the context of the original EEM structure.

1.3.4 Validation Model and Data Pre-processing

Validation is a crucial step for any model before it is applied to predict new data. This process is essential for the estimation of the predictive ability of the model, and it helps determine the correct complexity of the model. A practical validation model precisely predicts the Y-values using a validation set that typically represents new X-values. While having an independent validation set is rare, two standard methods for model validation exist. Cross-validation (CV) is the first way, which simulates how well the model predicts new data. The second method is model re-estimation, which estimates the probability of obtaining a good fit with random response data after randomizing the data[18]. In this project, cross-validation is employed as the chosen validation method because it uses the data more economically. It is sometimes referred to as the 'leave-one-out method' [14]. In this approach, all the data matrices are used only once. Specifically, CV is performed by dividing the data into several groups. Each group is sequentially removed and used as the test set, while the remaining groups serve as the training set. The model is calibrated on the training samples each time and then used to predict the samples of the removed group. So, several parallel comparisons are developed to calculate differences between actual and expected values. Then, the sum of squares of all these differences is represented as the Predictive Residual Sum of Squares (PRESS). This value indicates the proportion of effectiveness in the model's predictive ability.

The most common pre-processing techniques consist of scatter-correction methods and spectral derivates. The first category aims to decrease the contribution of the scattering phenomena of measurements. In contrast, the second category involves calculating the derivatives of measurements to mitigate the detrimental effect of the noise from the instrument, which often leads to variability in recorded data. One classic method widely used in spectroscopic data is the mean centering method, where the average value of each variable is subtracted from all data[15]. Another pre-processing method applied in this study is the Standard Normal Variate (SNV) method. The SNV is a normalization technique and is particularly valuable when the objective is to highlight differences between samples[19].

1.3.6 Software and Spectral Data Processing

Spectral data was collected using the software provided by the spectroscopic instruments and later transferred to spreadsheets in Origin Lab. This project's data was visualized as emission spectra, excitation spectra, and fluorescence maps. The main goal of the comprehensive study is the chemical interpretation and the identification of trends and patterns among the samples based on spectral characteristics. Subsequently, the spectral data was imported into the MATLAB platform, version R2015b. Specialized toolboxes designed for spectral data analysis, such as the PLS_Toolbox 8.1, are utilized to analyze and process spectral data. These toolboxes are tailored to the specific needs of the research[7].

Chapter 2: Extra Virgin Olive Oil

Olive oil falls into the broader category of edible vegetables. It offers many health benefits to consumers, such as cardioprotective, antioxidant, anti-inflammatory, and anti-tumor, causing low levels of unsaturated fatty acids and tocopherols[20]. Olive oil is a vital component of the Mediterranean diet, being extracted entirely from the fruits of the olive tree and being ready for consumption immediately after the extraction process[21]. Furthermore, olive oil appears in various flavors and qualities depending on the spice of olives, and olive oils have diverse uses, sources, and intended applications in both the culinary and industrial realms. Therefore, the production of olive oil is one of the fundamental products for the industry, contributing significantly to the economic system[22].

In this experiment, some samples were measured in a fluorometer to observe the fluorescence region of olive oil. Olive oil can fluoresce due to the presence of some substances mentioned below. Therefore, applying the fluorescence techniques leverages those substances' unique light emission properties to detect and analyze their presence in a sample, providing valuable information about their concentration and identity. More specifically, observing the fluorescence in various wavelengths determines what particular substances there are in olive oil. Finally, measuring the intensity of the fluorescence signal can be correlated with the concentration of the substance in the sample. This allows for quantitative analysis, providing information about the amount of the substance present.

2.1 The Categories of Olive Oil

This chapter focused on edible oil, specifically olive oil. Olive oil is divided into groups based on quality, and it is classified into the main categories below.

- Extra virgin olive oil: This category represents the highest quality from an organoleptic point of view. It has no defects and is fruity. Its acidity level shall not exceed 0.8%[23].

- Virgin olive oil: This category is fruity but has slight sensory defects. The acidity of virgin olive oil should not surpass 2%[23].

- Lampante olive oil: This category possesses the lowest quality virgin olive oil. It has substantial sensory defects (taste and smell), which can result from the lousy processing of the olives or weather incidents affecting olive fruits on the trees. Lampante olive oil must be refined to eliminate its defects. Following refinement, the resulting oil is known as 'refined olive oil' and cannot be directly sold to consumers[23].

- Refined olive oil: This category of olive oil has minimal or no olive aroma, flavor, or color. Refined olive oil cannot be sold to consumers. It is typically blended with extra virgin or virgin olive oil so it can be consumed[23].

This project focuses on studying extra virgin olive oil (EVOO), defined by specific criteria. It is obtained through mechanical or other physical processes under precise thermal conditions that don't cause oil deterioration. This category excludes oils obtained using solvents, adjuvants with chemical actions, re-esterification processes, or any mixtures with oils of other types. The conclusion is that olive oil can be determined as an extra virgin if certain factors affecting its quality are controlled, with the extraction and storage processes playing crucial roles.

The observation of olive oil exhibits information according to the origin and, more specifically, can determine the variety, climate, and terrain it comes from. This association with quality is essential for understanding the characteristics of the oil but also holds economic significance because olive oils are classified and priced according to quality that depends on acidity[11]. The most expensive and rare oil is the high-quality extra-virgin olive oil (EVOO), constituting only a tiny percentage of global oil production (around 2-2.5%)[7]. However, there is a concern about the mislabelling and adulteration of EVOO due to its high market value. Therefore, EVOO is much more expensive than other types of oil, and it has excellent organoleptic characteristics, such as aroma and taste, as well as nutritional and therapeutic value. Thus, ensuring the quality of olive oil is crucial for health reasons and maintaining the integrity of the economic aspects associated with different oil categories.

2.2 Chemical composition of olive oil

The composition of EVOO can be influenced by environmental conditions, fruit ripening, harvest time, and agricultural practices. Therefore, analyzing EVOO's chemical composition and structure is crucial as these factors significantly impact its quality.

Therefore, olive oil consists of the fatty phase at 98-99% and micro-components at a percentage of 1-2%[7]. In more detail, EVOO is rich in fatty acids, including a well-balanced combination of monounsaturated fatty acids (MUFA) and polyunsaturated fatty acids (PUFA), a high amount of MUFA and a low proportion of PUFA. Additionally, EVOO contains numerous bioactive compounds, such as hydrophilic phenols, phytosterols, tocopherols, and carotenes. All of those components contribute to the resistance of olive oil to oxidation. Overall, the chemical compounds that compose the EVOO are classified as metabolites, which are small molecules contributing to its overall profile[22].

Metabolites in EVOO can be categorized into primary and secondary metabolites. The first category exists in all cells and contributes to an organism's growth and survival. On the other hand, the secondary metabolites serve functions related to defense mechanisms, communication, or environmental adaptation. Understanding and monitoring these diverse components contribute to assessing and maintaining the quality of Extra Virgin Olive Oil[22].

Primary Metabolite

Lipids

Lipids serve as a primary energy source for all living organisms and play crucial roles in physiological functions. This diverse group of organic molecules is characterized by a notable abundance of monounsaturated fatty acids (MUFA), constituting approximately 65.2-80.8% of their composition. Within lipids, various bioactive compounds are present.

In Extra Virgin Olive Oil (EVOO), lipids manifest as triacylglycerols, predominantly featuring oleic acid as a constituent. Triacylglycerols, categorized under lipids, are composed of fatty acid molecules, with oleic acid being a prominent representative. Additionally, lipids encompass phospholipids and sterols.

Olive oil contains four classes of sterols, and their presence is closely linked to the oil's quality. Sterols can exist in two forms: as free molecules and as esterified compounds. The concentration of sterols in olive oil may be influenced by storage time, impacting the overall quality of the oil. Understanding the composition and variations of lipids, particularly the role of sterols, contributes to evaluating and maintaining the quality of Extra Virgin Olive Oil.

Table 2.1: Presentation of types of fatty acid and the respective percentages that occupy oil[22]

Fatty acids	Carbon chain: Double bond	Concentration%
Myristic acid	C14:0	0.05
Palmitic acid	C16:0	9.4 - 19.5
Palmitoleic acid	C16:1	0.6 - 3.2
Heptadecanoic acid	C17:0	0.07 - 0.13
Heptadecenoic acid	C17:1	0.17 - 0.24
Stearic acid	C18:0	1.4 – 3.0
Oleic acid	C18:1	63.1 - 79.7
Linoleic acid	C18:2	6.6 - 14.8
α-Linolenic acid	C18:3	0.46 – 0.69
Arachidic acid	C20:0	0.3 - 0.4
Eicosenoic acid	C20:1	0.2 - 0.3
Docosanoic acid	C22:0	0.09 - 0.12
Lignoceric acid	C24:0	0.04 - 0.05
MUFA		65.2 - 80.8
PUFA		7.0-15.5

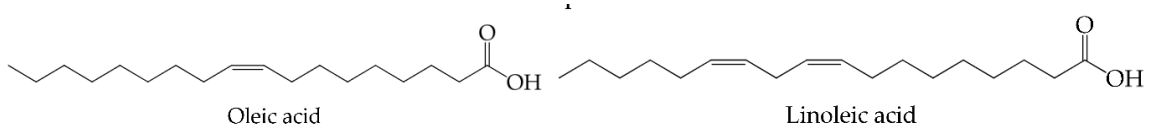

Figure 2.1: Chemical structure of lipids

Vitamins

Vitamins are considered part of the category of organic compounds involved in the primary metabolite category. They are bioactive components and demonstrate many benefits and effects on the organism. The main vitamin in olive oil is vitamin E, which includes four natural tocopherols and four tocotrienols. The α-tocopherol constitutes approximately 88.5% of the total amount of tocopherols in oil, the β- with γ- tocopherol composes 9.9%, and the remaining 1.6% percentage consists of δ-tocopherol. Olive oil produced from the core of oils has more tocopherols than the olive oil extracted from the fleshy part of the fruit. Therefore, the stability of olive oil in oxidation is influenced, for the most part, by the presence of tocopherols.

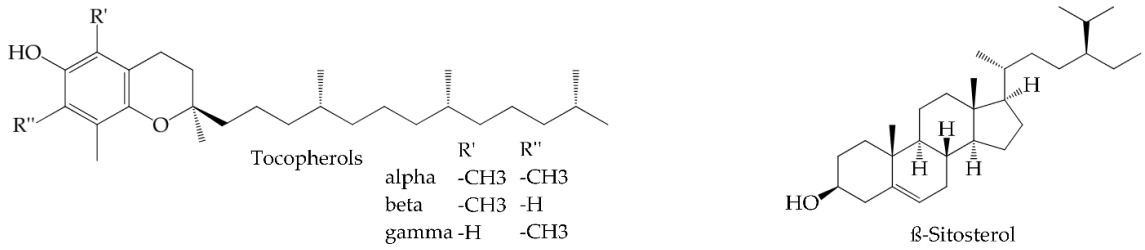

Figure 2.2: Chemical structure of two types of vitamins

Specifically, Tocopherols are high molecular weight heterocyclic compounds, and there is a fluctuation in the proportion of tocopherols in olive oil. These compounds are found in all vegetable oils. Furthermore, tocopherols are found as three isoforms in EVOO. The first is a-tocopherol, which exists in free form and is located in the most significant concentration in contrast to the other two types of Tocopherols. The β-Tocopherol, γ-Tocopherol, and δ-Tocopherol can be found in lower quantities in EVOO. Looking at **Figure 2.4**, it is evident that each tocopherol differs from the other due to the different positions of methyl groups.

Determining the proportion of tocopherols in EVOO contributes to the detection of adulteration with lower-quality oil because some seed oils, such as corn oil, are more decadent in tocopherols β and γ than EVOO.

Carbohydrates

In olive oil, two significant carbohydrates, β-carotene and squalene, play essential roles. The presence of carbohydrates in olive oil offers health benefits, such as restricting certain types of cancer. Among these carbohydrates, the presence of squalene exerts a substantial influence on the health associated with olive oil.

It is subject to variations based on factors such as the type of olive cultivation and the oil extraction technique. Moreover, the carbohydrate fraction in Extra Virgin Olive Oil (EVOO) includes triterpenes and diterpenes, isoprenoid polyolefins, hydrocarbons, and n-paraffins.

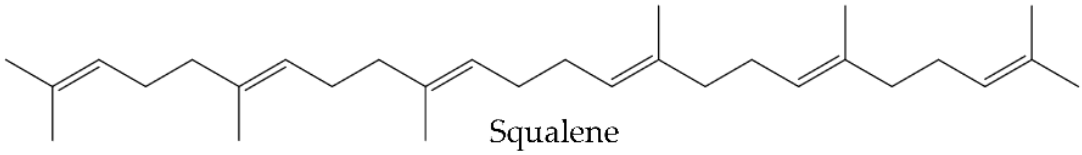

Figure 2.3: Chemical structure of squalene

Secondary Metabolite

Phenolic Compounds

Phenolic compounds come from the fruit and leaves of the olive and occupy the principal group of antioxidants. Phenolic compounds offer a range of benefits for human health, contributing to the prevention of various chronic diseases because they protect human cells from oxidative stress. These compounds have demonstrated selective toxicity against cancer cells, inducing apoptosis and protecting non-tumorigenic cells.

The phenolic compounds can exist in different forms, such as free, bound, or esterified, and have been identified in the olive fruit. The primary role of phenolics in olive oil is to protect it from the attack of atmospheric air, oxygen, and solar radiation. Therefore, olive oil rich in phenolic compounds has high protection and resists changes in its properties over time. Furthermore, the presence of phenols in oil helps determine the quality of the oil.

The main phenols found in olive oil are tyrosol and hydroxy-tyrosol. In 2012, the European Food Safety Authority (EFSA) proposed that the polyphenols in olive oil help protect blood lipids from oxidative stress if olive oil contains at least 250 mg of hydroxytyrosol and its derivatives per 1kg of olive oil.

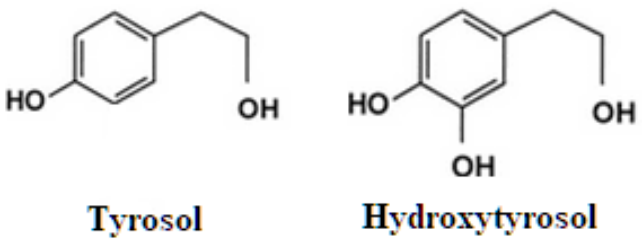

Figure 2.4: Chemical structure of two phenolic compounds[24]

Pigments

Pigments in olive oil often comprise phenolic compounds, contributing to the characteristic color of this valuable oil. The pigments exist as lipophilic carotenoids and chlorophyll in olive oil. Several factors, including the physicochemical

characteristics of the fruit, the geographic origin, climate, and irrigation conditions, influence the quantity of pigment in olive oil. Also, the mechanic extraction process, storage conditions, and final packaging can affect the pigment concentration.

Observing pigments in oil is a valuable tool for determining the quality and potential adulteration of Extra Virgin Olive Oil (EVOO). Pigments indicate freshness and antioxidant properties, essential elements that contribute to the overall quality of the oil. In addition, the ratio between the total amount of chlorophyll and carotenoids indicates the authentication of EVOO. Moreover, specific pigments such as violaxanthin and lutein can be used to identify a monovarietal EVOO. Many types of pigment can be maintained for more than a year in storage.

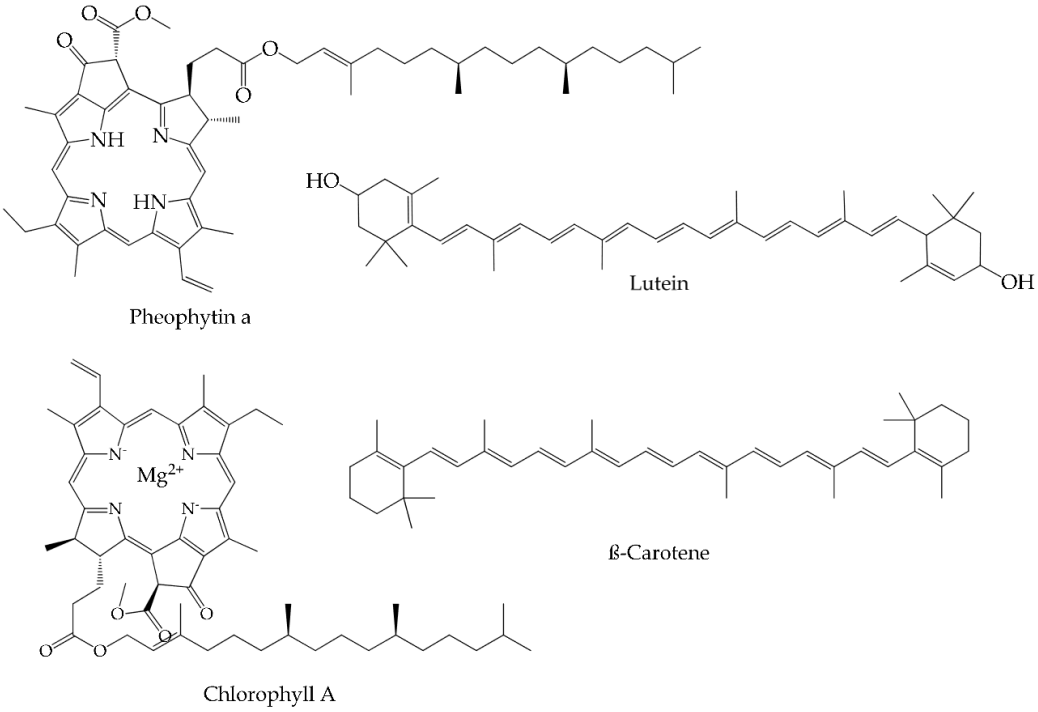

Figure 2.5: Chemical structure of pigments

2.3. Fluorescence spectrum of olive oil

The application of the fluorescence techniques is important because it detects the presence of some substances that compose the olive oil and have fluorescence properties, providing valuable information about their concentration and identity. More specifically, the presence of particular substances may be identified by observing the various wavelengths. Finally, measuring the intensity of the fluorescence signal can be correlated with the concentration of the substance in the sample. This allows for quantitative analysis, providing information about the amount of the substance present.

2.3.1 Experiment Process

In this study, fluorescence measurements of the olive oil were conducted using the Fluoromax-P instrument from Horiba. The experimental setup involved placing each

pure olive oil sample in quartz cuvettes with a 10-mm path length, positioning them in a front face geometry at an angle of 35 degrees.

A systematic scanning approach was employed to visualize these measurements, scanning a range of excitation wavelengths for each emission wavelength. The emission wavelength was examined from 200 nm to 800 nm, with an increment step of 2 nm and a scanning time of 0.2 seconds. Simultaneously, the excitation wavelength was scanned from 270 to 600 nm, with an increment step at 5 nm. This process resulted in 67 scans, providing a comprehensive dataset for thorough analysis. Additionally, the width of slits for both the excitation and emission beams was set at 3 nm.

2.3.2 Fluorescence Excitation-Emission Matrices (EEMs) of EVOO

Figure 2.6 visually depicts the fluorescence ranges exhibited by extra virgin olive oil. In images (a) and (b), the fluorescence measurements cover an emission wavelength range between 200 and 800 nm and an excitation wavelength range between 270 and 600 nm. Upon closer inspection of image (a), it is observed that there is intensity only at approximately 650 nm of emission wavelength, and the excitation wavelength is from 350 nm to 440 nm. Image (b) encompasses the same wavelength ranges but with a different intensity scale, revealing an additional region that fluoresces with lower intensity than the previous region.

Furthermore, image (c) zooms in on the region of interest in image (b), specifically concentrating on emission wavelengths between 250 and 600 nm and excitation wavelengths ranging from 250 to 500 nm. In this magnified view, it becomes apparent that the region contributing the most has excitation wavelengths from 270 nm to 400 nm and emission wavelengths between 300 and 550 nm. This meticulous analysis of fluorescence patterns assists in identifying specific spectral features and intensity variations in extra virgin olive oil, offering valuable insights into its composition and quality characteristics.

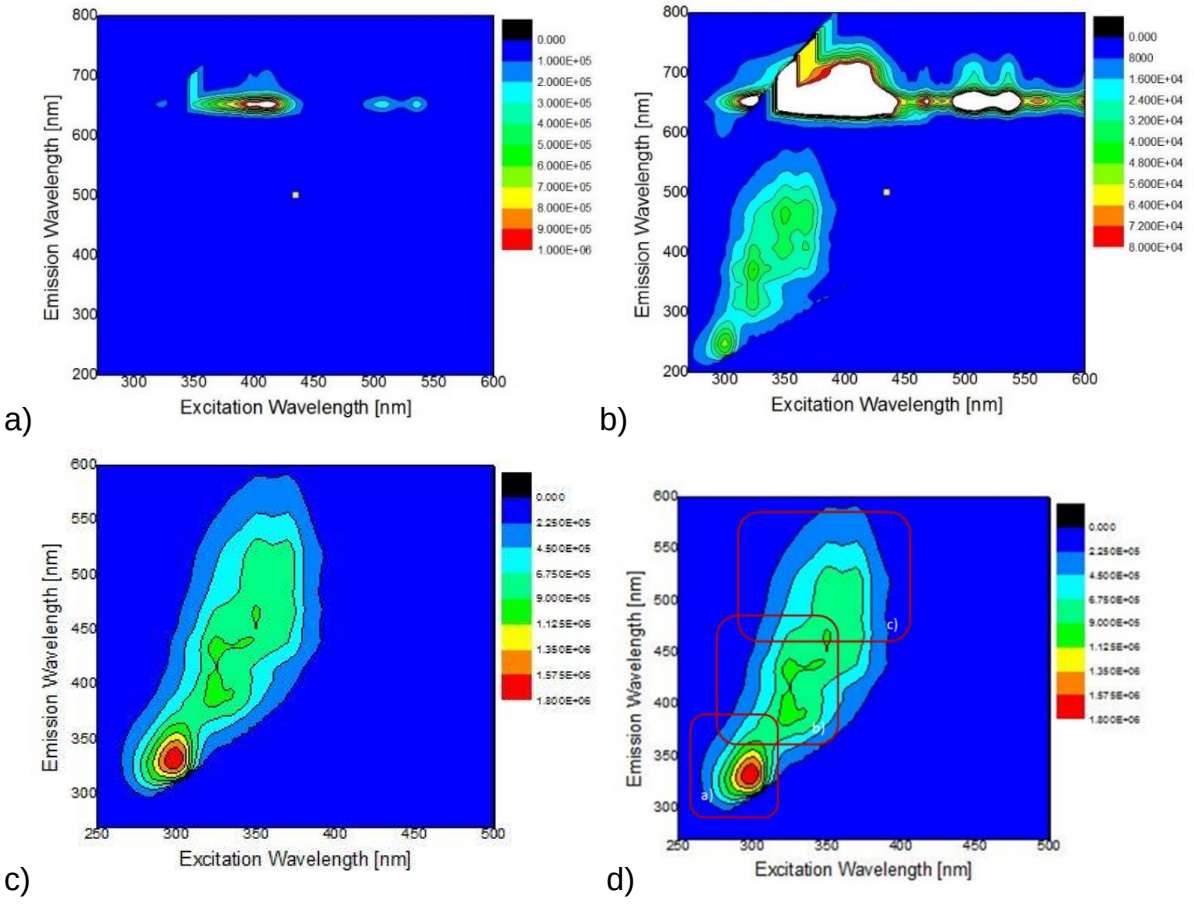

Figure 2.6: Fluorescence Excitation-Emission Matrices (EEMs) of Extra Virgin Olive Oil in different wavelength ranges

2.3.3 Matching of Fluorescence Regions with Olive Oil's Chemical Substances

The employ of fluorescence measurements to assess the quality of olive oils dates back to the early 20th century[11]. Researchers noted that olive oil exhibits distinctive fluorescence characteristics, which can be attributed to various compounds. As a result, fluorescence techniques have evolved into widely employed methods for studying the composition of olive oil.

A related paper[21] applies the fluorescence spectroscopy technique to determine the fluorescence region of substances that compose the EVOO. The research highlights two intense bands in the fluorescence spectra of Extra Virgin Olive Oil. The first band, termed short-wavelength, is characterized by excitation wavelengths between 270 and 400 nm and emission wavelengths around 290-580 nm. The second band, long-wavelength, displays excitation wavelengths from about 350 nm to 420 nm and emission wavelengths from 650 nm to 700 nm.

Furthermore, the paper associates these fluorescence regions with specific compounds in olive oil. Short fluorescence wavelengths are related to the presence of tocopherols, tocotrienols, and several phenolic compounds, with excitation wavelengths occurring from 270 nm to 320 nm and emission from 290 nm to 400 nm. The tyrosol and hydroxytyrosol are the main phenolic compounds that contribute to

this region. Additionally, oxidation products are attributed to fluorescence in the excitation wavelength range of 290 nm to 360 nm and emission wavelength between 350 nm and 480 nm. Furthermore, Vitamin E and carotenoids exhibit fluorescence between 300 nm and 400 nm excitation with emission between 450 nm and 580 nm. Lastly, pigments such as chlorophyll contribute to long-wavelength fluorescence with excitation from 350 nm to 420 nm and emission at about 650 nm to 700 nm.

Synthesizing information from the bibliography mentioned in the above text makes it feasible to elucidate the specific chemical components contributing to the fluorescence excitation-emission matrix in **Figure 2.5**. Therefore, the region is illuminated with excitation wavelengths from 330 nm to 550 nm, and emissions of approximately 620 nm and 700 nm are associated with chlorophylls. Furthermore, in **Figure 2.6** in the d picture, the (a) region corresponds to tocopherols, tocotrienols, and phenolic compounds. Also, region (b) appears due to oxidation products in olive oil. Ultimately, Vitamin E and carotenoids exhibit fluorescence in the region (c).

The comparison of different fluorescence regions in image (d) from **Figure 2.6** reveals that the phenolic compounds, tocopherols, and tocotrienols significantly contribute to the fluorescence, presenting higher intensity than the vitamins. This detailed analysis enhances our understanding of the distinct contributions of various chemical components to the fluorescence patterns observed in olive oil.

Chapter 3: Detection of Adulteration of Olive Oils with Seeds and Pomace Oils

As mentioned before, EVOO offers many health benefits to consumers and, as a result, has become a top-rated product in recent decades. However, the olive oil industry faces adulteration and intentional mislabelling challenges. Observing the fluorescence spectroscopic analysis in pure olive oils aims to learn about obtaining knowledge of olive oil fluorescence elements and their intensity. Therefore, those measurements help to discriminate the proportion that the olive oil contributes against the contribution of adulterants to the creation of fluorescence spectra of the spiked olive oils. This chapter presents the process followed for the preparation and measurements of samples, as well as the application of multivariate statistical analysis to detect adulterants in olive oil. This study is critical because the presence of these substances in olive oil influences the product's quality and safety. Conversely, the absence of safety measures can lead to severe harm or even fatalities among consumers.

3.1 Adulterants in Olive Oil

Adulteration typically involves blending pomace and seed oils such as soybean, sunflower, and corn oil with Extra Virgin Olive Oil to increase profitability[20]. This practice arises from the substantial price difference between EVOO and other oils, prompting the producers to mix cheaper oils with olive oil solely for financial gain. The deceptive similarity in physical characteristics between the adulterating component and EVOO makes detection difficult for consumers and retailers. This allows vendors to sell adulterated EVOO at the same price as pure EVOO, impacting both the economy and consumer health[2]. Therefore, food safety and quality are two essential terms that describe aspects of food products and the reputation of the processors producing[25].

Consequently, developing methods for identifying adulteration in Extra Virgin Olive Oil is essential. Several techniques have been employed to analyze EVOO, such as the analytical technique we mentioned in this project's introduction. But in this project, we study fluorescence spectroscopy with the combination of statistical analysis used to efficiently determine the presence of seeds or pomace oils in EVOO because this method is faster and more economical.

Adulterants commonly found in virgin olive oil include refined olive oil, pomace oil, residue oil, synthetic olive oil, glycerol products, seed oils, and nut oils. This study has focused on seed oils, including corn, soybean, sunflower, and pomace oil. The pomace oil is the residue of olive oil fruits after mechanical extraction of EVOO and is treated with organic solvents such as hexane. Additionally, the category of pomace oils includes crude olive pomace oil, which is deemed unsuitable for human consumption due to its processing methods and quality.

The main difference in composition of EVOO and adulterant and the reason that they show differences in fluorescence measurements is that EVOO possesses high levels of monounsaturated fatty acids (e.g., 78%) and low levels of saturated acids (e.g.,

14%) in contrast to seed oils (e.g., sunflower, corn, and soybean), which have high levels of polyunsaturated fats[26].

3.2. Fluorescence Spectroscopic Analysis of Pure Adulterants and Spiked Olive Oil

It is essential to employ analytical methods and techniques, such as fluorescence measurements, for detecting and preventing the adulteration of olive oil, contributing to maintaining product integrity and consumer trust. Hence, this part of the project presents the fluorescence excitation-emission matrices of the pure three seed oils and pomace oil and the blend of EVOO with the adulterants.

3.2.1 Preparation of Samples

For this research, the creation process of artificially adulterated olive oil samples was done in the previous work of this lab. This process involved using five different types of olive oils and four distinct adulterants. The pure olive oils used in this experiment were different. One came from the previous harvest, the other came from commercial olive oil, and the other three were different olive oils from the same crop year. For the adulterants, soybean, corn, sunflower, and pomace oil were used. Overall, 260 samples of adulterated olive oil were prepared. Specifically, a 4-decimal scale was used, and a certain amount of adulterant was added to 20 ml Vials each time. Thus, with this process, the final amount is approximately 10 gr of adulterated olive oil. These samples were created by combining the olive oils with various adulterants in different percentages (%w/w). Specifically, for each adulterant, 13 samples were prepared by mixing a certain adulterant with each type of olive oil, resulting in 52 adulteration samples for each olive oil. The concentration range spanned from 0.5% w/w to 30% w/w.

Subsequently, these samples were subjected to measurement in the fluorescence instrument. Each of the samples was located in quartz cuvettes with a 10-mm path length, and then this was placed in the front face geometry at 35^{o}. The ranges of spectra that were used for the measurements consisted of the emission wavelength range between 300 nm and 550 nm with increments of 2 nm. The time of each scan was 0.2 sec, and the excitation wavelength range was between 280 nm and 410 nm, with the scan's step equalling 5 nm. Thus, each sample was exposed in 27 scans, and the whole process took approximately 16 minutes for each sample. After all measurements were completed, the statistical and multivariate analysis techniques were applied to obtain fluorescence spectroscopic data to extract valuable insights.

3.2.2 Fluorescence Excitation-Emission Matrices (EEMs) of Adulterants

In the beginning, four different types of oil without any additional substance were measured in a fluorometer.

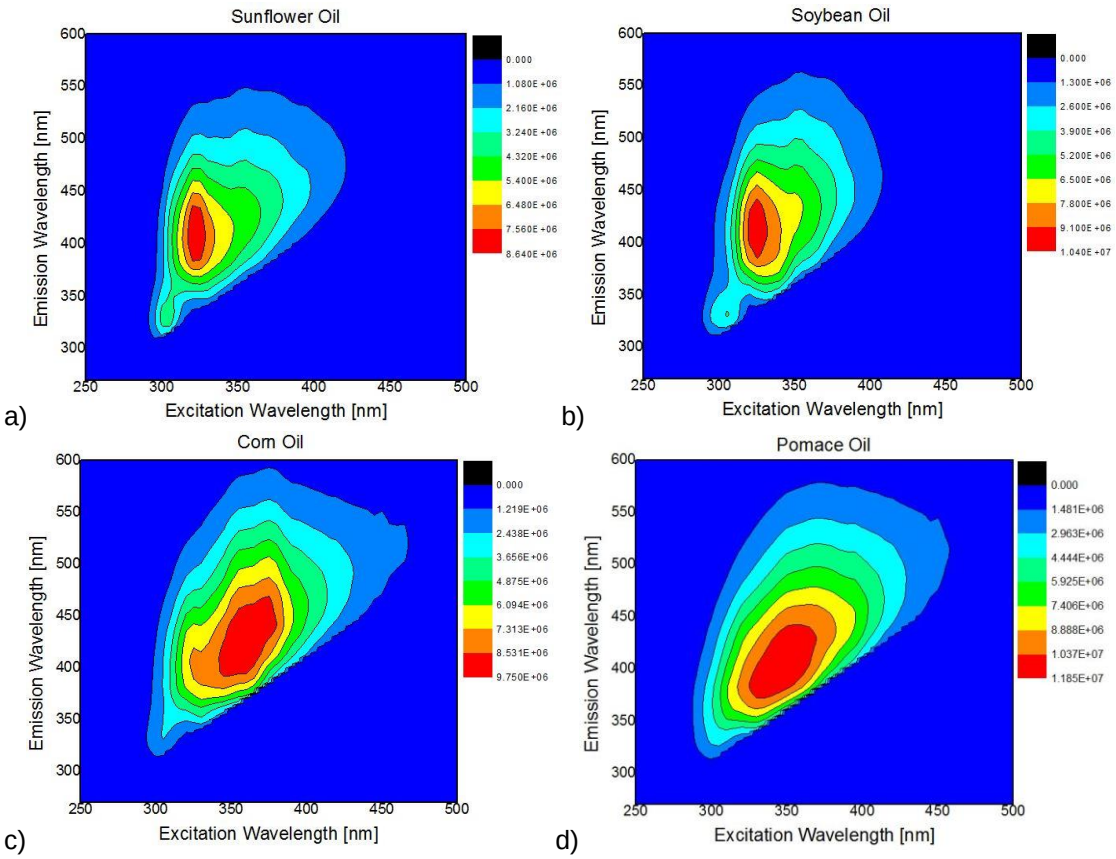

Figure 3.1: Fluorescence Excitation-Emission Matrices of different types of adulterant oil. a) Sunflower oil, b) Soybean oil, c) Corn oil, d) Pomace oil

Figure 3.1 depicts the ranges of wavelengths that those types of oil fluoresce. In more detail, it exhibits that sunflower oil and soybean oil present similar patterns because both of them reach the maximum intensity approximately at 330 nm of excitation wavelength, and respectively, the emission wavelengths range correspond to numbers from 390 nm to 440 nm. Furthermore, corn oil presents maximum intensity in a slightly bigger excitation wavelength than the other two oils. This number corresponds to the range of 350 nm and 380 nm. The emission wavelength of corn oil is between 390 nm and 460 nm, a slightly more extensive range than the other two compounds. Looking at the (d) picture, it is evident that the regions of fluorescence of pomace oil are very similar to the area that corn oil fluoresces, but the excitation wavelength range starts from 330 nm instead of 350 nm and the emission wavelength range finished a little under 450 nm.

3.2.3 Fluorescence Excitation-Emission Matrices (EEMs) of Adulterated EVOO

After the competition with the pure adulterants, the samples, which included EVOO mixed with different adulterants, were measured in a fluorometer. **Figure 3.2** illustrates the ranges of wavelengths that different types of mineral oil fluoresce. It is observed

that all of them fluoresce with maximum intensity in excitation wavelength equal to 320 nm, and the emission wavelength corresponds to the range from 390 nm to 450 nm.

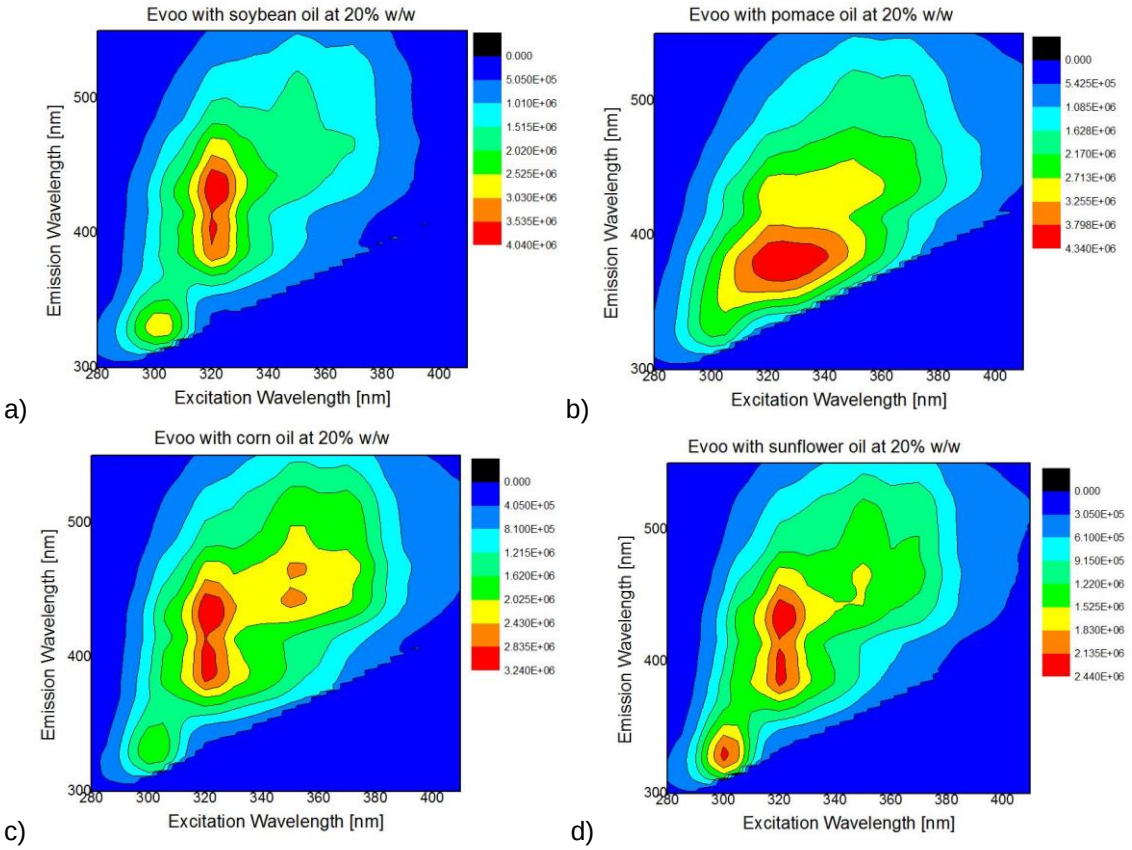

Figure 3.2: Fluorescence Excitation-Emission Matrices of different types of adulterant oil: a) Sunflower oil, b) Soybean oil, c) Corn oil, d) Pomace oil with concentration at 20%

The comparison of **Figure 2.6** and **Figure 3.2** shows that the fluorescence region with the maximum intensity of the above mixtures is due to the contribution of mineral oil because EVOO presents a lower intensity than the mineral oil in the same wavelengths. Also, according to **Figure 3.1**, it is evident that pure adulterant oil shows the maximum fluorescence intensity in approximately the same region as the above figure. Therefore, observing those three figures leads to the conclusion that the contribution of adulterant oils has a slightly more significant weight than the contribution of EVOO at 320 nm and 430 nm of excitation and emission wavelength, respectively, because, in this region, the EVOO presents fluorescence intensity one order of magnitude smaller than the adulterant fluorescence intensity.

3.3. Statistical Analysis

A multivariate statistical analysis is needed to understand fluorescence data and extract meaningful insights. Specifically, the PLS model for observation of the limits of adulterant concentration in EVOO that fluorescence spectroscopy can detect. Also, for the visualization of different categories and the prediction of a sample into the right group, the OPLS-DA was used, and those methods were described in **Chapter 1**.

Those methods were combined with the loading plots that present the weight of the contribution of the Latent Variables.

3.3.1 Partial Least Square

This project applied statistical analysis to 260 artificially adulterated EVOO samples and five pure EVOO. Therefore, **Figure 3.3** presents a PLS graph employed in spectral data to determine the adulterants proportion in EVOO. This method leads to the conclusion of what spectral data contribute to creating the above graph and the known proportions of adulterants in EVOO. As mentioned in **section 1.3.2**, this multivariate statistical analysis requires two data tables. The first table (X) is determined as the independent variable and contains the intensities of fluorescence spectra for each sample. The fluorometer measured these data in the emission spectra range between 300 and 550 nm and the excitation wavelengths between 280 and 410 nm. The second table (Y) is the dependent variable, composed of the actual concentration of adulterant oil for each sample. In the above data, the smoothing and mean centering were applied as the pre-process.

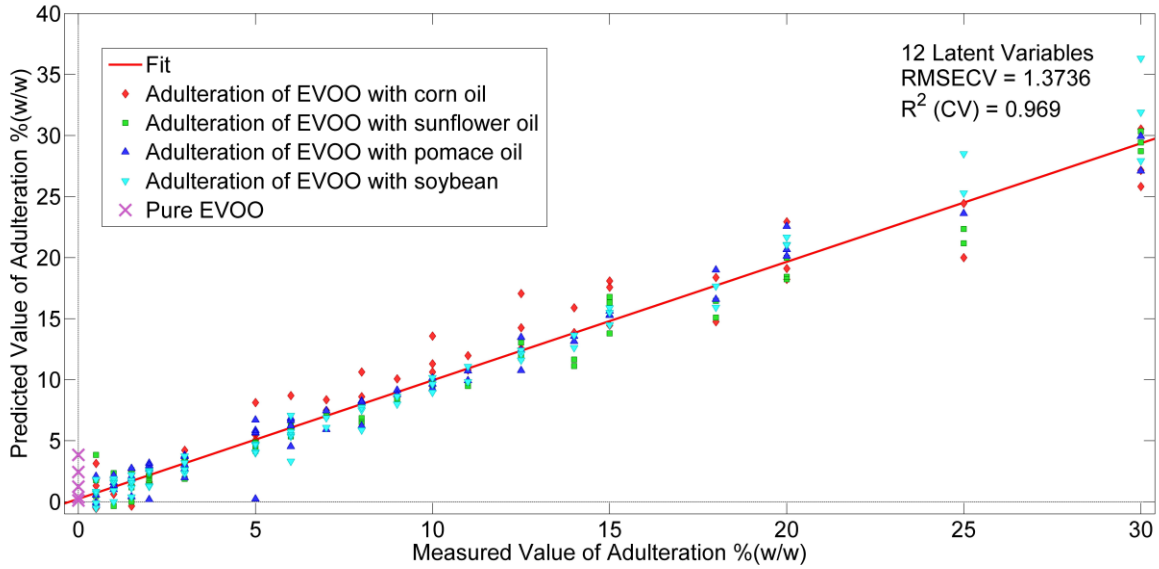

Figure 3.3: PLS regression model plot of predicted function with measured concentrations of oil mixtures

The predictive ability of the PLS model was checked by internal cross-validation by evaluating parameters such as the correlation coefficient R^2 and the root mean square error of cross-validation (RMSECV). According to the above picture, the numbers of R^2 and RMSECH equal 0.969 and 1.3736, respectively. Hence, this model presents satisfactory results regarding the correlation between the predictive and actual concentrations because the value of R^2 is pretty close to 1, and the RMSECV is slightly higher than 0. Applying the smoothing and mean center pre-processes gave better results, leading to **Figure 3.3**. The respective loading plots are presented in **Figure 3.4**. This picture shows the proportions of wavelengths that contribute the most.

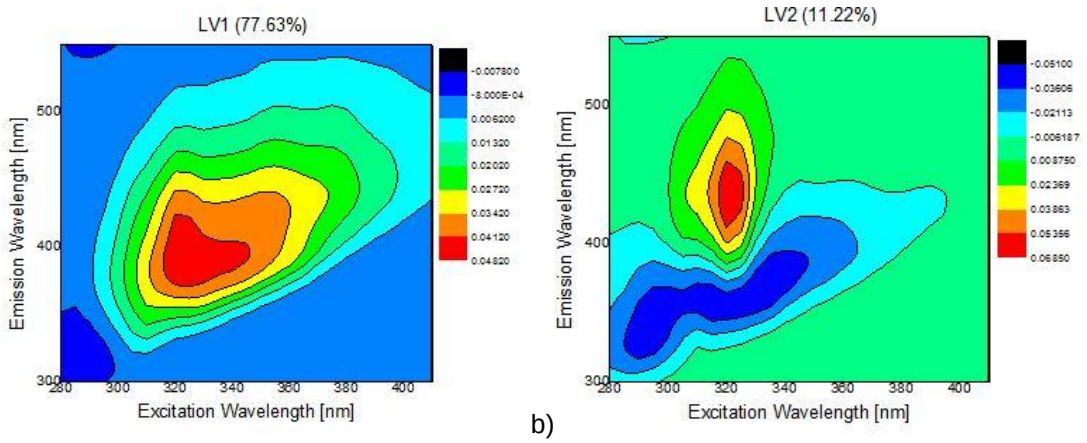

a) b)

Figure 3.4: Loading plot of the a) first latent variables (77.63%) and b) second latent variable (11.22%)

Looking at **Figure 3.4**, it is observed that the LV1 contributes with a proportion of 77.63%, and the significant regions of wavelengths to the creation of the PLS graph are approximately between 320 nm and 360 nm and from 360 nm to 440 nm of excitation and emission wavelength respectively. Also, this picture illustrates the LV2 contribution by 11.22% and the critical role wavelengths play in the regions between 280 and 350 nm and from 300 to 400 nm of excitation and emission wavelength, respectively, and the other area appears in 320 nm of excitation wavelength with emission wavelength at 400 until 500 nm.

3.3.2 Orthogonal Partial Least Squares Discriminant Analysis

The OPLS-DA method was used to discriminate different types of adulterants in oil. This statistical method helped visualize the possible grouping of adulterated olive oil samples mixed with various adulterants. The results of this process are presented in the form of a loading plot and score plot, which appear in **Figure 3.5** and **Figure 3.6**, respectively. A score plot illustrates the association among the samples, thus leading to possible discrimination in the categories of samples. A loading plot depicts the relationship between latent variables and the wavelengths that contribute to the placement of the sample in the correct category. Additionally, **Table 3.1** presents the successful classification rate achieved by the pre-processed when they were chosen. The result below arose from the employment of smoothing and SNV pre-processes. This combination led to better results than the other techniques that were used.

According to **Table 3.1**, it is evident that this technique can predict the correct group of a sample with high percentages. More specifically, the spiked EVOO with pomace oil is predicted more accurately than the other substances in EVOO with 96.72%. The slight difference regarding the correct classification above the categories of adulterated EVOO is affected by the fact that all of them exhibit different characteristic fluorescence regions.

Table 3.1: OPLS-DA classification (confusion matrix) of adulterated oil samples (total 256) using fluorescence spectra

	Spiked EVOO with corn oil	Spiked EVOO with sunflower oil	Spiked EVOO with Pomace oil	Spiked EVOO with soybean oil
Predicted as spiked EVOO with corn oil	56	0	0	0
Predicted as spiked EVOO with sunflower oil	7	61	0	8
Predicted as spiked EVOO with pomace oil	1	0	59	0
Predicted spiked EVOO with soybean	1	4	2	57
Correct classification (%)	86.15%	93.85%	96.72%	87.69%

Looking at **Figure 3.5**, it is evident that there is discrimination between the categories of spiked EVOO. Furthermore, it is observed that the separation between the spiked EVOO with corn oil and sunflower held mostly according to LV7, and the mixtures of EVOO with pomace oil and soybean oil are categorized due to the contribution of LV1.

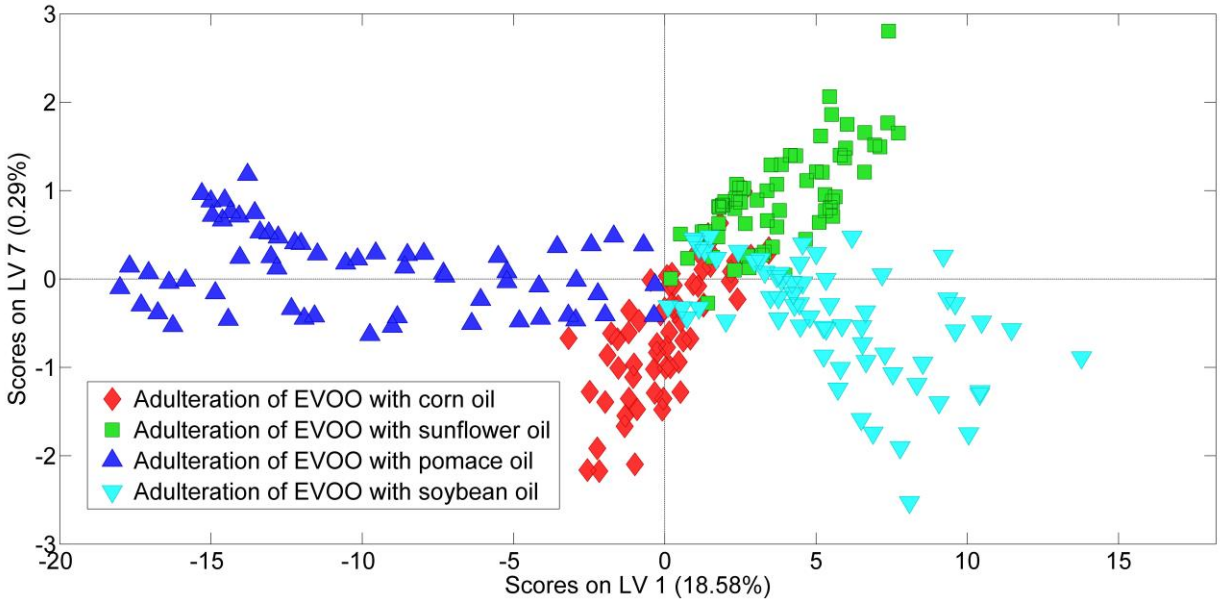

Figure 3.5: Discrimination of adulterated extra virgin olive oil with different types of oils by using OPLS-DA

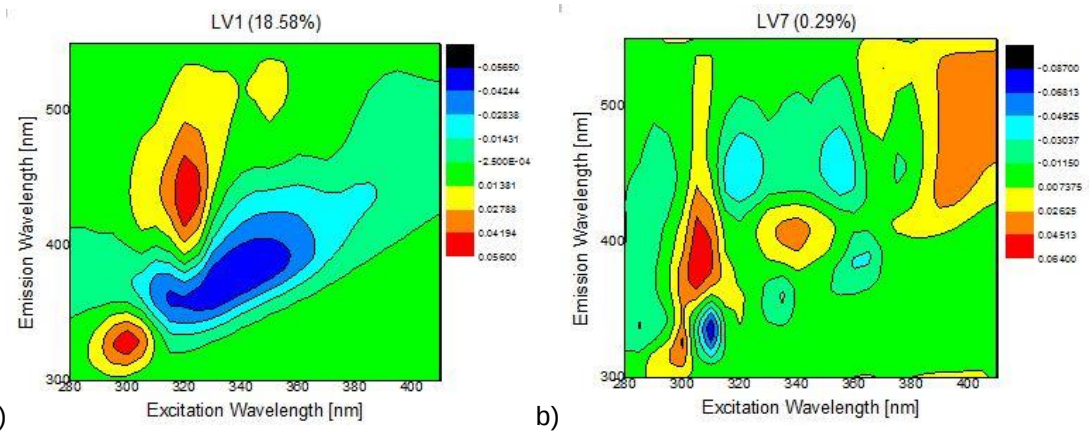

a) b)

Figure 3.6: Loading plot of the a) first latent variable (18.58) and b) seventh latent variable (0.29%)

Figure 4.9 presents the loading plot of LV1 and LV7, providing insight into the regions contributing significantly to the discrimination. In the classification of the adulteration of EVOO with pomace oil, the first latent variable's loading plot consistently highlights the region's significance with an emission wavelength from 350 to 400 nm and an excitation wavelength ranging from 310 to 360 nm. One more region contributing to LV1 is at 320 nm of excitation wavelength with emission wavelength between 400 and 500 nm. The final area in LV1 is at 300 and 330 nm of excitation and emission wavelength, respectively. On the other hand, the loading plot of the second latent variable (LV2) reveals that the specific wavelengths, which play a crucial role in classification, appear in regions between 380 and 410 nm of excitation wavelength with the mission wavelength in the range of 410 and 550 nm. The other two contributing points are the 340/400 nm and 310/ 310 nm excitation /emission wavelengths. The final region that affects the classification in LV2 is at approximately 310 nm of excitation wavelength and from 350 to 500 nm of emission wavelength.

3.4 Conclusions

This chapter crafted a novel analytical tool utilizing optical spectroscopic techniques to identify and measure the adulteration of extra virgin olive oil with lower-quality edible oils, such as seed and pomace oil. The method employed fluorescence spectroscopy, and the obtained results were further analyzed using multivariate statistical techniques, including Partial Least Squares (PLS) and Partial Least Squares Discriminant Analysis (PLS-DA).

The PLS score plot illustrated the tool's capability to determine adulteration in EVOO, while the PLS-DA score plot demonstrated its ability to infer the type of adulterant present. To enhance understanding, the loading plots were generated to visualize the predominant wavelength ranges contributing to the production of these plots. This step facilitated the comparison of wavelengths between loading plots and those obtained from the spectrometer, aiding in identifying substances contributing to the observed patterns. The PLS model yielded statistical parameters with a correlation coefficient of 0.969 and a root mean square error of prediction of 1.3736 units. Also, the corresponding loading plot indicates that the mineral oils contribute to predicting the correct concentration in PLS because the wavelengths that appear at high intensity in

the loading plot fit with the fluorescence wavelength of pure adulterants. These results indicate relatively low detection limits for adulteration in the specific analyzed oil samples. The developed analytical tool, combining fluorescence spectroscopy with multivariate statistical methods, effectively detected and characterized adulteration in EVOO.

In previous work[23], the prediction of adulterant concentration in olive oil was also held with other methodologies such as FT-IR, Raman, and absorption in the region of UV, Vis, and NIR of electromagnetic radiation. The results of this project fluctuated between 0.617 and 0.990 for the value of $R^{2,}$ and the RMSECV appeared values between the range 4.5051 and 0.766, where the better result was for the data set without the mixed olive oil with pomace oil. Therefore, the fluorescence technique is chosen because the PLS model in this method retains more accuracy in predicting the actual concentrations than the other optical spectrometry methods containing the data of pomace oil. More specifically, the results with pomace oil are the same as those without this type of adulteration. Furthermore, the range of scans used in those measurements is continuous, and it is unnecessary to detect some regions of the spectrum separately. Finally, one more advantage of the fluorescence method is that it is possible to discriminate adulterated extra virgin olive oil into different groups according to the substance they are mixed with through the PLS-DA statistical analysis. In that case, the correct classification reached a proportion of 86% in all the adulterated EVOO groups.

Chapter 4: Contaminants in Olive Oil

The consumption of olive oil has increased every day worldwide, so determining olive oil's safety is essential. However, assessing the overall quality of food products is a complex undertaking due to the potential presence of undetected pathogenic organisms, toxic chemicals, or physical hazards that may threaten human health.

Contamination can occur during various stages of edible oil production, such as harvesting, manufacturing, transportation, and storage processes[27]. Furthermore, sources of contamination in olive oil may be the new industrial processes, agricultural practices, environmental pollution, and climate change.

The contaminant substances in olive oil are pesticide residues, heavy metals, and mycotoxins in edible oils, mineral oils, and fats. More specifically, mycotoxins are small molecular organic compounds, not complex protein molecules, so antibodies cannot be produced in the body, nor can they be immune to the body. They could be reduced by controlling the temperature during the production process. The following very well-known product that contaminates olive oil is pesticide residues. The most widely used organic chlorinated pesticides (OCPs) are applied to prevent pets and disease in plant growth. The priority of research is the effective detection and reduction of pesticide residues in edible olive oil. In addition, the long-term and large-scale use of chemical fertilizers and pesticides during crop cultivation increases the pollution of olive oil by heavy metals such as cadmium (Cd), mercury (Hg), lead (Pb), chromium (Cr), and zinc (Zn). The United States Environmental Protection Agency (USEPA) lists these heavy metals as essential control contaminants because of their potential toxicity, persistence, and irreversibility[28]. Finally, mineral oil is another contaminant often found in olive oil. It comprises petrogenic hydrocarbons and includes oil-saturated hydrocarbons (MOSH) and the mineral oil-aromatic hydrocarbons (MOAH). Due to the carcinogenic effects of MOAH, their detection in food is undesirable.

Mineral oil contamination in various foods has been highly concerning due to its potential adverse health effects. In this chapter, the primary focus is on studying the detection of mineral oils in olive oil. The contaminants under consideration are petrogenic hydrocarbons commonly used globally and in various commercial products, such as diesel, gasoline, kerosene, and lubricant oils[29]. Of particular interest is the presence of lubricant oils, a critical petrogenic hydrocarbon, in olive oil. Mineral oils are frequently added to lubricant oils to enhance their properties, serving as additives along with typical salts of organic acids and metallic ions, forming complex mixtures of hydrocarbons.

The sources of mineral oil contamination in food include packaging materials, processing aids, and machine lubricants[27]. More specifically, lubricant oils utilized in machinery such as vehicle motors, tractors, industrial machines (e.g., vacuum pumps and compressors), and aviation and marine applications represent a notable source of mineral oil contamination [24]. Also, the lubricant oils protect metallic surfaces from corrosion, providing cooling and facilitating cleaning in various mechanical devices. Potential contamination methods include using lubricant oils during olive oil manufacturing, minerals in olive skin, and intentional addition by producers.

Developing effective detection methods is crucial, given the potential health risks of mineral oil consumption. Detecting and quantifying mineral oil contamination in olive oil is essential for ensuring food safety. Therefore, this research delves into seeing mineral oils as contaminants in olive oil using fluorescence. It also involves using multivariate statistical analysis to rapidly and accurately identify mineral oil contaminants in olive oil, contributing to broader efforts to enhance food quality and safety, ensuring consumers' well-being.

4.1 Chemical Composition and Structure of Minerals Oil

The petrogenic hydrocarbons consist of mineral oil hydrocarbons (MOH), which contain 10 to about 50 carbon atoms. MOH can be derived from crude minerals and alternative sources, such as coal, natural gas, and biomass, within the category of mineral oil products. Mineral oil products consist of two primary types of hydrocarbons: oil-saturated hydrocarbons (MOSH) and mineral oil-aromatic hydrocarbons (MOAH)[27].

MOH consists of three major classes of hydrocarbon compounds:

- Paraffines are composed of alkanes, encompassing both branched and unbranched.
- Naphthenes, which include cycloalkanes, particularly cyclopentane, and cyclohexanes, alkylated and non-alkylated, mono-, di- and higher ring systems
- Polyaromatic hydrocarbons (PAHs)

Technical grades of MOH typically contain 15-35 % MOAH[30]. However, determining the specific concentration of individual MOH components is challenging due to the complexity of MOH. Nevertheless, it is feasible to quantify the concentration of total MOSH and MOAH fractions.

Additionally, certain petroleum products may contain sulfur compounds at low concentrations, which are formed as aromatic compounds, such as thiophenes, benzothiophenes, dibenzothiophenes, and benzonaphthothiophenes.

Figure 4.1 illustrates the structure of MOH. The first thirteen structures in the figure correspond to MOSH, while the subsequent structures are included in the MOAH category. This graphical representation aids in visualizing the diverse structures that constitute mineral oil hydrocarbons and underscores the complexity of analyzing and characterizing these compounds.

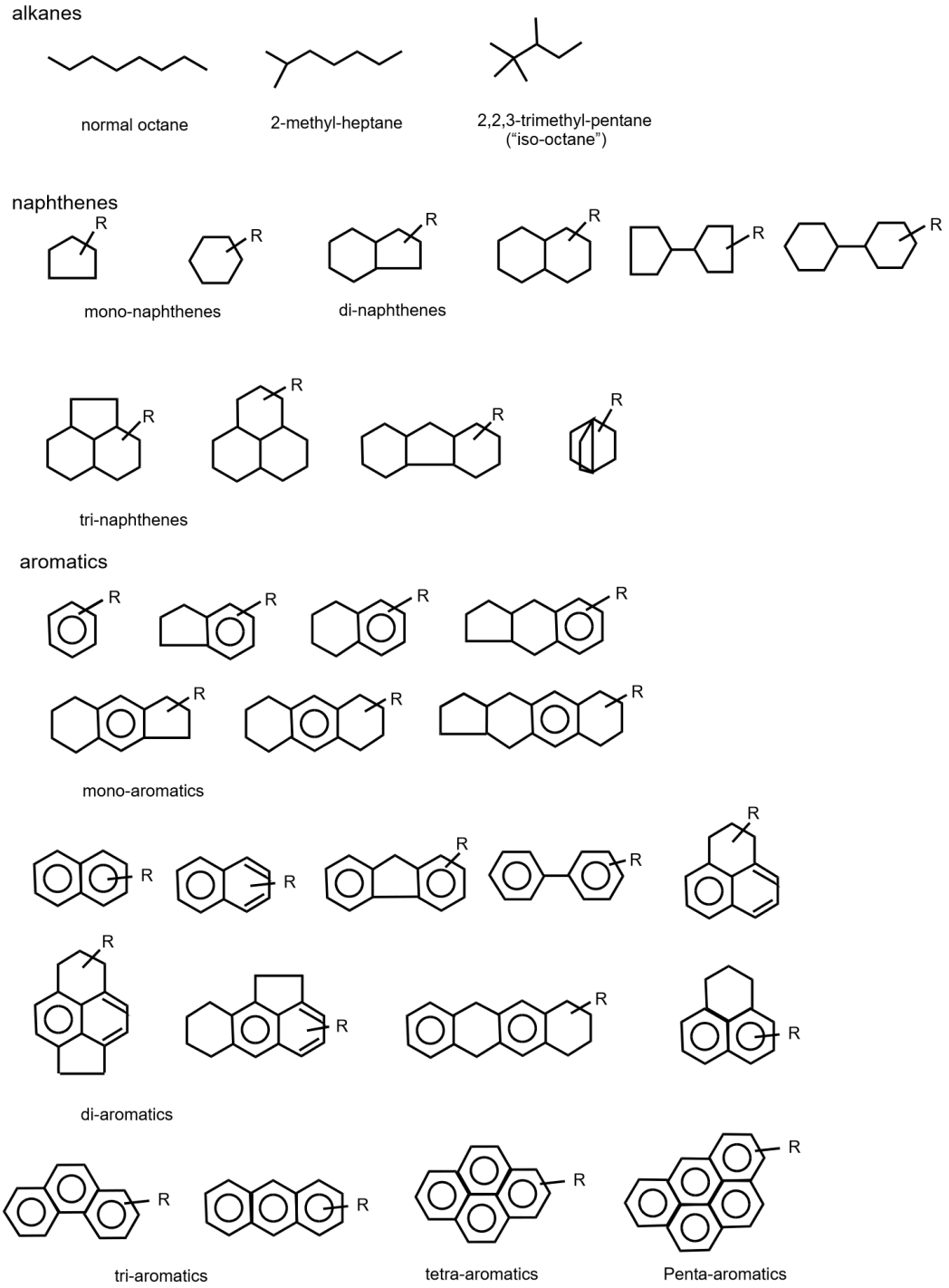

Figure 4.1: The structures of different classes of hydrocarbons[30]

Incorporating petroleum oil into a product significantly shapes its performance characteristics and physical attributes. Some observed physical properties are density, viscosity, refractive index, pour point, and boiling point. Those properties provide information regarding the chemical composition of petroleum oil. These physical properties are notably influenced by the substantial presence of aromatic compounds, particularly polyaromatic hydrocarbons (PAH), which have a similar

structure to mineral oil. Therefore, aromatic compounds, a significant component of the chemical makeup of petroleum oil, contribute to its complexity.

PAHs are contained in engine lubricants and are known to be good fluorophores[31]. Structurally, PAHs consist of two or more aromatic rings without existing heteroatoms. More specifically, PAHs are divided into two categories. The first is the small PAHs, containing up to six aromatic rings, and the second is the large PAHs, comprising more than six aromatic rings. The origins of PAHs can be pyrogenic, petrogenic, and biological.

In previous work, the PAHs were measured in a fluorometer, and now those spectra are compared with the fluorescence spectroscopical analysis of mineral oil, which is presented below. With this comparison, it is possible to see the corresponding fluorescence peaks of mineral oils with one or more PAHs. This happened because a part of mineral oil's structure contains PAH's structure. Therefore, **Figure 4.2** visually depicts the Fluorescence Excitation-Emission Matrices of major PAHs, complemented by their respective structural representations. This approach leverages the unique fluorescence spectrum exhibited by PAHs to identify and quantify the presence of mineral oils in olive oil samples.

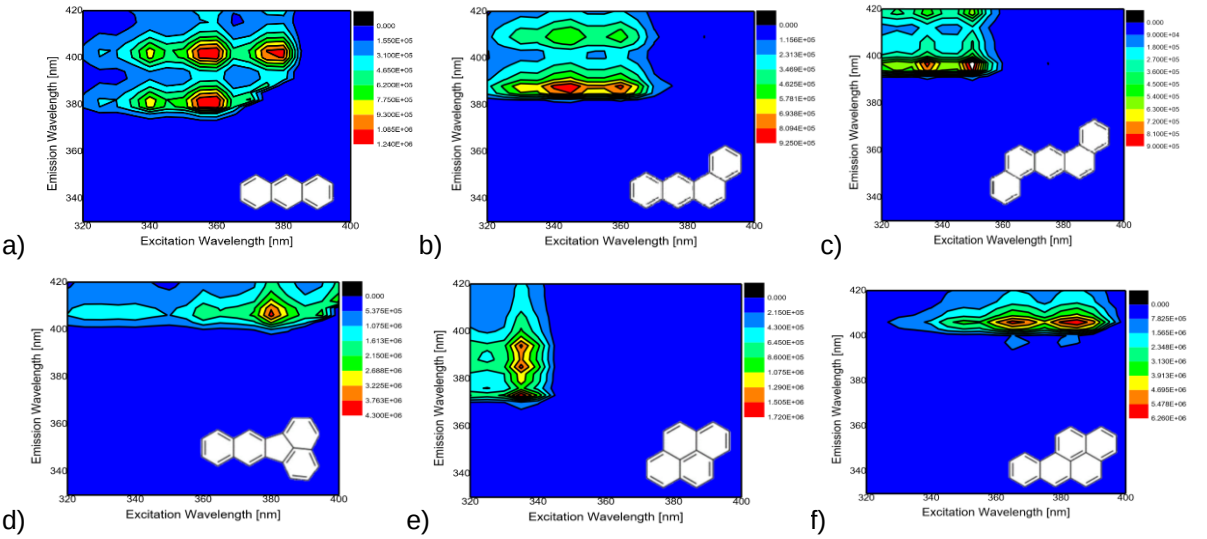

Figure 4.2: Fluorescence Excitation-Emission Matrices PAHs with the concentration of 20ppm, a) Anthracene, b) Benzo[a]anthracene, c) Dibenzo[a,h]anthracene, d) Benzo[k]fluoranthene, e) Pyrene, f) Benzo[a]pyrene

The anthracene appears in the fluorescence region in the excitation wavelength range at approximately 355 nm to 380 nm and the emission wavelengths from 380 nm to 400 nm. Furthermore, the Benz[a] anthracene presents maximum fluorescence intensity from 345 nm to 365 nm and 385 nm to 410 nm for the excitation and emission wavelengths, respectively. Also, image (c) shows the fluorescence regions of Dibenzo[a,h]anthracene, which are smaller than the other PAH. It fluoresces between 335 nm and 350 nm of excitation wavelengths with emission wavelengths from 395 nm to 400 nm. In addition, the maximum fluorescence intensity that Benzo[k] fluoranthene irradiates is at 380 nm and 405 nm of excitation and emission wavelength, respectively. Picture (e) illustrates that at 335 nm of excitation wavelength, the Pyrene exhibits the maximum intensity between 375 nm and 400 nm

of emission wavelength. Finally, the fluorescence region in the Benzo[a]pyrene is located in the excitation wavelengths from 360 nm to 390 nm and the emission wavelengths from 400 nm to 410 nm.

The findings from a published article[29] reveal a significant relationship between the weight of the PAH molecule and the range of emission wavelengths with maximum intensity. This research indicates that a molecule with multiple aromatic rings, which inherently has a higher weight, tends to emit radiation at a higher wavelength. Therefore, this observation sheds light on the rationale behind **Figure 4.2**, which illustrates different regions of fluorescence among various PAHs.

In conclusion, it is essential to detect mineral oil in olive oil because the European Food Safety Authority (EFSA)[30] investigation estimated that the daily exposure range for people to mineral oil-saturated hydrocarbons (MOSH) is between 0.03 and 0.3 mg/kg by body weight (b.w). Notably, the study found that children are exposed to a higher amount of MOSH compared to adults. PAHs in mineral oils play a critical role in human health. That happens because PAHs are rapidly absorbed through the gastrointestinal tract or the pulmonary epithelium once ingested, inhaled, and distributed in various tissues, especially those rich in fat. PAHs undergo extensive metabolism in multiple organs, including the lung, skin, esophagus, colon, liver, and placenta. Also, PAHs are known to possess mutagenic, teratogenic, and carcinogenic effects, primarily due to benzo[a]pyrene (BaP). BaP has been identified as the sole PAH classified as a Group 1 carcinogen by the International Agency for Research on Cancer. In response to this, the European Union has established the first-ever maximum limits for BaP in foods, setting the top levels at 2 µg/kg for BaP and 10 µg/kg for the sum of four PAHs (benzo[a]pyrene, benzo[a]anthracene, benzo[b]fluoranthene, and chrysene) in oils and fats intended for direct human consumption or use as an ingredient in foods. These regulatory measures aim to mitigate health risks associated with PAH exposure through food consumption.

4.2. Spectroscopic analysis of Spiked olive oil and mineral oil with fluorescence spectrum

Determining Polycyclic Aromatic Hydrocarbons (PAHs) in foods poses challenges due to their low concentrations and the complex structure of food matrices. To address potential health hazards linked to human exposure to mineral oils through food consumption, a recommended approach involves utilizing high-performance liquid chromatography combined with gas chromatography and flame ionization detection (LC-GC-FID) for analyzing both Mineral Oil oil-saturated hydrocarbons (MOSH) and Mineral Oil Aromatic Hydrocarbons (MOAHs) in food products. The use of such traditional analytical methods for the characterization of mineral oils in olive oil is vital due to the complexity of the hydrocarbon combination that composes the structure of mineral oils. The advantage of this method is that it reaches low limits and minimizes interferences from food components. Still, those analytical methods often involve expensive sampling, extraction, and separation sequences, which take a long time.

Therefore, it is crucial to establish simple and precise analytical procedures for determining mineral concentration levels. Optical spectroscopy techniques provide a

different perspective in food analysis with their wide applications. Specifically, fluorescence spectroscopy, one of many optical spectroscopic techniques, is promising for detecting mineral oils in food. Thus, fluorescence spectroscopy is a valuable method for identifying specific compounds containing aromatic hydrocarbon rings, such as MOAHs and PAHs, leveraging their natural fluorescence properties. This technique offers high sensitivity, selectivity, and non-destructiveness, along with advantages like simplicity, rapidity, and potential portability, making it suitable for laboratory and field applications. Therefore, this method was established to decrease the time and cost of the whole process.

4.2.1 Samples Preparation

The monitoring of the presence of mineral oils in EVOO is accomplished with an alternative perspective with the rapid use of fluorescence spectroscopy and a relatively cheap technique due to the needless sample pretreatment or the requirement of complex instrumentation. Each sample was located in quartz cuvettes with a 10-mm path length, which was placed in the front face geometry at 35^{o}.

Three different companies have used and purchased a diverse set of mineral oils. The first company produced mineral oil, regenerating double-distillation mineral oil tailored for external use. This oil is designed for chain lubrication in chainsaws and is a fuel. The second company supplied four different mineral oil products. Among them are two diverse base oils with versatile applications, including usage as cleaning agents, in metalworking fluids, for fuel lubrication, in agrochemicals, and within road and construction contexts. Another product, derived from petroleum, finds extensive industrial use, particularly in deasphalting processes, while cylinder oil is designed primarily for diesel engines. The third company provided four distinct lubricants. The initial one is a distillate hydrotreated heavy paraffinic, which is a complex blend of hydrocarbons resulting from the hydrotreatment of a heavy paraffinic petroleum fraction, predominantly containing hydrocarbons within the carbon range of C20 to C50. The second lubricant is a distillate solvent dewaxed light paraffinic oil, obtained through the removal of normal paraffin via solvent crystallization, primarily consisting of hydrocarbons in the carbon range of C15 to C30. The third lubricant, a distillate hydrotreated light paraffinic, is chiefly composed of hydrocarbons within the carbon range of C15 to C30 and is produced through hydrotreatment. Lastly, the fourth lubricant from the third company is a distillate solvent dewaxed heavy paraffinic, and it has a complex hydrocarbon blend obtained through solvent crystallization, primarily comprising hydrocarbons within the carbon range of C20 to C50.

For the different mineral oils mentioned before, a series of spiked samples were performed in olive oil. The sample creation process starts with manufacturing an initial compound containing 49.5gr of EVOO and 0.5gr of mineral oil. Thus, these mixtures were created for each mineral oil with a concentration of 1%. To produce those mixtures, a weight scale was used with an accuracy of four decimal digits. Then, spiked samples with various concentrations were created using the initial compound at the beginning of measurements of different types of mineral oil. Those samples were produced by taking a part of the initial mixture and adding the proper amount of the mineral oil measured as ml. Finally, the concentrations measured with a fluorescence instrument started with a high amount of mineral oil. They ended with a smaller proportion of mineral oil in EVOO until the mineral oil was no longer detected

in EVOO. The last concentration that was measured depended on the type of mineral oil each time because some samples were fluorescing strongly in areas where the EVOO wasn't fluorescing. Thus, these samples were able to be detected in smaller concentrations.

Specifically, for the mineral oil A, 18 spiked samples in olive oil were conducted in the range of concentrations from 1000 ppm to 40 ppm. Then, 18 spiked samples in olive oil were performed in the range of concentrations from 1000 ppm to 40 ppm for the mineral oil B. Then 18 spiked samples in olive oil were created for the mineral oil C, which they were conducted in the range of concentrations from 1000 ppm to 40 ppm, for the mineral oil D 16 spiked samples in olive oil were performed in the range of concentrations from 1000 ppm to 60 ppm, for the mineral oil E 16 spiked samples in olive oil were conducted in the range of concentrations from 1000 ppm to 60 ppm, for the mineral oil F 16 spiked samples in olive oil were performed in the range of concentrations from 1000 ppm to 60 ppm, for the mineral oil G 9 spiked samples in olive oil were conducted in the range of concentrations from 1000 ppm to 350 ppm, for the mineral oil H 6 spiked samples in olive oil were performed in the range of concentrations from 1000 ppm to 500 ppm, for the mineral oil I 15 spiked samples in olive oil were conducted in the range of concentrations from 1000 ppm to 80 ppm and for the mineral oil J 12 spiked samples in olive oil were performed in the range of concentrations from 1000 ppm to 200 ppm. This method allowed for a comprehensive examination of the behavior and properties of each mineral oil within the spiked olive oil samples. Additionally, to enhance the scope of the study, extra virgin olive oil samples were carefully selected to represent a diverse range of varieties, brands, and geographical origins. This diverse set of EVOO samples was then compared with the spiked samples containing different mineral oils, providing a comprehensive perspective on the interaction between mineral oils and olive oils across various conditions.

4.2.2 Fluorescence Excitation-Emission Matrices (EEMs) of Pure Mineral Oil

This study employed a spectrofluorometer to obtain fluorescence excitation-emission matrices for observing mineral oil. 11 samples of different mineral oil were measured in the same wavelength range. For those measurements, each mineral oil was diluted with Hexane, where 10 gr of Hexane was added to 0.1 gr of mineral oil to create the 1 % (10000 ppm) concentration. The precision of those compos was achieved with a weight scale. The condition of the fluorescence instrument for the emission wavelength was 2 nm of the increment step, the time of each scan was at 0.2 sec, and both excitation and emission slits were at 3 nm. The observations spanned a range of emission wavelengths between 270 nm and 600 nm, and the excitation wavelengths were set from 250 nm to 500 nm with an increment step of 5 nm. Thus, 51 scans were created, and the whole process lasted approximately 40 minutes for each sample.

The results of fluorescence measurements are shown in **Figure 4.3** as a contour plot of the Excitation-Emission matrices (EEM) of different types of mineral oils. This fluorescence results from their complex composition, containing various compounds with aromatic rings, including MOAH and PAHs. While all mineral oil products share the general feature of fluorescence, there are differences in the intensity of this fluorescence among different products due to variations in the composition and

concentration of MOAH and PAH. The pictures below help to determine particular wavelength ranges that contribute to detecting mineral oil in spiked EVOO.

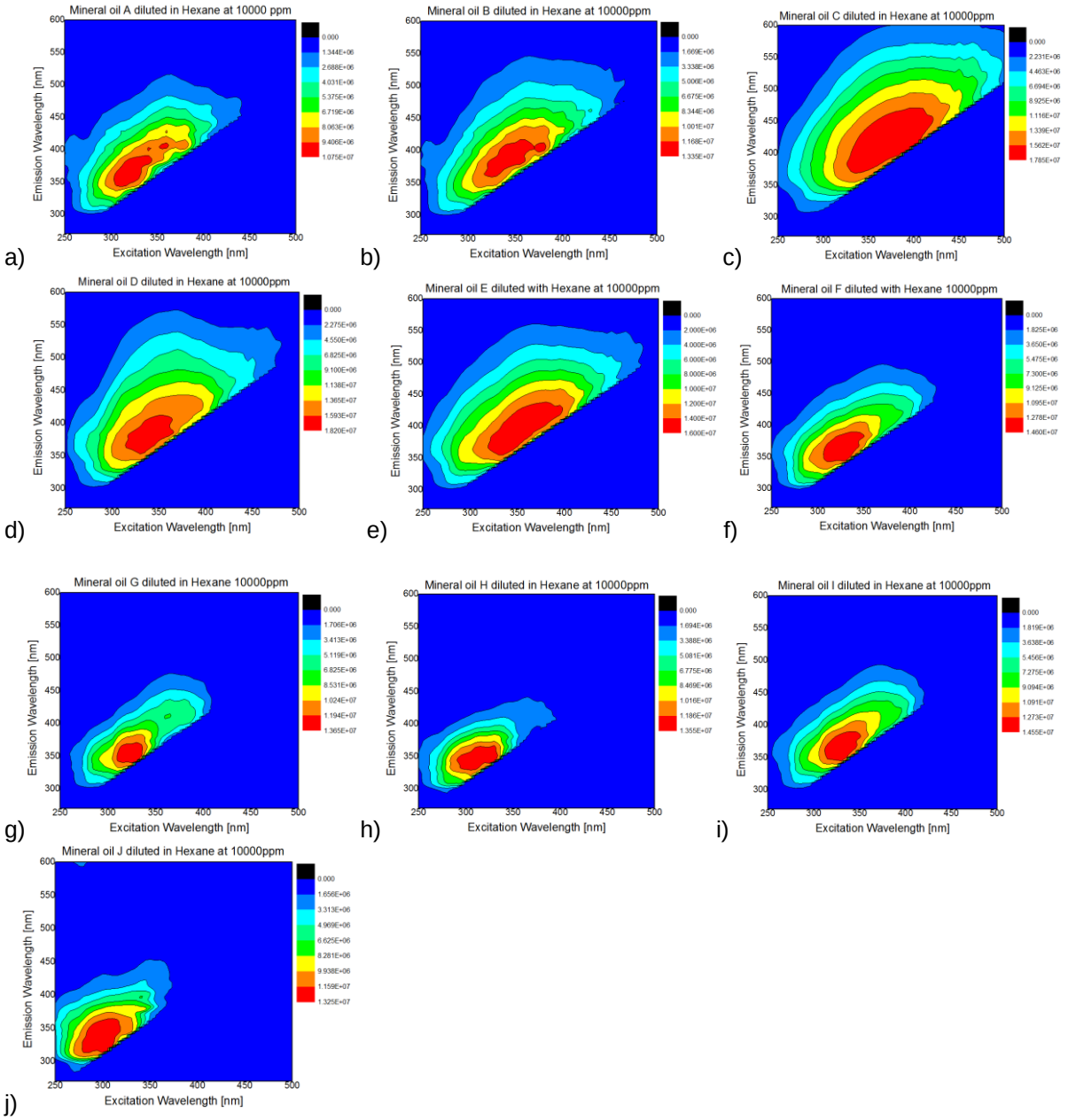

Figure 4.3: Fluorescence Excitation-Emission Matrices of the different mineral oil products diluted in hexane (1 %w/v): a) Mineral oil A, b) Mineral oil B, c) Mineral oil C, d) Mineral oil D, e) Mineral oil E, f) Mineral oil F, g) Mineral oil G, h) Mineral oil H, i) Mineral oil I, j) Mineral oil J

Looking at **Figure 4.3**, it is observed that all mineral oils contribute in the same wavelengths as olive oil. With more details, mineral oils (h) and (j) appear almost in the same wavelengths, such as an excitation range between 250 nm and 350 nm, and the corresponding range of emission wavelengths is from 300 nm to 400nm. Also, the mineral oil (k) appears to have the same fluorescence wavelengths as the previous two minerals. However, this mineral peaks at emission and excitation wavelengths of 290 nm and 280 nm, respectively. Furthermore, the intensity of most mineral oils in **Figure 4.3** is maximized in wavelengths of approximately 330nm and 350nm of

excitation and emission wavelength, respectively. This fact is shown in pictures (f), (g), and (i), which appear fluoresce on emission wavelength from 270 nm to 400 nm, and the emission wavelength range of that mineral oil is between 300 nm and approximately 450 nm. Turning to pictures (a), (b), and (d), it is shown that the mineral oil in the two first pictures exhibits a more extensive range of wavelengths than the previous mineral oils. Specifically, the maximum intensity appears in the 340 nm and 400 nm emission wavelength, and the excitation range corresponds to wavelengths between 330nm and 390nm. Furthermore, the mineral oil (c) presents the same ranges with a slightly smaller intensity. On the other hand, the mineral in picture (e) has the same range of excitation wavelength, but it has a different range of emission wavelength that ranges from 350 nm to 420nm. In addition, it is observed that the mineral oils in the (c) image present the maximum intensity relocated in a slightly higher excitation wavelength. Also, they possess a more extensive range of maximum intensity. Thus, the ranges of this mineral oil appear from 360 nm to 450 nm and between the range of 330 nm and 420 nm for the emission wavelength and excitation wavelength, respectively.

The measurements conducted on various mineral oils reveal that most of these oils exhibit fluorescence patterns in wavelength ranges similar to those observed in extra virgin olive oil (EVOO). This conclusion is drawn from **Figure 2.6**, where it was previously discussed that the maximum intensity of EVOO occurred at 300 nm and 330 nm for excitation and emission wavelengths, respectively. Consequently, when comparing these findings with the fluorescence patterns of mineral oils represented in **Figure 4.2**, it becomes apparent that detecting the presence of mineral oils in EVOO is challenging due to the overlapping of their fluorescence wavelengths.

4.2.3 Fluorescence Excitation-Emission Matrices (EEMs) of Spiked EVOO

For the measurements of fluorescence spectra of spiked EVOO, each sample was located in a quartz cuvette with a 10mm light path length. The excitation and emission beams occupy 3 and 3 nm bandwidths, which are controlled with the opening of slits. Moreover, all spiked samples of EVOO were analyzed in the excitation wavelength range from 320 nm to 400 nm with an excitation step at 2 nm and emission wavelength range from 330 nm to 420 nm with an emission step at 2 nm with the time of each emission scan was at 0.2 sec. The total scans of measurements were 56, and the whole process lasted about 25 minutes. All contour plots, emission, and excitation spectra of all measured spiked samples are presented in **Appendix B** from **Figure B4** and **Figure B21.**

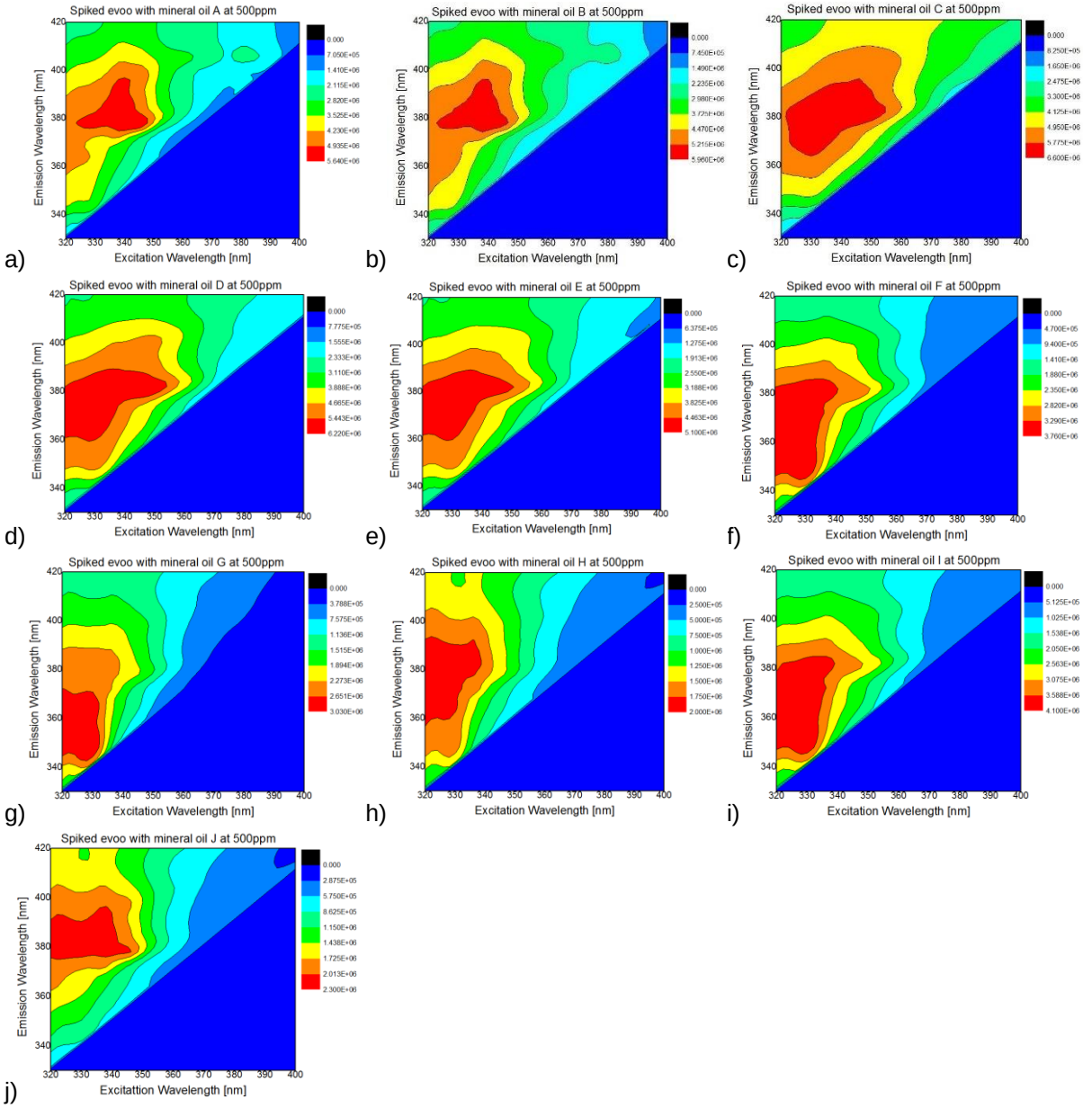

Figure 4.4: Fluorescence Excitation-Emission Matrices of spiked EVOO with the different mineral oil products at 500 ppm with a) Mineral oil A, b) Mineral oil B, c) Mineral oil C, d) Mineral oil D, e) Mineral oil E, f) Mineral oil F, g) Mineral oil G, h) Mineral oil H, i) Mineral oil I, j) Mineral oil J

With the comparison of **Figure 4.4** and **Figure 4.2**, it is concluded that PAHs present significant fluorescence intensity in the above spectra. Therefore, those spectra are essential for detecting mineral oil in EVOO because the chemical structure of PAHs includes mineral oil. As a result, it influences the fluorescence spectra of mineral oils. The fluorescence intensity in excitation wavelength at 380 nm and emission wavelength at 406 nm I due to structures containing the benzo[K]fluoranthene, anthracene, and Benzo[a]pyrene. It is observed from **Figure 4.4** that only the spiked EVOO with mineral oils A, B, C, and D fluoresce at this point. Also, the above structure affects the fluorescence intensity in 360 nm and 406 nm excitation and emission wavelength, respectively. Furthermore, the fluorescence intensity in excitation wavelength at 360 nm and emission wavelength at 380 nm is caused by the structure of anthracene. In excitation wavelength at 340 nm and emission wavelength at 380

nm, the structures of Benz[a]anthracene, pyrene, and anthracene play a significant role in the display of fluorescence intensity. Finally, in the same excitation wavelength and at 400 nm of emission wavelength, fluorescence intensity is due to the structures of anthracene, benzo[a]pyrene, and dibenzo[a,h]anthracene.

Therefore, the comparison of **Figure 4.4** and **Figure 2.6** reveals noticeable differences in fluorescence regions between pure Extra Virgin Olive Oil (EVOO) and EVOO spiked with mineral oils. In the specific areas of the fluorescence spectra, the spiked EVOO with mineral oils exhibits higher fluorescence intensity, while pure EVOO shows lower contributions in the identical fluorescence spectra. This discrepancy suggests that mineral oils may be detectable based on their fluorescence intensity distributions, which contain wavelengths in areas where EVOO contributes less fluorescence. In comparing those two figures, it is observed that specific regions in the mineral oils can contribute to fluorescence excitation-emission matrices of spiked EVOO. These distinct areas are identified in emission spectra with constant excitation wavelengths around 360 nm, 380 nm, and 400 nm. In excitation spectra, stable emission wavelengths at 380 nm and 400 nm also serve as potential points of differentiation between pure EVOO and EVOO spiked with mineral oils.

In summary, comparing fluorescence intensity distributions in specific wavelength regions allows for the potential detection of mineral oils in EVOO, as these regions exhibit differences in fluorescence behavior between pure EVOO and EVOO contaminated with mineral oils. Hence, each sample was measured in constant excitation or emission wavelength.

4.2.4 Fluorescence Spectrum of Spiked Samples Shown as Line Graph

In this project, four emission and two excitation spectra were measured to discriminate the fluorescence spectrum of different mineral oils. Expressly, the slits of the spectrometer were set at 3 and 3 nm for both emission and excitation radiation. Also, the time of each wavelength was at 1 sec, and for those measurements, an increment step at 1 nm.

All those separate spectra are presented in **Figure 4.5**, where the first spectra in picture (a) occupy a constant excitation wavelength at 340 nm and a range of emission wavelengths from 350 nm to 500 nm. The second spectra in the picture (b) acquire an emission spectrum from 370 nm to 500 nm with a constant excitation wavelength at 360 nm. Picture (c) illustrates an emission spectrum between 390 nm and 500 nm with a constant excitation wavelength at 380 nm. The following emission spectrum is shown in picture (d) with an excitation wavelength at 400 nm and a spectrum range of 410 nm up to 500 nm. Furthermore, the constant emission wavelength at 380 nm is presented in the image (e) with a range of excitation wavelengths from 300 nm to 370 nm. Finally, the (f) image depicts the excitation wavelength between 300 and 395 nm with an emission wavelength of 406 nm.

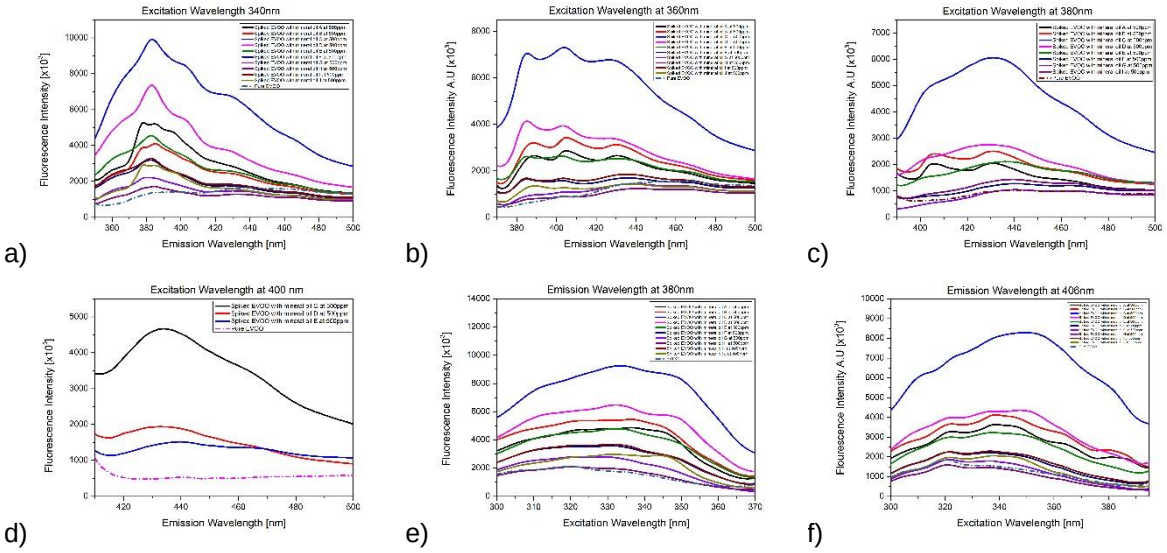

Figure 4.5: Emission and Excitation fluorescence spectra of spiked EVOO with the different types of mineral oils and pure EVOO with a) Excitation wavelength at 340 nm, b) Excitation wavelength at 360 nm, c) Excitation wavelength at 380 nm, d) Excitation wavelength at 400 nm, e) Emission wavelength at 380 nm, f) Emission wavelength at 406 nm

Specifically, picture (e) presents peaks at 330 nm and 350 nm of excitation wavelength, and the (f) image shows peaks at 320, 350, and 380 nm. The difficulty of determination is affected by the fact that the fluorescence intensity is decreased while the concentration of mineral oils in EVOO is reduced. As a result, the peaks of spiked and pure EVOO don't stand out. Image (a) shows three peaks that characterize the emission spectrum at 340 nm excitation wavelength. The first peak is 385 nm, the second is 400 nm, and the third is 430nm. The spectrum of constant excitation wavelength at 360 nm is presented in image (b), where the characterization peaks are located at approximately 385, 405, and 430 nm of emission wavelength. Furthermore, in picture (c), the peaks that contribute to the spectrum exist at 405, 435, and 465 nm of emission wavelength. Finally, picture (d) indicates the 425 and 465 nm emission wavelength as the characteristic peaks. The conclusions of the emission spectra with constant excitation wavelength are that the most significant peaks for the determination of mineral oil in EVOO are 385 nm of emission wavelength with an excitation wavelength of 360 nm. Also, the peaks at 405 nm and 430 nm of emission wavelength with constant excitation wavelength at 380 nm

4.3. Multivariate Statistical Analysis

The multivariate statistical analysis described in the first chapter of this project was applied to the data derived from the fluorescence measurements. More specifically, the PLS-DA and OPLS-DA, combined with the appropriate pre-process type into the data, were used to discriminate pure EVOO from the spiked EVOO with mineral oil and categorize the sample into the right group. Also, this technique visualizes the classification of spiked EVOO with mineral oils from different companies.

4.3.1 Analysis of Data from Excitation-Emission Fluorescence Matrices

Table 4.1 presents the prediction percentages derived from the PLS-DA model using

data from EEM matrices with mean center pre-processing. According to the table, the model achieved a 100% correct classification for pure EVOO samples and a 90.27% correct classification for contaminated EVOO, with only 14 misclassified samples out of 144. The score plot in **Figure 4.6** visually represents the discrimination between pure EVOO and degraded samples. The first latent variable explaining the 94.44% of the data matrix variance plays a significant role in this discrimination. **Figure 4.7** illustrates the loading plots of the first and second latent variables in contour plots following the reverse transformation process.

Examining the loading plot of the first latent variable, it is observed that the characteristic region is located at the emission wavelength of 380 nm and an excitation wavelength ranging from 330 to 360 nm, emerging as crucial for discriminating between pure EVOO and mineral oil-contaminated samples. Furthermore, the loading plot also reveals additional spectral regions that contribute to the discrimination, with varying degrees of significance. Lower emission wavelengths, particularly in the emission of 360 nm, demonstrate substantial contributions. Additionally, wavelengths corresponding to an emission of 405 nm exhibit noteworthy influence in the discriminatory capacity of the model. These identified regions are directly associated with the unique fluorescence characteristics of the studied mineral oil products.

Table 4.1: Partial least squares discriminant analysis classification of samples into pure EVOO and EVOO contaminated with mineral oil products based on fluorescence spectroscopic data by EEM

	Pure EVOO	Spiked EVOO with mineral oil
Predicted as pure EVOO	23	12
Predicted as spiked EVOO with mineral oil	0	132
Correct classification (%)	100%	91,7 %

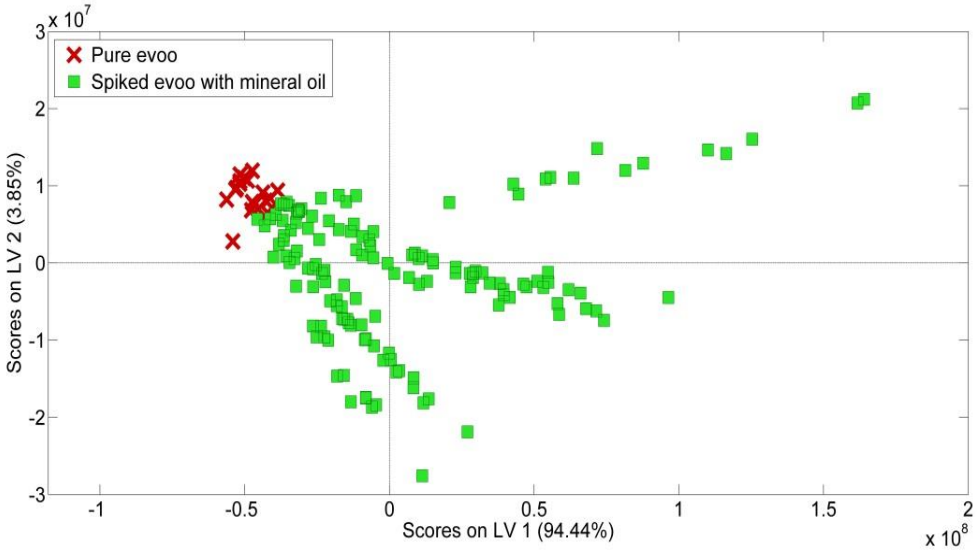

Figure 4.6: Score plot of first (LV 1) and second (LV 2) latent variables for the discrimination of pure olive oil (n = 23) and contaminated olive oil with mineral oil products (n = 144) from partial least squares discriminant analysis (PLS-DA) model of fluorescence data by EEM

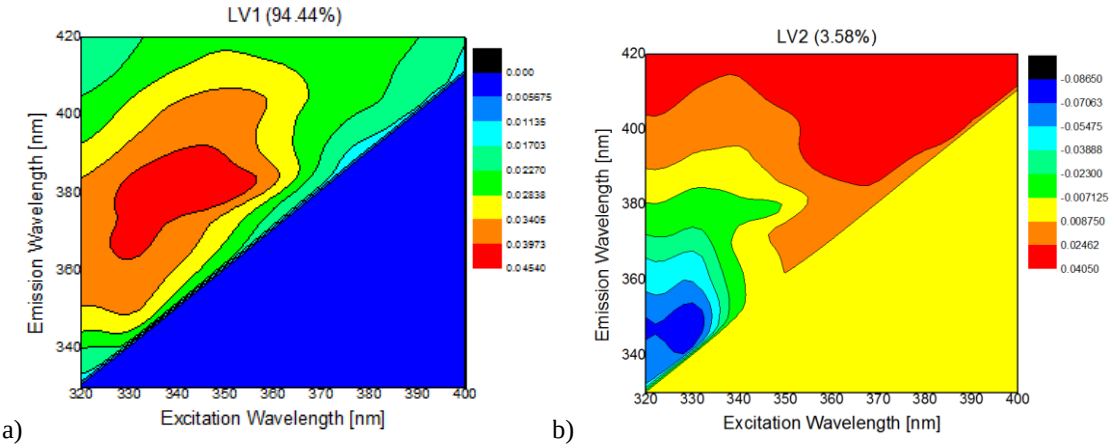

a) b)

Figure 4.7: Loading plot of LV 1 and LV 2 latent variables for the discrimination of pure and contaminated olive oil with mineral oil products from the PLS-DA model of fluorescence data by EEM

The methodology of Partial Least Squares Discriminant Analysis (PLS-DA) was also employed to visualize the separation of three different companies associated with mineral oil contamination. This analysis involved the transformation of Excitation-Emission Matrix (EEM) data, the construction of models, and subsequent interpretation through loading plots. The mean center was used as a pre-processing step for the data. **Table 4.2** provides an overview of the classification outcomes from PLS-DA, presenting predictive accuracy for the categories of pure Extra Virgin Olive Oil (EVOO) and EVOO contaminated with minerals from Companies A, B, and C.

The model demonstrated remarkable accuracy in discerning pure EVOO samples, achieving a 100% correct classification rate. However, the model's ability to correctly classify contaminated samples decreased, providing varied predictive proportions among the companies. Company C presents the highest classification rate at 93.5%. **Figure 4.8** shows the score plot of the PLS-DA model, illustrating the separation of pure EVOO from contaminated samples originating from different companies. It is observed that the first latent variable (LV 1) played a pivotal role in achieving the discrimination between pure and contaminated EVOO, capturing 94.54% of the data matrix variance. Additionally, the second latent variable, which captures 3.78% of the data matrix variance, showcases the discrimination of contaminated olive oil with mineral oil products across the three companies.

Figure 4.9 presents the loading plot of LV 1 and LV 2, providing insight into the regions contributing significantly to the discrimination. In the discrimination between pure and contaminated EVOO with mineral oils, the first latent variable's loading plot consistently highlights the region's significance with an emission wavelength of 380 nm and an excitation wavelength ranging from 330 to 360 nm. On the other hand, the loading plot of the second latent variable (LV2) reveals the most significant contributors to the discrimination of contamination originating from distinct companies. This loading plot emphasizes the crucial role of specific wavelengths, particularly the excitation wavelength of 330 nm with emission wavelengths at approximately 345 nm.

Table 4.2: Partial least squares discriminant analysis classification of samples into pure EVOO and EVOO contaminated with mineral oil products from the different companies based on fluorescence spectroscopic data by EEM

	Pure EVOO	Spiked EVOO with mineral oil from Company A	Spiked EVOO with mineral oil from Company B	Spiked EVOO with mineral oil from Company C
Predicted as pure EVOO	23	5	3	2
Predicted as spiked EVOO with mineral oil from company A	0	31	11	0
Predicted as spiked EVOO with mineral oil from Company B	0	0	48	1
Predicted as spiked EVOO with mineral oil from Company C	0	0	0	43
Correct classification (%)	100%	86.11%	77.4%	93.5%

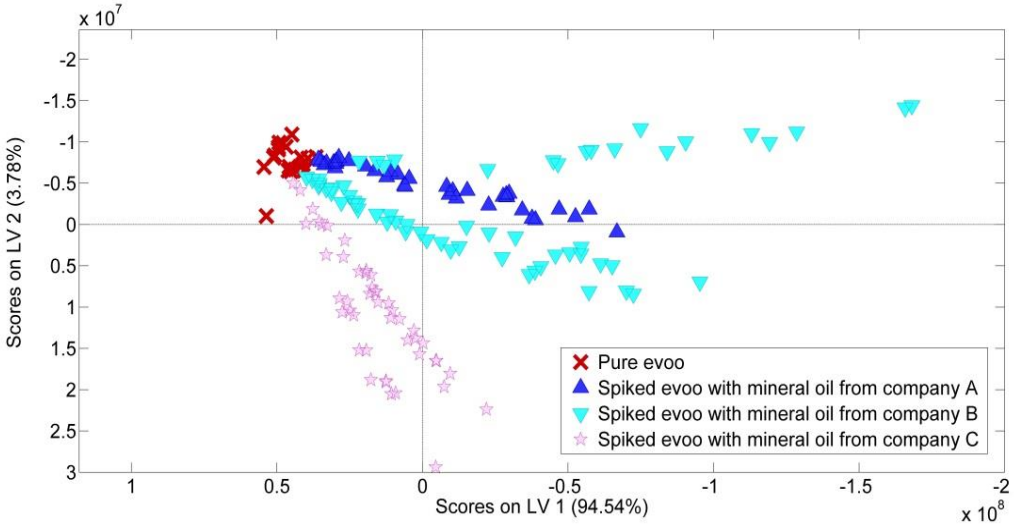

Figure 4.8: Score plot of first (LV 1) and second (LV 2) latent variables for the discrimination of pure olive oil (n = 23) and contaminated olive oil with mineral oil products from the different companies (Company A n = 36, Company B n = 62, Company C n = 46) from PLS-DA model of fluorescence data by EEM

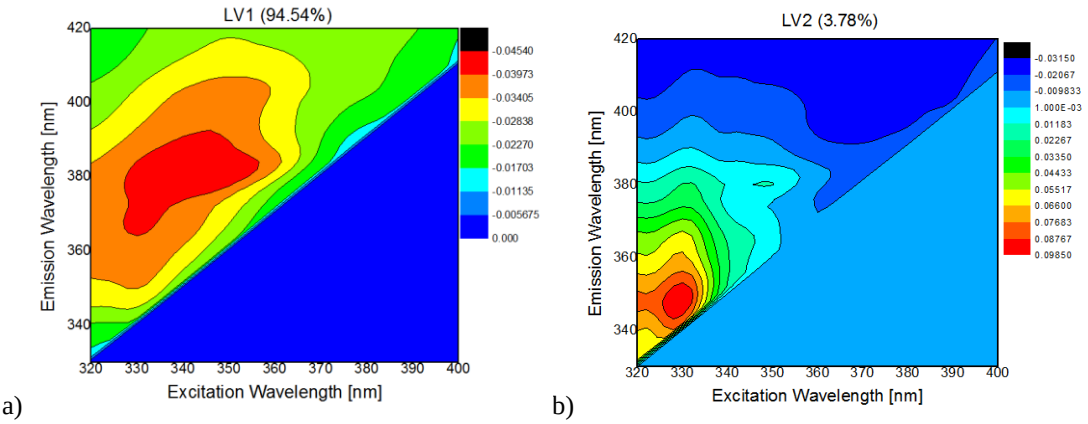

a) b)

Figure 4.9: Loading plot of LV 1 and LV 2 latent variables for the discrimination of pure and contaminated olive oil with mineral oil products from different companies from the PLS-DA model of fluorescence data by EEM

After applying statistical analysis to fluorescence data by EEM, following the analysis of intensity data that came from the emission and excitation spectra. In the data derived from those fluorescence measurements were employed PLS-DA or OPLS-DA for the discrimination of pure and contaminated EVOO with mineral oils, as well as the distinguish between pure EVOO and EVOO spiked with mineral oils originating from different companies. Also, the loading plots are used to understand the relationships between the variables and the wavelengths that contribute the most to the data discrimination into the different categories.

4.3.2 Analysis of Data from Line Graph of Fluorescence Spectrum

Excitation spectrum with emission wavelength at 406 nm

Specifically, orthogonal partial least square (OPLS-DA) was used to classify EVOO from spiked EVOO using fluorescence data from excitation spectrum measurements in regions between 300 and 370 nm with a constant emission wavelength at 380 nm. Those results are represented in **Table 4.3** with the mean center used for data pre-processing. According to the table, the model achieved a 100% correct classification for pure EVOO samples and a 94.4% correct classification for contaminated EVOO, with only 8 misclassified samples out of 144. The score plot in **Figure 4.10** visually represents the discrimination between pure EVOO and contaminated samples. The first latent variable explaining 94.44% of the spectrum data plays a significant role in this discrimination, and LV 2 occupies 28.61% of the data. **Figure 4.11** illustrates the loading plots of the first and second latent variables, where it is observed that the excitation wavelengths that contribute the most to the correct classification are 325, 340, and 355 nm. LV 2 presents the 350 nm excitation wavelength as a crucial region in the classification.

Table 4.3: OPLS-DA discriminant analysis classification of samples into pure EVOO and EVOO contaminated with mineral oil products based on fluorescence spectroscopic data from emission wavelength at 380 nm

	Pure EVOO	Spiked EVOO with mineral oil
Predicted as pure EVOO	23	8
Predicted as spiked EVOO with mineral oil	0	136
Correct classification (%)	100%	94.4%

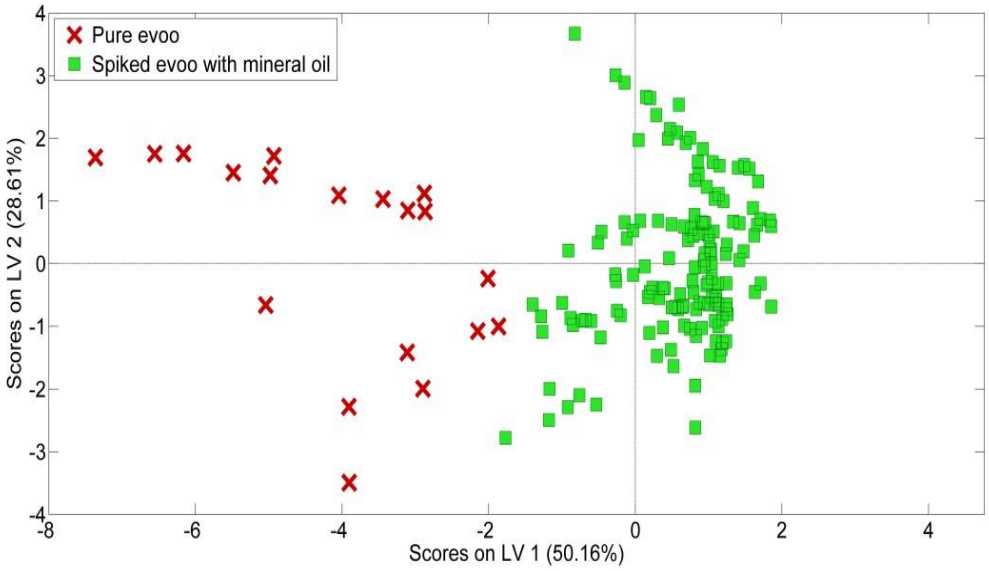

Figure 4.10: Score plot of first (LV 1) and second (LV 2) latent variables for the discrimination of pure olive oil (n = 23) and contaminated olive oil with mineral oil products (n = 144) from OPLS-DA model of fluorescence data for emission wavelength at 380 nm

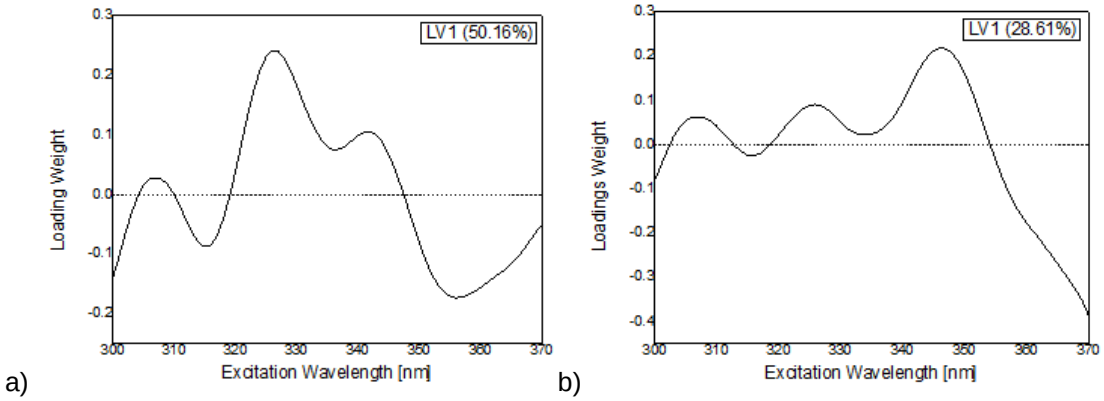

a) b)

Figure 4.11: Loading plot of LV 1 and LV 2 latent variables for the discrimination of pure and contaminated olive oil with mineral oil products from the OPLS-DA model of fluorescence data from emission wavelength at 380 nm

In the visualization of the separation of three different companies associated with mineral oil contamination for the fluorescence data from emission wavelength at 380nm, the Orthogonal Partial Least Squares Discriminant Analysis (PLS-DA) methodology was employed. The pre-processing types used in data in this spectrum

were smoothing SNV and mean center. Therefore, **Table 4.4** provides an overview of the classification outcomes from OPLS-DA, presenting predictive accuracy for the categories of pure and spiked EVOO with minerals from Companies A, B, and C.

The model demonstrated remarkable accuracy in distinguishing pure EVOO samples, achieving a 100% correct classification rate. However, the different companies' correct classification numbers of contaminated samples vary. Company C presents the highest classification rate at 93.5%. **Figure 4.12** shows the score plot of the OPLS-DA model, illustrating the separation of pure EVOO from contaminated samples originating from different companies. It is observed that LV 1 played an important role in achieving the discrimination between pure and contaminated EVOO, capturing 60.27% of the spectrum data. Additionally, the second latent variable, which captures 21.78% of the data, showcases the discrimination of contaminated olive oil with mineral oil products across the three companies.

Figure 4.13 presents the loading plot of LV 1 and LV 2, providing insight into the regions of wavelengths contributing significantly to the discrimination. This figure shows that combining those two latent variables contributes to the discrimination between pure and spiked EVOO with minerals from different companies. Specifically, LV 1 indicates the excitation wavelengths at 320 nm and 350 nm as the most critical regions for the discrimination. On the other hand, LV 2 shows the excitation wavelength at approximately 350 nm with significant degrees of significance.

Table 4.4: OPLS-DA discriminant analysis classification of samples into pure EVOO and EVOO contaminated with mineral oil products from the different companies based on fluorescence spectroscopic data from emission wavelength at 380 nm

	Pure EVOO	Spiked EVOO with mineral oil from Company A	Spiked EVOO with mineral oil from Company B	Spiked EVOO with mineral oil from Company C
Predicted as pure EVOO	23	8	3	2
Predicted as spiked EVOO with mineral oil from Company A	0	28	13	0
Predicted as spiked EVOO with mineral oil from Company B	0	0	43	1
Predicted as spiked EVOO with mineral oil from Company C	0	0	3	43
Correct classification (%)	100%	77.8%	69.4%	93.5%

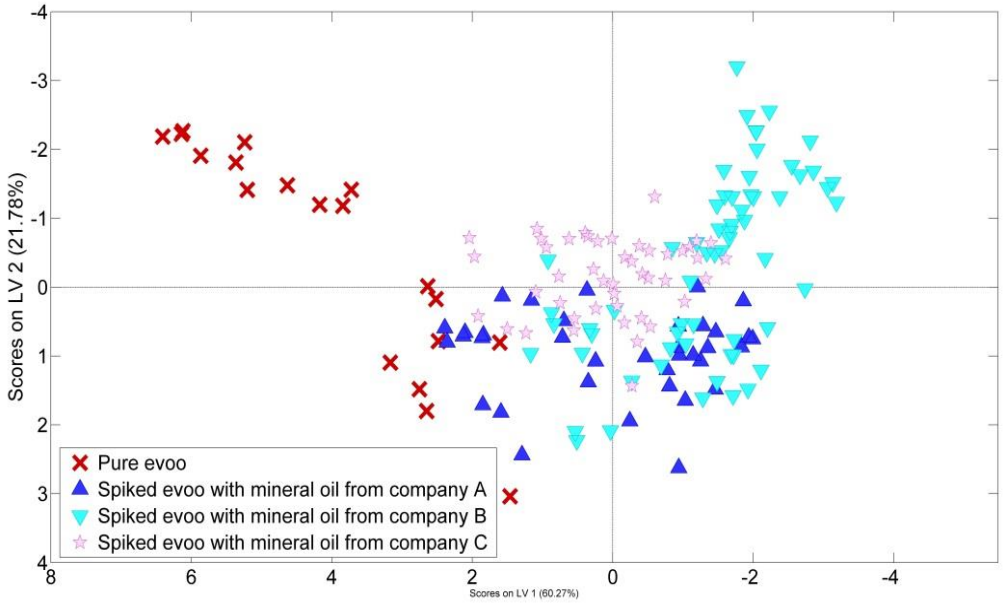

Figure 4.12: Score plot of first (LV 1) and second (LV 2) latent variables for the discrimination of pure olive oil (n = 23) and contaminated olive oil with mineral oil products from the different companies (Company A n = 36, Company B n = 62, Company C n = 46) from PLS-DA model of fluorescence data from emission wavelength at 380 nm

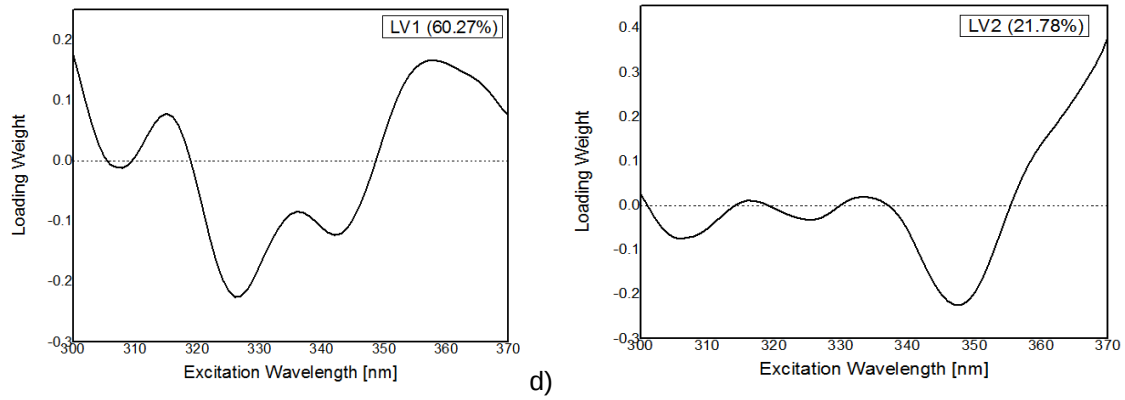

c) d)

Figure 4.13: Loading plot of LV 1 and LV 2 latent variables for the discrimination of pure and contaminated olive oil with mineral oil products from different companies from the OPLS-DA model of fluorescence data from emission wavelength at 380 nm

Excitation spectrum with emission wavelength at 406 nm

Furthermore, the partial least square (PLS-DA) was used to classify EVOO from spiked EVOO by using fluorescence data from excitation spectrum measurements in regions between 300 and 395 nm with a constant emission wavelength at 406 nm. Those results are represented in **Table 4.5** with the smoothing, SNV, and mean center used to pre-process data. According to the table, the model achieved a 100% correct classification for pure EVOO samples and a 93.1% correct classification for contaminated EVOO, with only 10 misclassified samples out of 144. The score plot in **Figure 4.14** visualizes the discrimination between pure EVOO and contaminated samples. The first latent variable corresponds to 74.53% of the spectrum data, which plays a significant role in this discrimination, and LV 2 reaches 14.19% of the data.

Figure 4.15 depicts the loading plots of the first and second latent variables, and it is observed that the excitation wavelengths that contribute the most to the correct classification are 320 and 345 nm. LV 2 appears to have significant wavelengths in similar regions to LV 1.

Table 4.5: PLS-DA discriminant analysis classification of samples into pure EVOO and EVOO contaminated with mineral oil products based on fluorescence spectroscopic data from emission wavelength at 406 nm

	Pure EVOO	Spiked EVOO with mineral oil
Predicted as pure EVOO	23	10
Predicted as spiked EVOO with mineral oil	0	134
Correct classification (%)	100%	93.1%

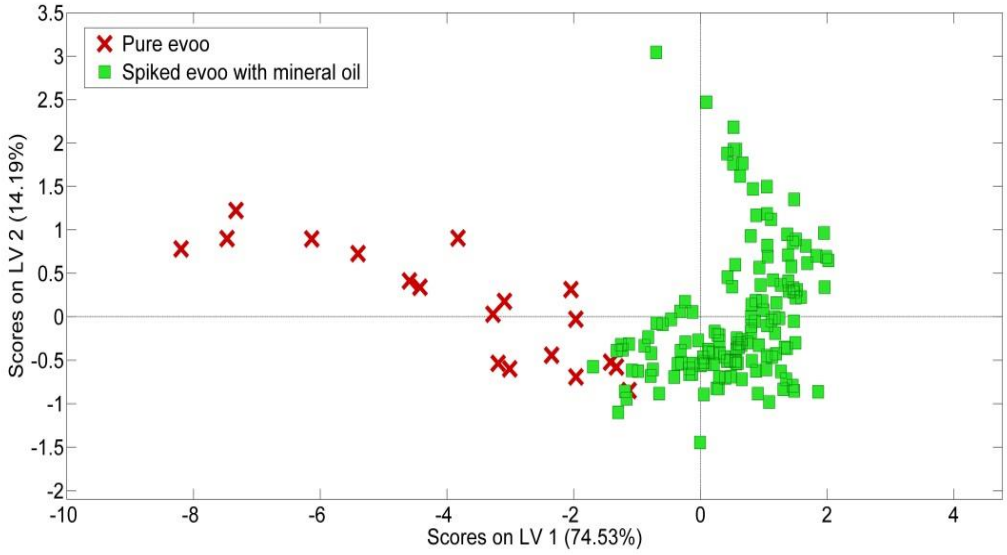

Figure 4.14: Score plot of first (LV 1) and second (LV 2) latent variables for the discrimination of pure olive oil (n = 23) and contaminated olive oil with mineral oil products (n = 144) from PLS-DA model of fluorescence data for emission wavelength at 406 nm

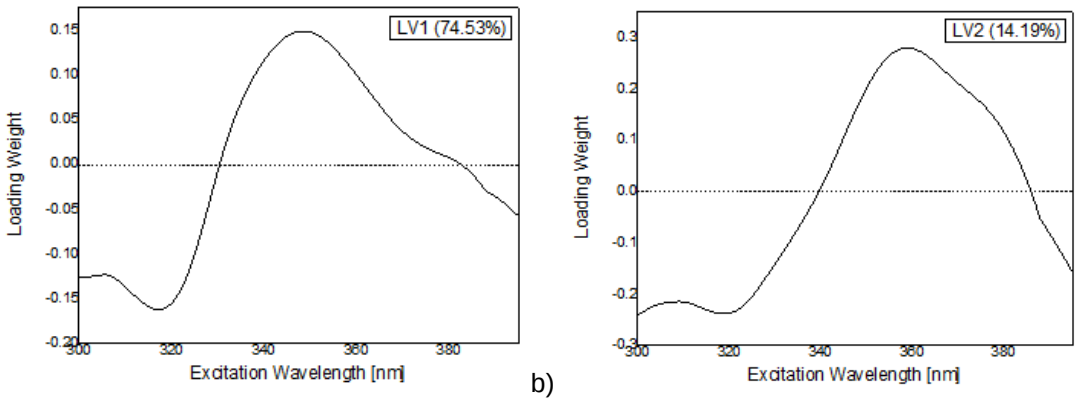

a) b)

Figure 4.15: Loading plot of LV 1 and LV 2 latent variables for the discrimination of pure and contaminated olive oil with mineral oil products from the PLS-DA model of fluorescence data from emission wavelength at 406 nm

In the visualization of the separation of three different companies associated with mineral oil contamination for the fluorescence data from emission wavelength at 406 nm, the methodology of Partial Least Squares Discriminant Analysis (PLS-DA) was employed, with the use of smoothing, SNV, and mean center as pre-processing of data. Therefore, **Table 4.6** provides an overview of the classification outcomes from PLS-DA, presenting predictive accuracy for the categories of pure and spiked EVOO with minerals from Companies A, B, and C.

The model demonstrated remarkable accuracy in distinguishing pure EVOO samples, achieving a 91.3% correct classification rate, and the most significant proportion of correct classification of contaminated samples corresponds to Company C, which presents the highest classification rate at 93.5%. **Figure 4.16** shows the score plot of the PLS-DA model, illustrating the separation of pure EVOO from contaminated samples originating from different companies. It is observed that LV 1 played an important role in achieving the discrimination between pure and contaminated EVOO, capturing 80.07% of the spectrum data. Additionally, the second latent variable, which captures 8.67% of the data, showcases the discrimination of contaminated olive oil with mineral oil products across the three companies.

Figure 4.17 presents the loading plot of LV 1 and LV 2, providing insight into the regions of wavelengths contributing significantly to the discrimination. This figure shows that combining those two latent variables contributes to the discrimination between pure and spiked EVOO with minerals from different companies. Specifically, LV 1 indicates the excitation wavelengths at 320 nm and 350 nm as the most critical regions for the discrimination. On the other hand, LV 2 shows the excitation wavelength at approximately 360 nm with significant degrees of significance and 335 nm with smaller contributions to classification.

Table 4.6: PLS-DA discriminant analysis classification of samples into pure EVOO and EVOO contaminated with mineral oil products from the different companies based on fluorescence spectroscopic data from emission wavelength at 406 nm

	Pure EVOO	Spiked EVOO with mineral oil from Company A	Spiked EVOO with mineral oil from Company B	Spiked EVOO with mineral oil from Company C
Predicted as pure EVOO	21	5	3	2
Predicted as spiked EVOO with mineral oil from Company A	0	29	3	0
Predicted as spiked EVOO with mineral oil from Company B	0	1	46	2
Predicted as spiked EVOO with mineral oil from Company C	2	1	10	42
Correct classification (%)	91.3%	80.6%	74.2%	91.3%

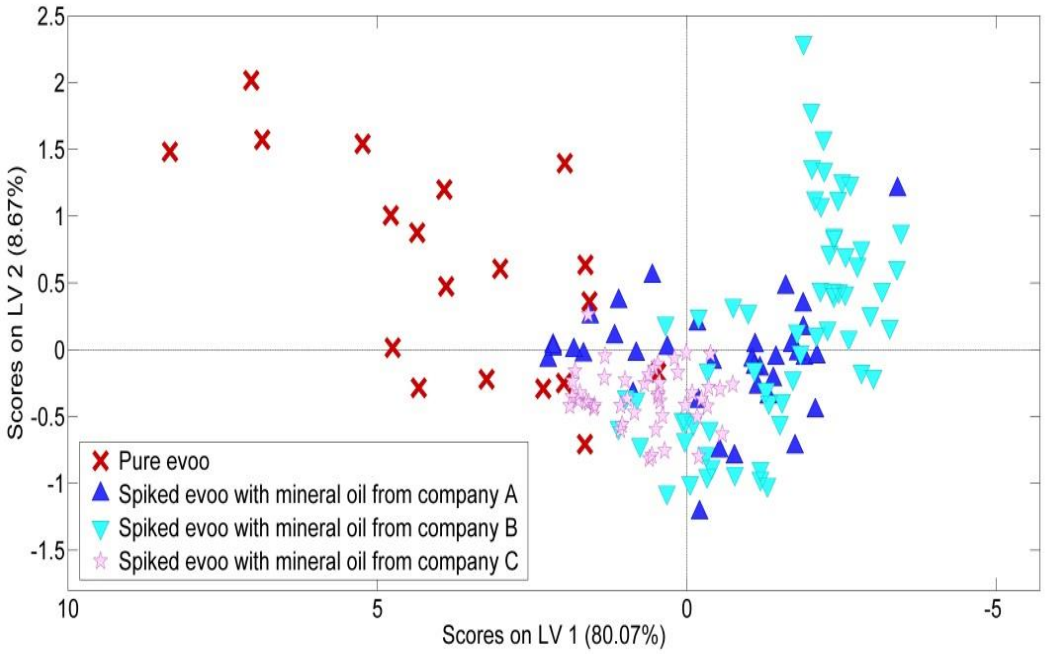

Figure 4.16: Score plot of first (LV 1) and second (LV 2) latent variables for the discrimination of pure olive oil (n = 23) and contaminated olive oil with mineral oil products from the different companies (Company A n = 36, Company B n = 62, Company C n = 46) from PLS-DA model of fluorescence data from emission wavelength at 406 nm

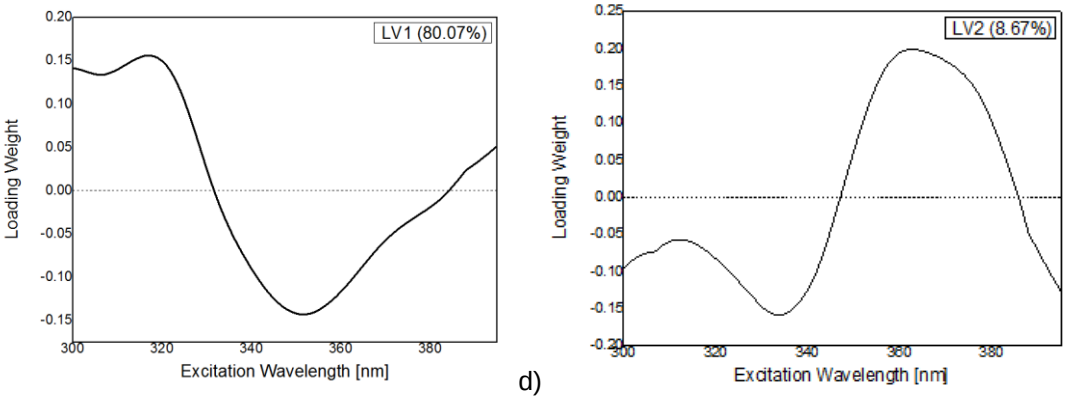

c) d)

Figure 4.17: Loading plot of LV 1 and LV 2 latent variables for the discrimination of pure and contaminated olive oil with mineral oil products from different companies from the OPLS-DA model of fluorescence data from emission wavelength at 406 nm

Emission spectrum with Excitation Wavelength at 340nm

The next region where the partial least square (PLS-DA) was used to classify EVOO from spiked EVOO using fluorescence data is between 350 nm and 500 nm of emission wavelength with constant excitation wavelength at 340 nm. Those results are represented in **Table 4.7** with the smoothing and mean center used for data pre-processing. According to the table, the model achieved a 100% correct classification for pure EVOO samples and an 88.9% correct classification for contaminated EVOO, with only 16 misclassified samples out of 144. The score plot in **Figure 4.18** visualizes the discrimination between pure EVOO and contaminated samples. The first latent variable corresponds to 97.45% of the spectrum data, which plays a significant role in this discrimination. **Figure 4.19** depicts the loading plots of the first and second latent variables, and it is observed that the excitation wavelengths that contribute the most to the correct classification are 390 nm.

Table 4.7: PLS-DA discriminant analysis classification of samples into pure EVOO and EVOO contaminated with mineral oil products based on fluorescence spectroscopic data from excitation wavelength at 340 nm

	Pure EVOO	Spiked EVOO with mineral oil
Predicted as pure EVOO	23	16
Predicted as spiked EVOO with mineral oil	0	128
Correct classification (%)	100%	88.9%

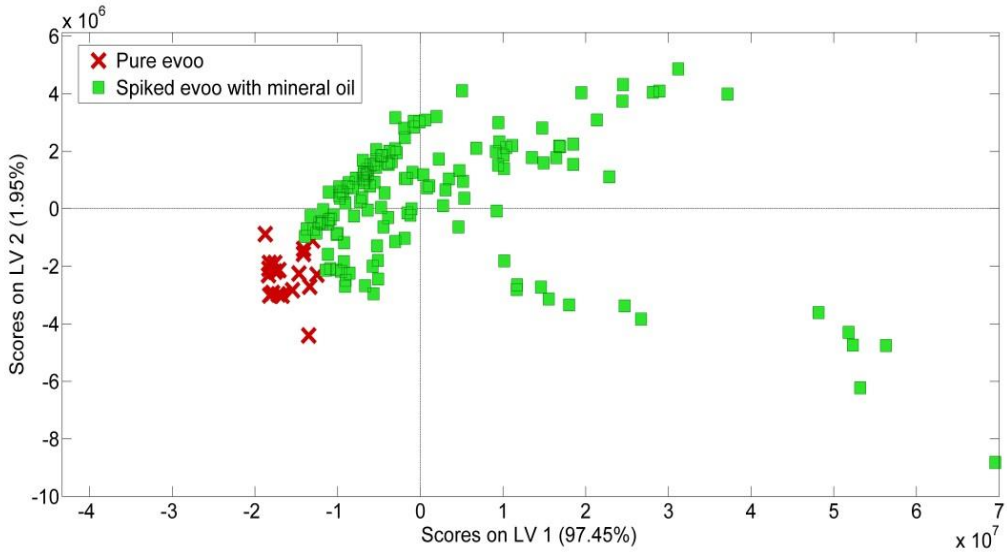

Figure 4.18: Score plot of first (LV 1) and second (LV 2) latent variables for the discrimination of pure olive oil (n = 23) and contaminated olive oil with mineral oil products (n = 144) from PLS-DA model of fluorescence data for excitation wavelength at 340 nm

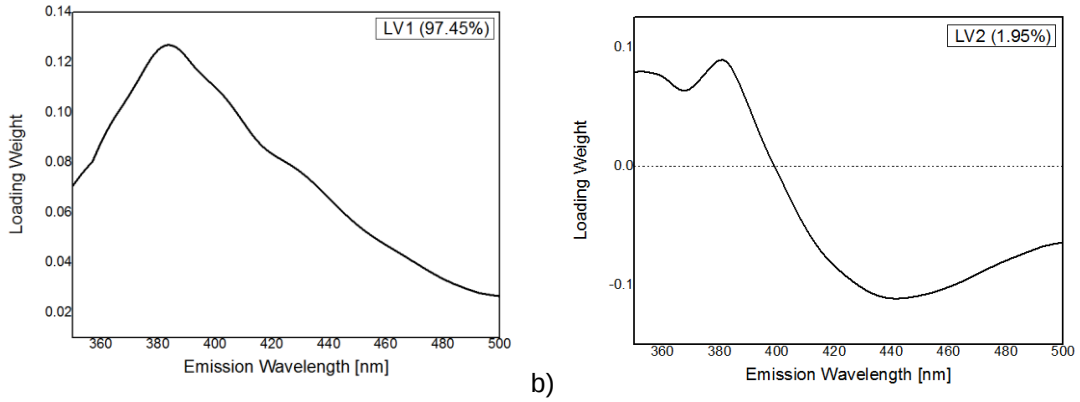

a) b)

Figure 4.19: Loading plot of LV 1 and LV 2 latent variables for the discrimination of pure and contaminated olive oil with mineral oil products from the PLS-DA model of fluorescence data from excitation wavelength at 340 nm

For the illustration of four different categories that indicate the companies of mineral oils contamination and pure EVOO, the methodology of Partial Least Squares Discriminant Analysis (PLS-DA) was employed. The smoothing and mean center were used to pre-process fluorescence data from emission spectrum measurements with excitation wavelength at 340 nm. **Table 4.8** provides an overview of the classification outcomes from PLS-DA, presenting predictive accuracy for the categories of pure and contaminated EVOO with minerals from Companies A, B, and C. The model demonstrated remarkable accuracy in discerning pure EVOO samples, achieving a 100% correct classification rate. However, Company C presents the highest classification rate at 93.5% of the other two spiked EVOO categories, with mineral oils originating from different companies. **Figure 4.20** shows the score plot of the PLS-DA model, illustrating the separation of pure EVOO from contaminated samples originating from other companies. It is observed that the first latent variable (LV 1)

played an essential role in achieving the discrimination between pure and contaminated EVOO, capturing 97.48% of the spectrum data. Additionally, the second latent variable, which captures 1.77% of the data, showcases the discrimination of contaminated olive oil with mineral oil products across the three companies.

Figure 4.21 presents the loading plot of LV 1 and LV 2, providing insight into the regions contributing significantly to the discrimination. In the discrimination between pure and contaminated EVOO with mineral oils, the loading plot of the first latent variable exhibits the emission wavelength at 385 nm as a region with high weight on distribution. On the other hand, the loading plot of the second latent variable (LV2) reveals the most significant contributors to the discrimination of contamination originating from distinct companies. This loading plot emphasizes the crucial role of specific wavelengths, particularly the emission wavelengths at around 365 nm and 440 nm.

Table 4.8: PLS-DA discriminant analysis classification of samples into pure EVOO and EVOO contaminated with mineral oil products from the different companies based on fluorescence spectroscopic data from excitation wavelength at 340 nm

	Pure EVOO	Spiked EVOO with mineral oil from Company A	Spiked EVOO with mineral oil from Company B	Spiked EVOO with mineral oil from Company C
Predicted as pure EVOO	23	9	7	2
Predicted as spiked EVOO with mineral oil from company A	0	27	11	0
Predicted as spiked EVOO with mineral oil from Company B	0	0	31	1
Predicted as spiked EVOO with mineral oil from Company C	0	0	13	43
Correct classification (%)	100%	75%	50%	93.5%

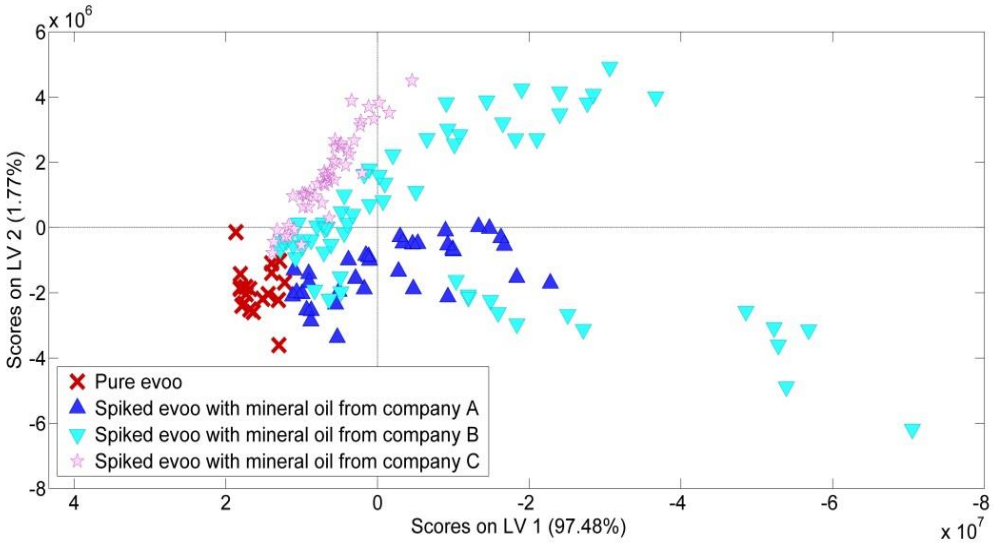

Figure 4.20: Score plot of first (LV 1) and second (LV 2) latent variables for the discrimination of pure olive oil (n = 23) and contaminated olive oil with mineral oil products from the different companies (Company A n = 36, Company B n = 62, Company C n = 46) from PLS-DA model of fluorescence data from excitation wavelength at 340 nm

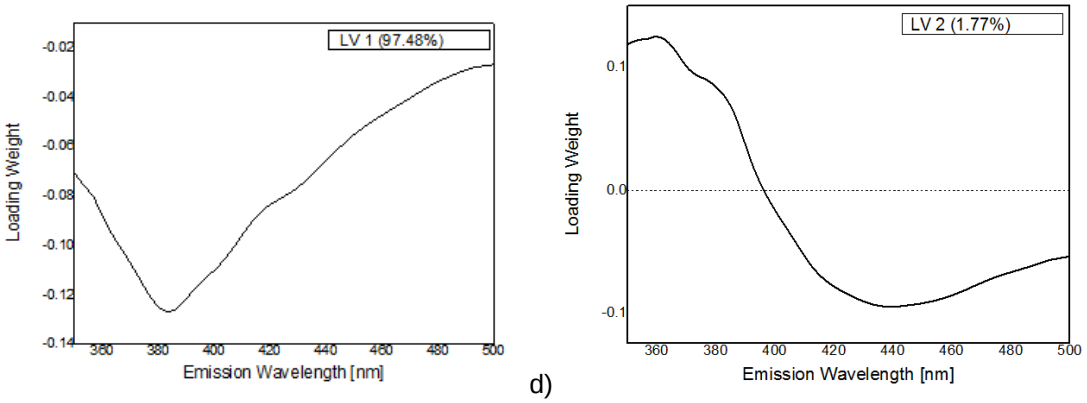

c) d)

Figure 4.21: Loading plot of LV 1 and LV 2 latent variables for the discrimination of pure and contaminated olive oil with mineral oil products from different companies from the OPLS-DA model of fluorescence data from excitation wavelength at 340 nm

Emission spectrum with Excitation Wavelength at 360nm

To classify EVOO from spiked EVOO with mineral oils, fluorescence data from the emission fluorescence measurements in regions between 370 nm and 500 nm with constant excitation wavelength at 360 nm were analyzed with partial least square (PLS-DA). Those results are represented in **Table 4.9** with the smoothing, SNV, and mean center used to pre-process data. According to the table, the model achieved a 100% correct classification for pure EVOO samples and a 95.1% correct classification for contaminated EVOO, with only 7 misclassified samples out of 144 spiked EVOO samples. The score plot in **Figure 4.22** visualizes the discrimination between pure EVOO and contaminated samples. The first latent variable corresponds to 61.86% of the spectrum data, which plays a significant role in this discrimination. **Figure 4.23** depicts the loading plots of the first and second latent variables, and it is observed that

the excitation wavelengths that contribute the most to the correct classification are 380 and 420 nm.

Table 4.9: PLS-DA discriminant analysis classification of samples into pure EVOO and EVOO contaminated with mineral oil products based on fluorescence spectroscopic data from excitation wavelength at 360 nm

	Pure EVOO	Spiked EVOO with mineral oil
Predicted as pure EVOO	23	7
Predicted as spiked EVOO with mineral oil	0	137
Correct classification (%)	100%	95.1%

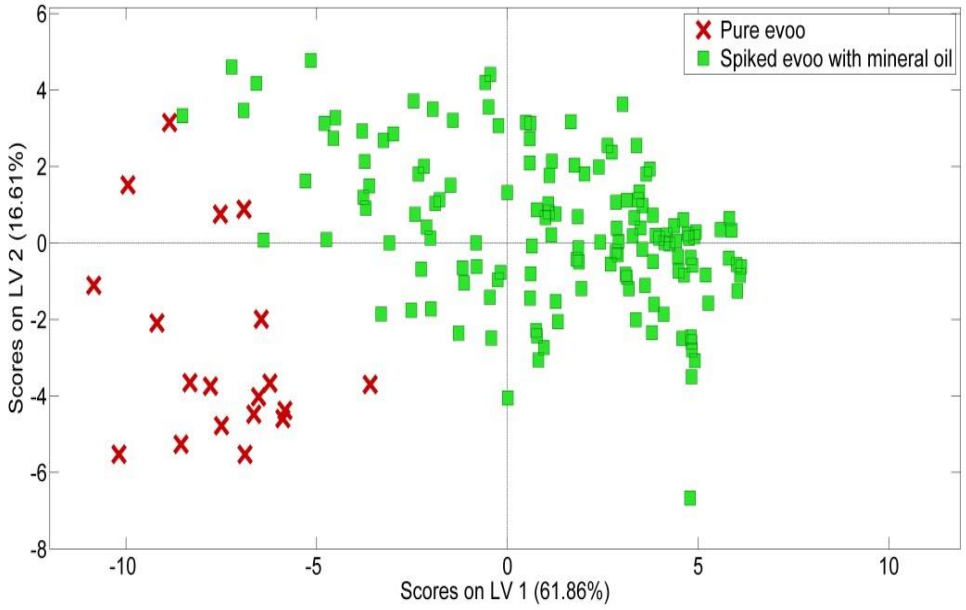

Figure 4.22: Score plot of first (LV 1) and second (LV 2) latent variables for the discrimination of pure olive oil (n = 23) and contaminated olive oil with mineral oil products (n = 144) from PLS-DA model of fluorescence data for excitation wavelength at 360 nm

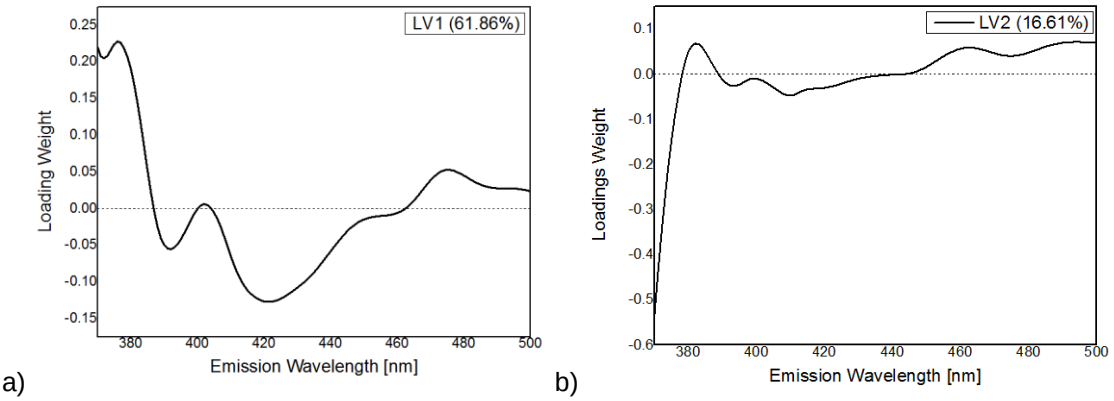

a) b)

Figure 4.23: Loading plot of LV 1 and LV 2 latent variables for the discrimination of pure and contaminated olive oil with mineral oil products from the PLS-DA model of fluorescence data from excitation wavelength at 360 nm

In the visualization of the separation of three different companies associated with mineral oil contamination for the fluorescence data from excitation wavelength at 360 nm, the methodology of Partial Least Squares Discriminant Analysis (PLS-DA) was employed, with the use of derivative, SNV, and mean center as pre-processing of data. Therefore, **Table 4.10** provides an overview of the classification outcomes from PLS-DA, presenting predictive accuracy for the categories of pure and spiked EVOO with minerals from Companies A, B, and C.

The model demonstrated a 91.3% correct classification rate in distinguishing pure EVOO samples, and the better classification of contaminated samples corresponds to Company A, with a rate of 94.4%. **Figure 4.24** presents the score plot of the PLS-DA model, illustrating the separation of pure EVOO from contaminated samples originating from different companies. It is observed that LV 1 played an important role in achieving the discrimination between pure and contaminated EVOO, capturing 61.58% of the spectrum data. Additionally, the second latent variable captures 11.09% of the data, contributing to the discrimination of contaminated olive oil with mineral oil products across the three companies.

Figure 4.25 presents the loading plot of LV 1 and LV 2, providing insight into the regions of wavelengths contributing significantly to the discrimination. This figure shows that combining those two latent variables contributes to the discrimination between pure and spiked EVOO with minerals from different companies. Specifically, LV 1 indicates the emission wavelengths at 415 nm as the most critical regions for the discrimination, and it helps mainly to separate the pure EVOO from spiked. On the other hand, LV 2 shows large degrees of significance in the emission wavelength at approximately 370 and 390 nm. Also, it appears to have smaller contributions at 430 and 480 nm of emission wavelength.

Table 4.10: PLS-DA discriminant analysis classification of samples into pure EVOO and EVOO contaminated with mineral oil products from the different companies based on fluorescence spectroscopic data from excitation wavelength at 360 nm

	Pure EVOO	Spiked EVOO with mineral oil from Company A	Spiked EVOO with mineral oil from Company B	Spiked EVOO with mineral oil from Company C
Predicted as pure EVOO	22	0	0	1
Predicted as spiked EVOO with mineral oil from Company A	0	34	1	0
Predicted as spiked EVOO with mineral oil from Company B	1	2	52	2
Predicted as spiked EVOO with mineral oil from Company C	0	0	9	43
Correct classification (%)	95.65%	94.4%	83,9%	93.5%

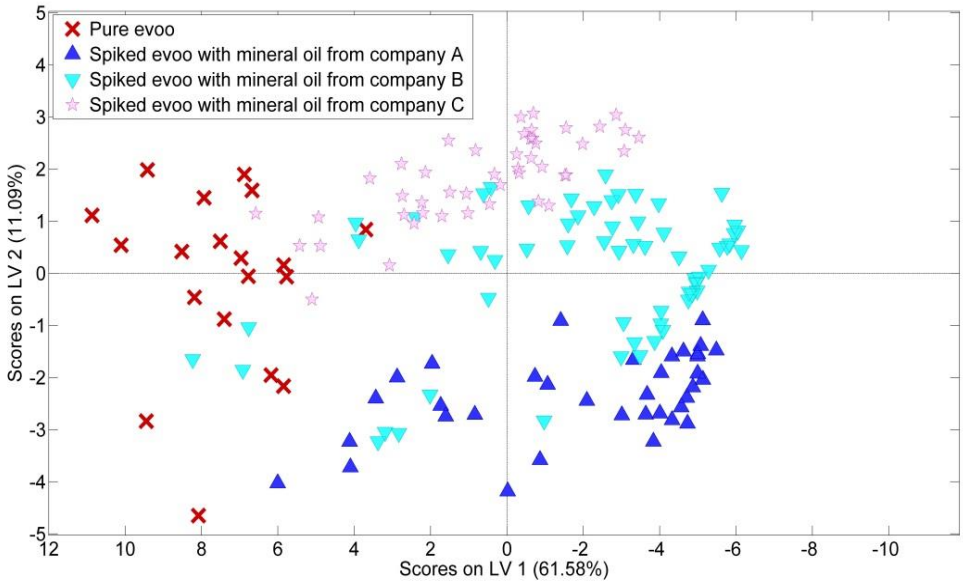

Figure 4.24: Score plot of first (LV 1) and second (LV 2) latent variables for the discrimination of pure olive oil (n = 23) and contaminated olive oil with mineral oil products from the different companies (Company A n = 36, Company B n = 62, Company C n = 46) from PLS-DA model of fluorescence data from excitation wavelength at 360 nm

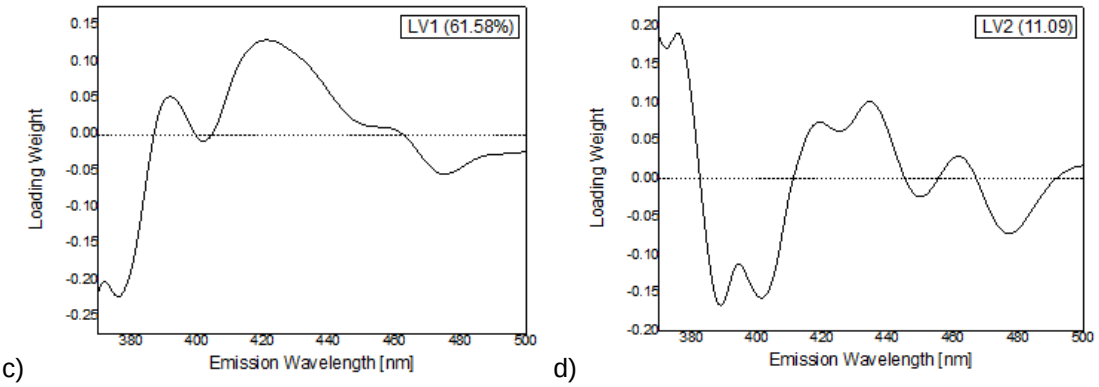

c) d)

Figure 4.25: Loading plot of LV 1 and LV 2 latent variables for the discrimination of pure and contaminated olive oil with mineral oil products from different companies from the OPLS-DA model of fluorescence data from excitation wavelength at 360 nm

Emission Spectrum with Excitation Wavelength at 380nm

For the classification of EVOO from spiked EVOO with mineral oils, fluorescence data from the emission fluorescence measurements in regions between 390 nm and 500 nm with constant excitation wavelength at 380 nm were analyzed with the application of orthogonal partial least square (OPLS-DA). Those results are represented in **Table 4.11** with the derivative, SNV, and mean center used for data pre-processing. According to the table, the model reached the proportion of 95.24% achievement to correct classification for pure EVOO samples and a 94.24% correct classification for contaminated EVOO with only seven misclassified samples out of a total of 144 spiked EVOO samples. The score plot in **Figure 4.26** depicts the discrimination between pure EVOO and contaminated samples. The first latent variable corresponds to 37.95% of the spectrum data, which plays a significant role in this discrimination. **Figure 4.27** illustrates the loading plots of the first and second latent variables, and it is observed that the excitation wavelengths at 400 and 440 nm contribute the most to the correct classification.

Table 4.11: OPLS-DA discriminant analysis classification of samples into pure EVOO and EVOO contaminated with mineral oil products based on fluorescence spectroscopic data from excitation wavelength at 380 nm

	Pure EVOO	Spiked EVOO with mineral oil
Predicted as pure EVOO	20	7
Predicted as spiked EVOO with mineral oil	1	119
Correct classification (%)	95.24%	94.44%

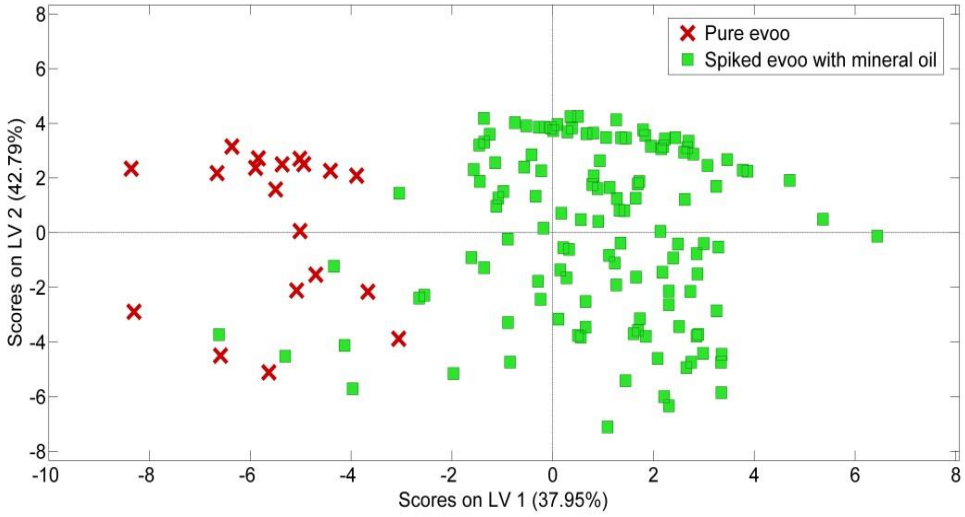

Figure 4.26: Score plot of first (LV 1) and second (LV 2) latent variables for the discrimination of pure olive oil (n = 21) and contaminated olive oil with mineral oil products (n = 126) from OPLS-DA model of fluorescence data for excitation wavelength at 380 nm

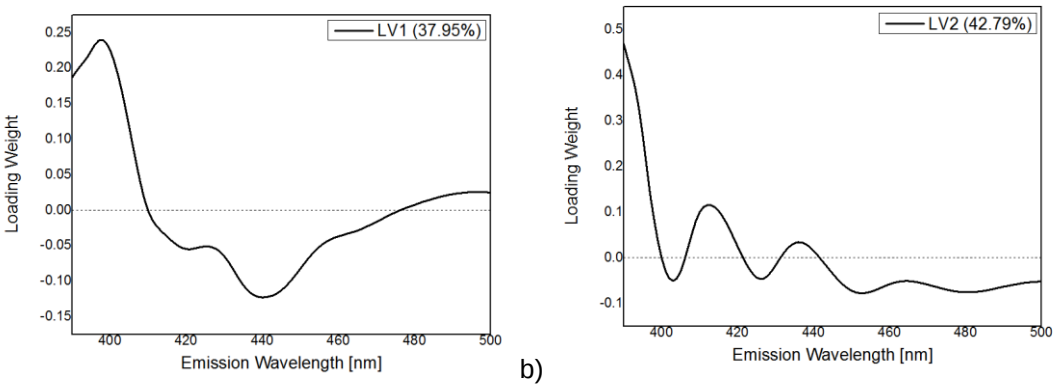

a) b)

Figure 4.27: Loading plot of LV 1 and LV 2 latent variables for the discrimination of pure and contaminated olive oil with mineral oil products from the OPLS-DA model of fluorescence data from excitation wavelength at 380 nm

PLS-DA methodology was employed to observe the separation of three companies associated with mineral oil contamination for the fluorescence data from excitation wavelength at 360 nm, using derivative, SNV, and mean center as data pre-processing. Therefore, **Table 4.12** provides an overview of the classification outcomes from PLS-DA, presenting predictive accuracy for the categories of pure and spiked EVOO with minerals from Companies A, B, and C.

The model demonstrated a 90.48% correct classification rate in distinguishing pure EVOO samples, and the better classification of contaminated samples corresponds to Company A, with 100%. **Figure 4.28** presents the score plot of the PLS-DA model, illustrating the separation of pure EVOO from contaminated samples originating from different companies. It is observed that LV 1 played an important role in achieving the discrimination between pure and contaminated EVOO, capturing 65.41% of the spectrum data. Additionally, the second latent variable captures 23.02% of the data, contributing mainly to the discrimination of spiked EVOO with mineral oil from Company A from the three other categories.

Figure 4.29 presents the loading plot of LV 1 and LV 2, providing insight into the regions of wavelengths that contribute significantly to categorizing the data. It specifies that LV 1 indicates the emission wavelengths at approximately 430 nm as the most critical regions for the discrimination, mainly pure from spiked EVOO. On the other hand, LV 2 shows large degrees of significance in the emission wavelength at approximately 390, 410 nm, and 430 nm, acquiring a smaller contribution weight.

Table 4.12: PLS-DA discriminant analysis classification of samples into pure EVOO and EVOO contaminated with mineral oil products from the different companies based on fluorescence spectroscopic data from excitation wavelength at 380 nm

	Pure EVOO	Spiked EVOO with mineral oil from Company A	Spiked EVOO with mineral oil from Company B	Spiked EVOO with mineral oil from Company C
Predicted as pure EVOO	19	0	2	4
Predicted as spiked EVOO with mineral oil from Company A	0	36	0	0
Predicted as spiked EVOO with mineral oil from Company B	2	0	42	1
Predicted as spiked EVOO with mineral oil from Company C	0	0	6	35
Correct classification (%)	90.48%	100%	84%	87.5%

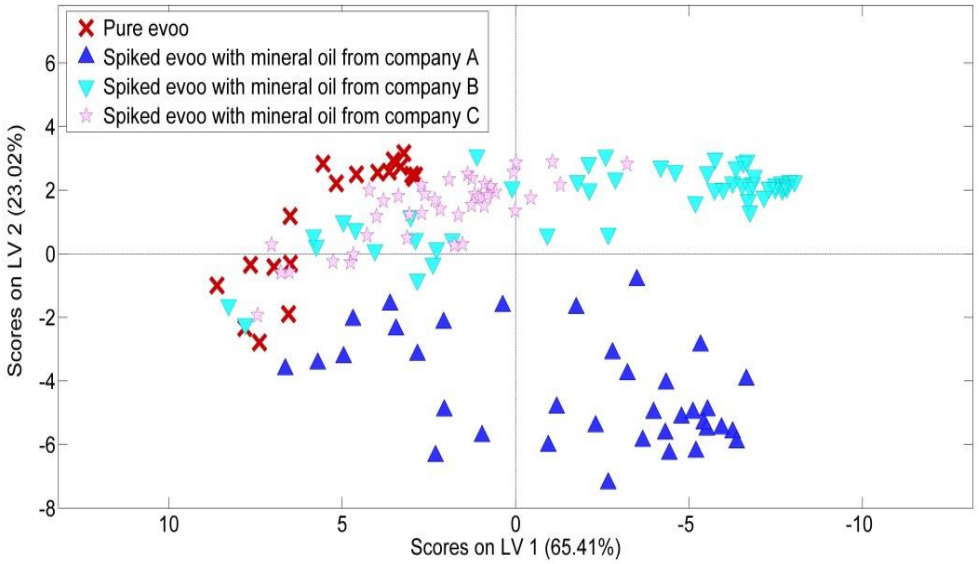

Figure 4.28: Score plot of first (LV 1) and second (LV 2) latent variables for the discrimination of pure olive oil (n = 23) and contaminated olive oil with mineral oil products from the different companies (Company A n = 36, Company B n = 50, Company C n = 40) from PLS-DA model of fluorescence data from excitation wavelength at 380 nm

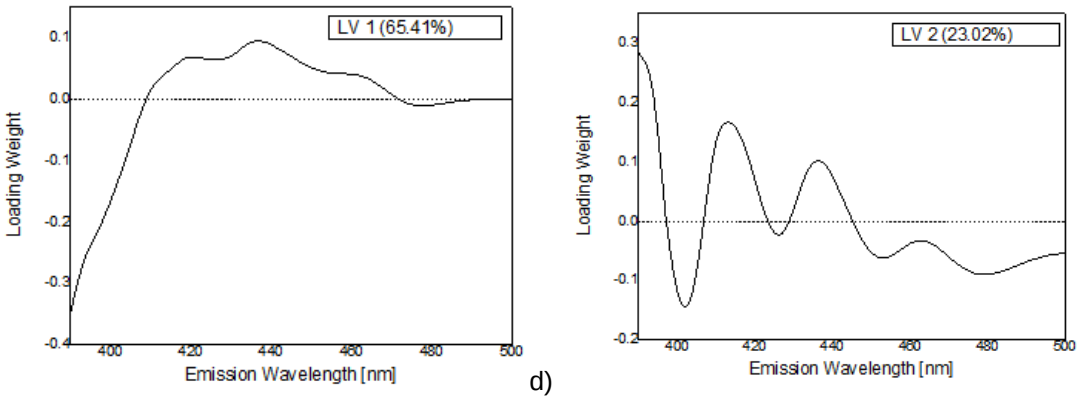

c) d)

Figure 4.29: Loading plots of emission spectra in the range of wavelength at 390nm-500nm: c) Spiked EVOO with mineral oil per company in variable LV1, d) Spiked EVOO with mineral oil per company in variable LV2

Emission Spectrum with Excitation Wavelength at 400nm

Finally, this project studied the classification of EVOO from spiked EVOO with mineral oil using fluorescence data from the emission fluorescence measurements in regions between 410 nm and 500 nm with constant excitation wavelength at 400 nm and analyzed by applying PLS-DA. Those results are represented in **Table 4.13** with the derivative, SNV, and mean center used for data pre-processing. According to the table, the model reached the proportion of 93.75% achievement to correct classification for pure EVOO samples and a 92% correct classification for contaminated EVOO with only four misclassified samples out of a total of 144 spiked EVOO samples. The score plot in **Figure 4.30** depicts the discrimination between pure EVOO and contaminated samples. The first latent variable corresponds to 82.72% of the spectrum data. **Figure 4.31** illustrates the loading plots of the first and second

latent variables, and it is observed that at LV 1, the emission wavelengths at 410 possess a higher loading weight.

In the excitation wavelength at 400 nm, the only samples that presented fluorescence intensity accepted EVOO was the spiked EVOO with mineral oils from Company B. Therefore, there was no reason for the visualization of PLS-DA score plot of discrimination of pure EVOO and contaminated EVOO with mineral oil products from the different companies.

Table 4.13: PLS-DA discriminant analysis classification of samples into pure EVOO and EVOO contaminated with mineral oil products based on fluorescence spectroscopic data from excitation wavelength at 400 nm

	Pure EVOO	Spiked EVOO with mineral oil
Predicted as pure EVOO	15	4
Predicted as spiked EVOO with mineral oil	1	46
Correct classification (%)	93.75%	92%

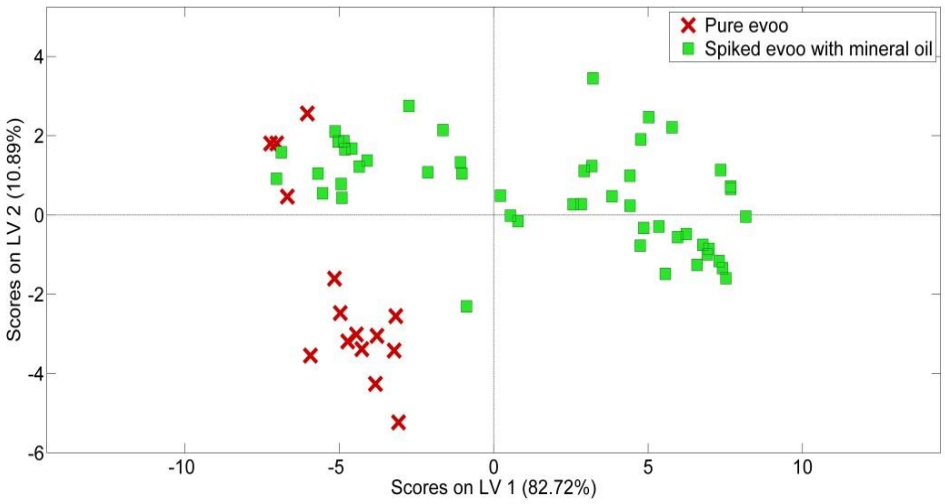

Figure 4.30: Score plot of first (LV 1) and second (LV 2) latent variables for the discrimination of pure olive oil (n = 20) and contaminated olive oil with mineral oil products (n = 50) from PLS-DA model of fluorescence data for excitation wavelength at 400 nm

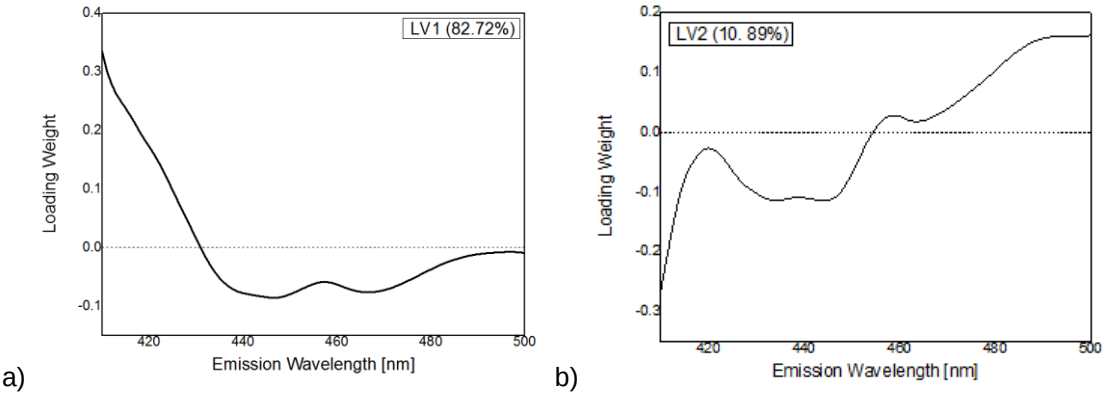

a) b)

Figure 4.31: Loading plot of LV 1 and LV 2 latent variables for the discrimination of pure and contaminated olive oil with mineral oil products from the OPLS-DA model of fluorescence data from excitation wavelength at 400 nm

4.3 Conclusions

In this part of the thesis, an investigation was conducted on extra virgin olive oil (EVOO) contaminated with mineral oils obtained from various companies. The analysis involved using a fluorometer to observe the fluorescence region of the samples. The fluorescence data were exposed to multivariate statistical analysis, specifically Partial Least Squares Discriminant Analysis (PLS-DA) and Orthogonal Partial Least Squares Discriminant Analysis (OPLS-DA). Those methods were employed to categorize the samples into groups based on whether they were pure EVOO or spiked with mineral oils. Additionally, the data was further grouped based on the specific companies from which the mineral oils originated.

The study's findings indicate that in most instances, correct classification between pure EVOO and spiked EVOO was achieved with 100% accuracy using fluorescence data. However, there were certain cases where correct classification dipped below 90%. Those cases come from applying statistical analysis to data obtained at excitation wavelengths of 380 and 400 nm. Therefore, the data analysis by excitation-emission matrices gives better results than the analysis of data from a line graph of the fluorescence spectrum.

The PLS-DA score plot in **Figure 4.6** visually represents the classification, demonstrating a clear distinction between the two groups. The importance of Latent Variable 1 (LV1) in segregating the data into distinct categories was highlighted. Further analysis of **Figure 4.7** revealed that emission at approximately 380 nm and excitation at 350 nm significantly determined LV1. Pure EVOO exhibited lower fluorescence intensity at these wavelengths than mineral oils. As a result, it was suggested that the presence of mineral oils in spiked EVOO could be detected by examining fluorescence around these specific wavelengths. The detection limit was around 60 ppm of mineral oil in EVOO. This concentration corresponds to 15-35% of MOAH, which influences the fluorescence ability of minerals. Thus, the MOAH detected in contaminated EVOO is around 9-21 ppm.

Finally, the fluorescence technique can classify the contaminated EVOO with mineral oil from different companies, as shown in **Figure 4.8**. This result is essential for understanding the various operations that a company follows.

Appendix A of Extra Virgin Olive Oil mixed with adulterant oils

EVOO A with corn oil

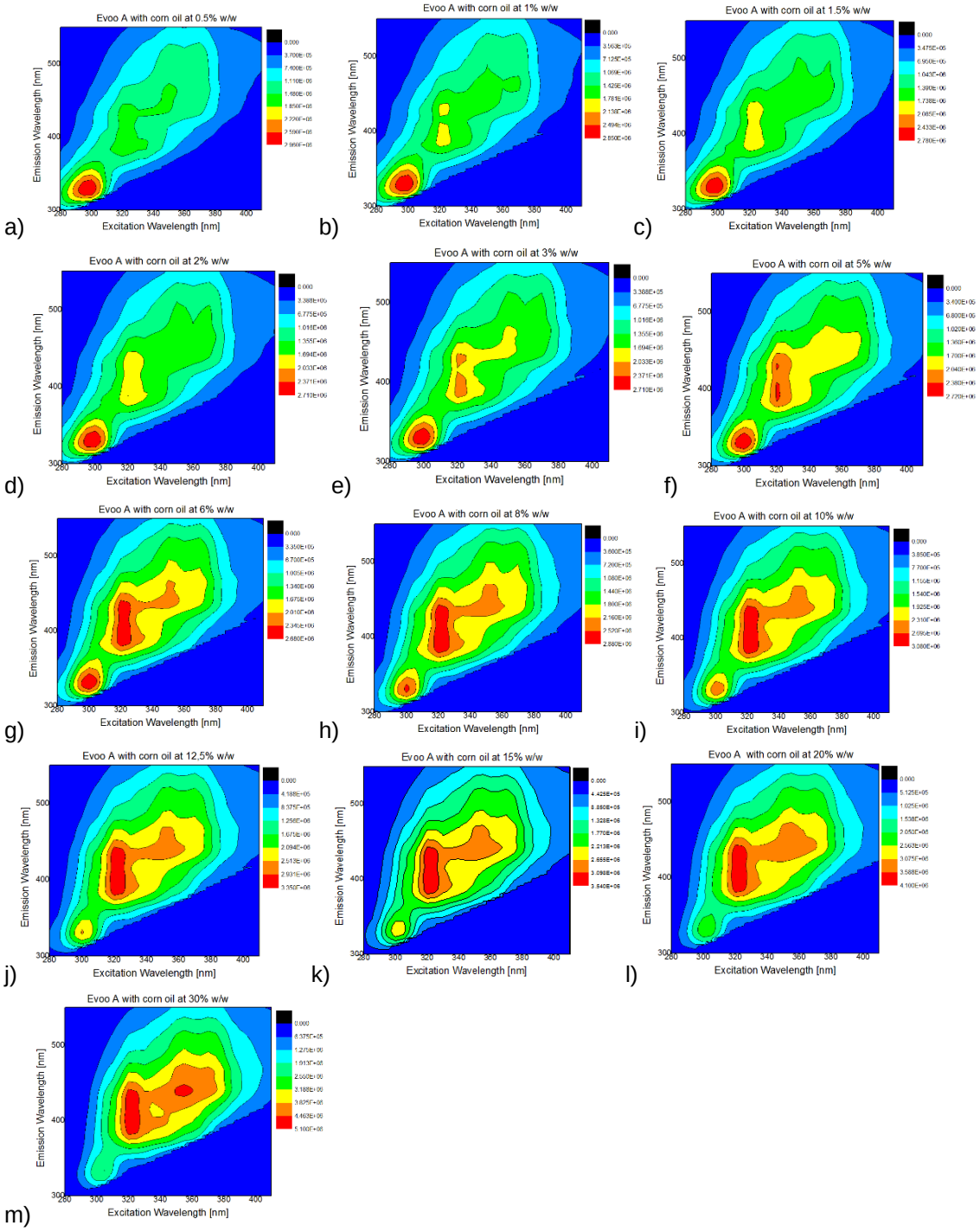

Figure A1. Fluorescence Excitation-Emission Matrices (EEMs) of EVOO A with corn oil in different concentrations at a) 0.5% w/w, b) 1% w/w, c) 1.5% w/w, d) 2% w/w, e) 3% w/w, f) 5% w/w, g) 6% w/w, h) 8% w/w, i) 10% w/w, j) 12.5% w/w, k) 15% w/w, l) 20% w/w, m) 30% w/w

EVOO A with sunflower oil

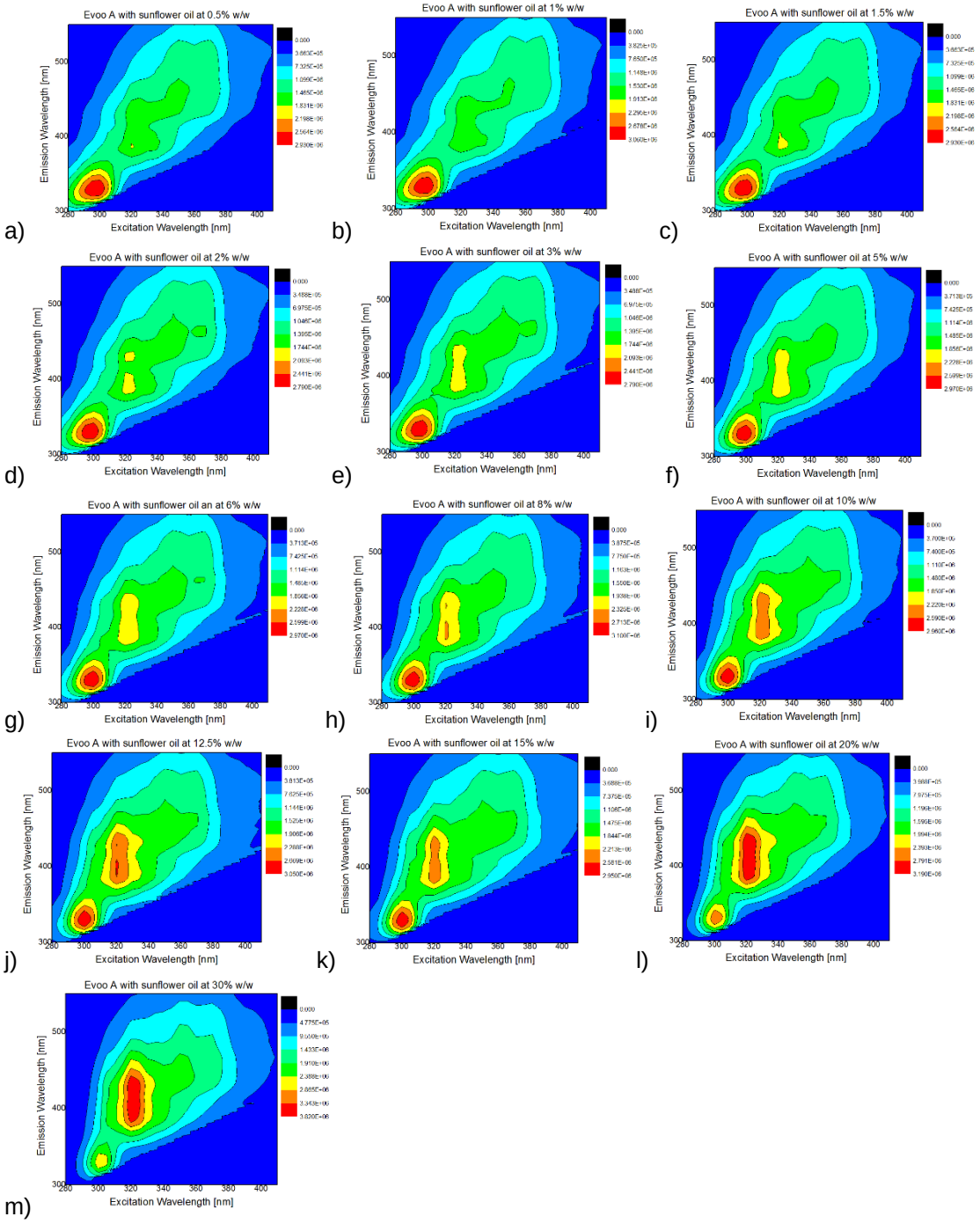

Figure A2. Fluorescence Excitation-Emission Matrices (EEMs) of EVOO with sunflower oil in different concentrations at a) 0.5% w/w, b) 1% w/w, c) 1.5% w/w, d) 2% w/w, e) 3% w/w, f) 5% w/w, g) 6% w/w, h) 8% w/w, i) 10% w/w, j) 12.5% w/w, k) 15% w/w, l) 20% w/w, m) 30% w/w

EVOO A with Pomace oil

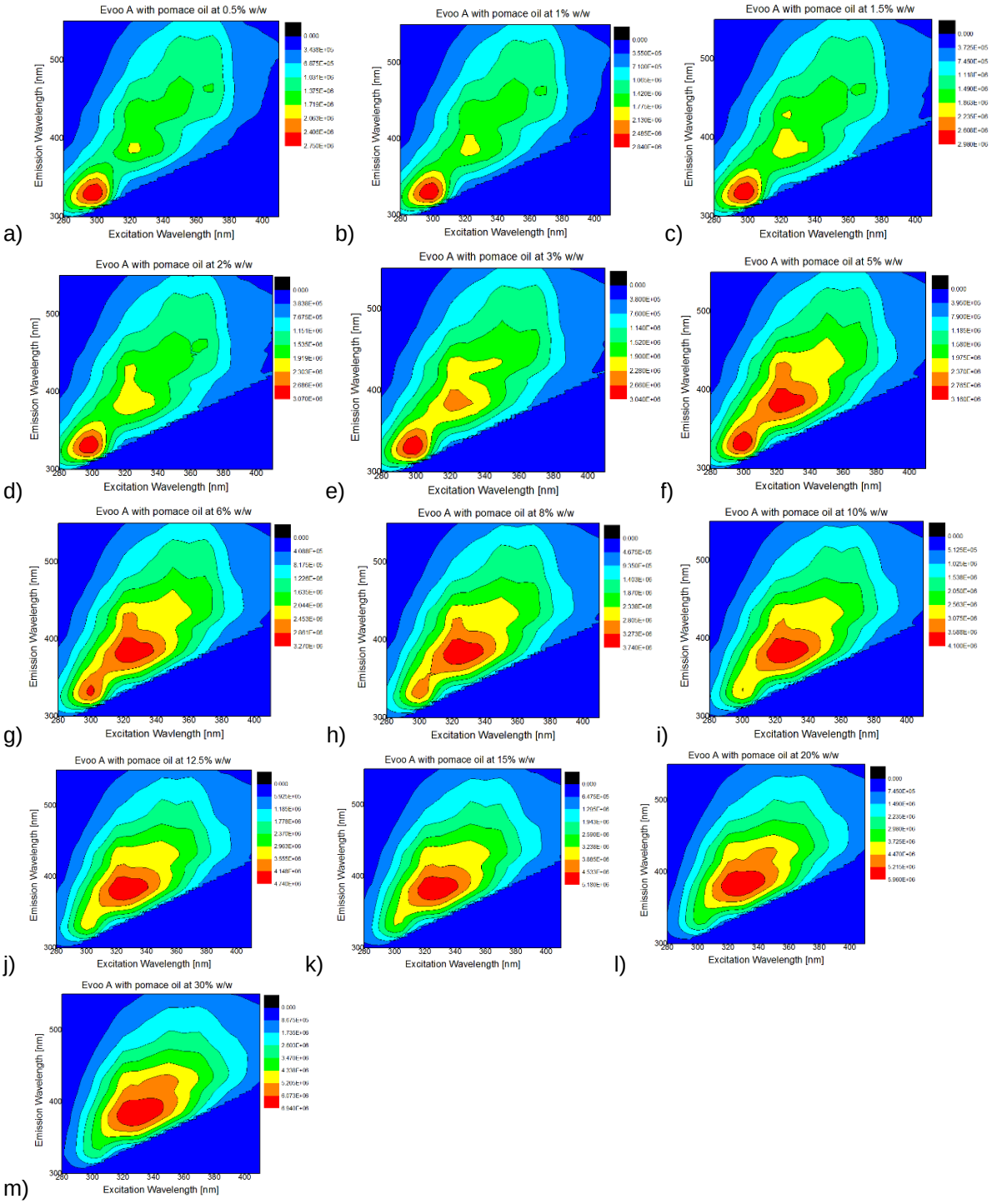

Figure A3. Fluorescence Excitation-Emission Matrices (EEMs) of EVOO A with pomace oil in different concentrations at: a) 0.5% w/w, b) 1% w/w, c) 1.5% w/w, d) 2% w/w, e) 3% w/w, f) 5% w/w, g) 6% w/w, h) 8% w/w, i) 10% w/w, j) 12.5% w/w, k) 15% w/w, l) 20% w/w, m) 30% w/w

EVOO A with soybean oil

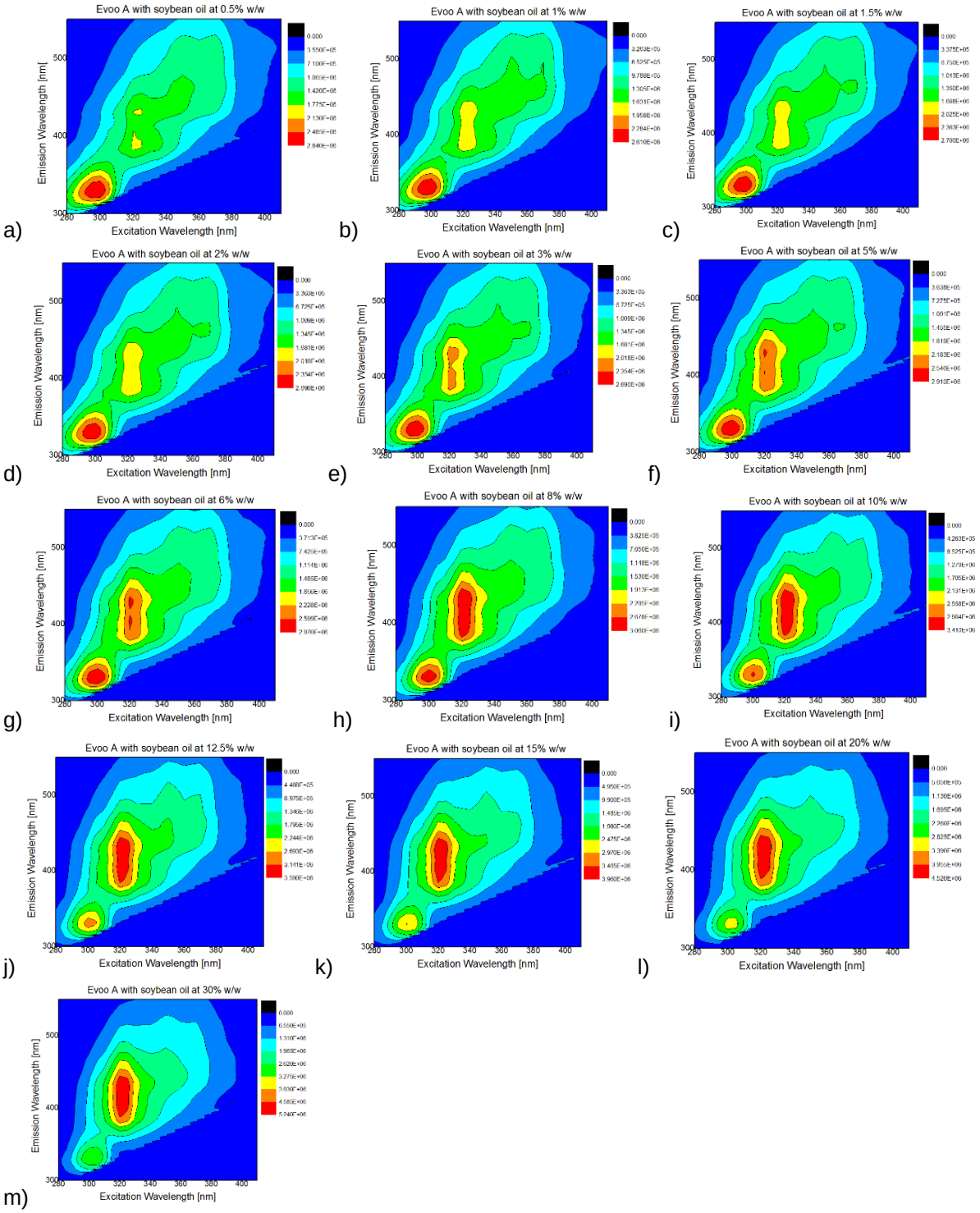

Figure A4. Fluorescence Excitation-Emission Matrices (EEMs) of EVOO A with soybean oil in different concentrations at a) 0.5% w/w, b) 1% w/w, c) 1.5% w/w, d) 2% w/w, e) 3% w/w, f) 5% w/w, g) 6% w/w, h) 8% w/w, i) 10% w/w, j) 12.5% w/w, k) 15% w/w, l) 20% w/w, m) 30% w/w

EVOO B with corn oil

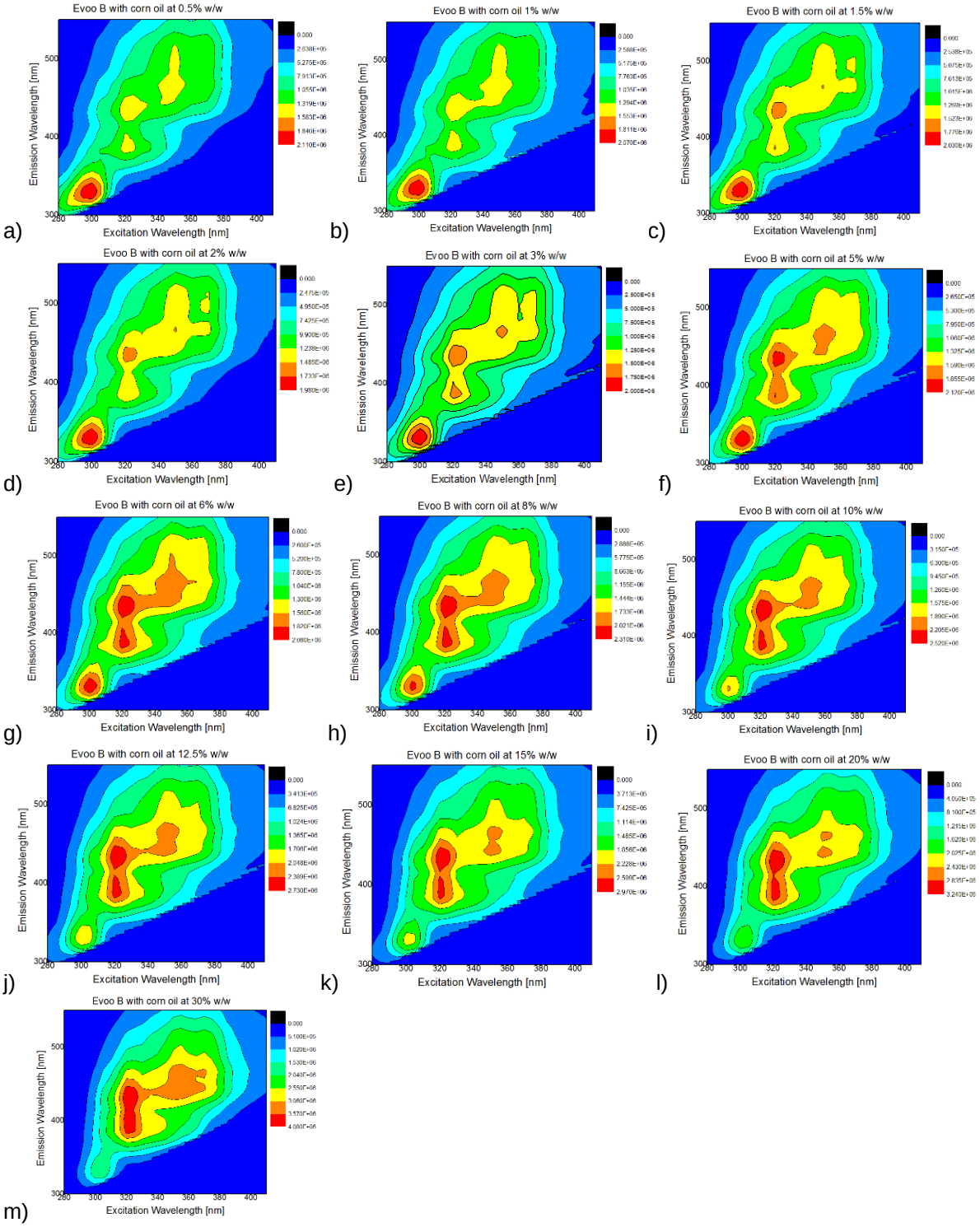

Figure A5. Fluorescence Excitation-Emission Matrices (EEMs) of EVOO B with corn oil in different concentrations at a) 0.5% w/w, b) 1% w/w, c) 1.5% w/w, d) 2% w/w, e) 3% w/w, f) 5% w/w, g) 6% w/w, h) 8% w/w, i) 10% w/w, j) 12.5% w/w, k) 15% w/w, l) 20% w/w, m) 30% w/w

EVOO B with Sunflower oil

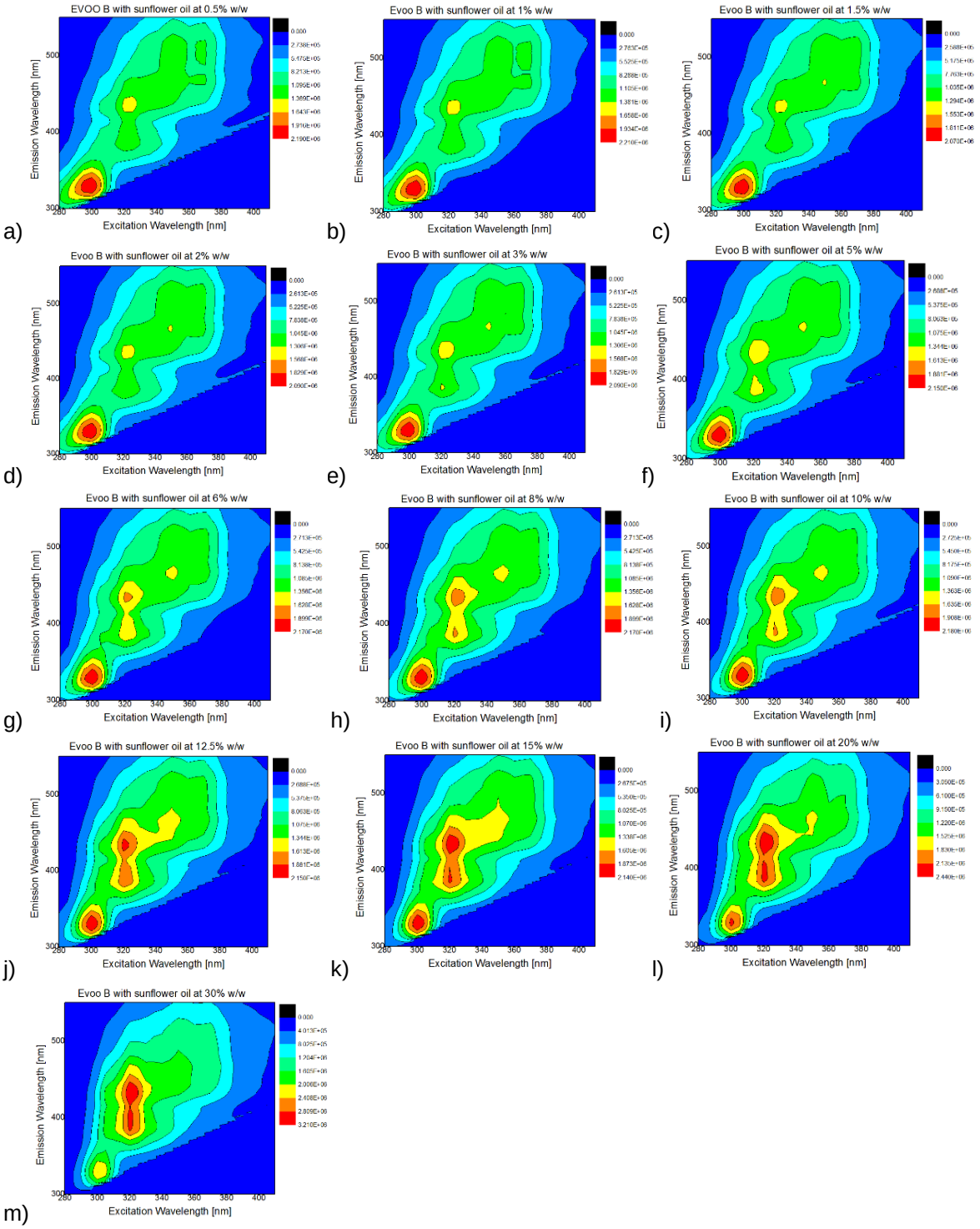

Figure A5. Fluorescence Excitation-Emission Matrices (EEMs) of EVOO B with sunflower oil in different concentrations at a) 0.5% w/w, b) 1% w/w, c) 1.5% w/w, d) 2% w/w, e) 3% w/w, f) 5% w/w, g) 6% w/w, h) 8% w/w, i) 10% w/w, j) 12.5% w/w, k) 15% w/w, l) 20% w/w, m) 30% w/w

EVOO B with pomace oil

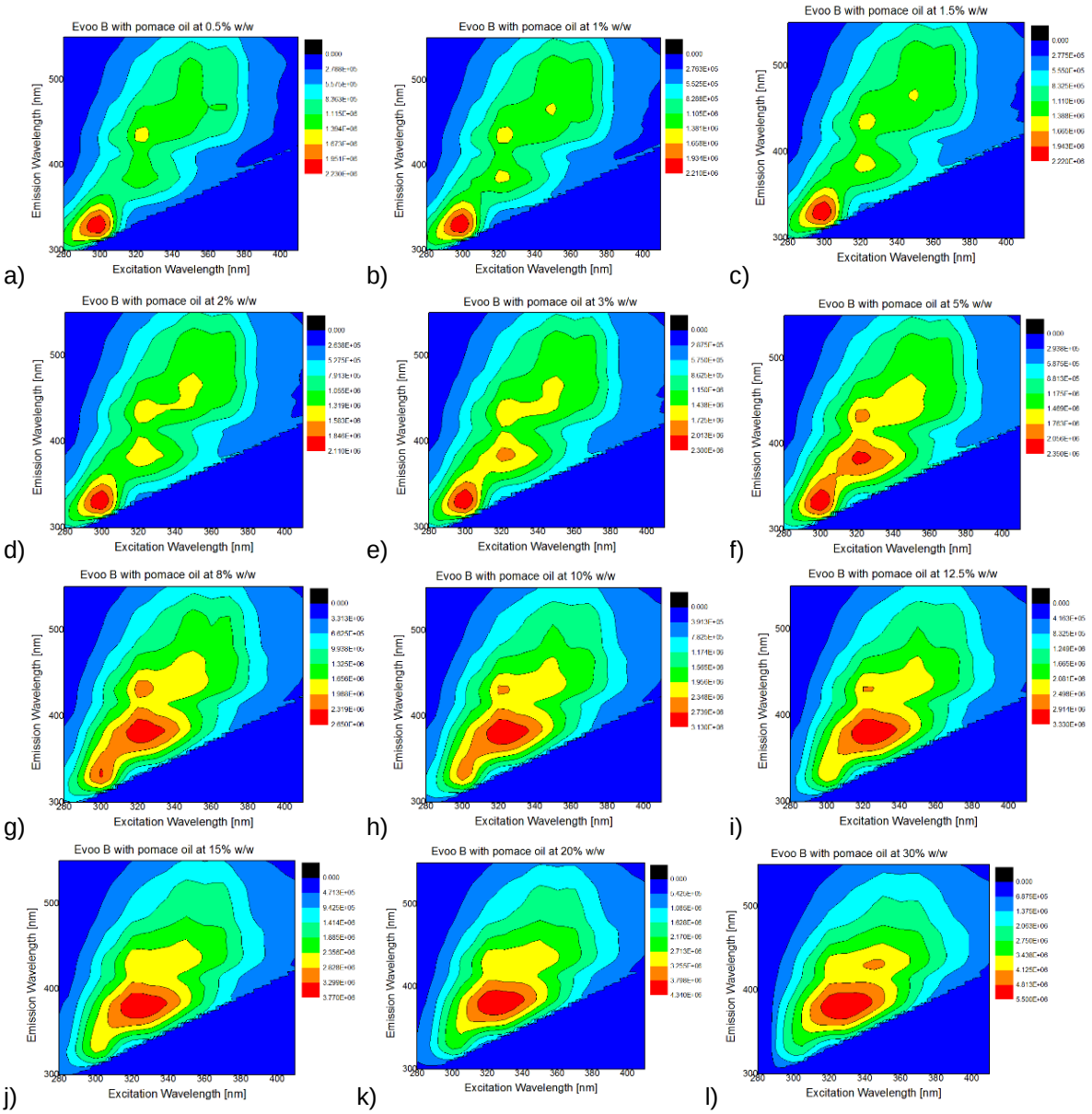

Figure A6. Fluorescence Excitation-Emission Matrices (EEMs) of EVOO B with pomace oil in different concentrations at: a) 0.5% w/w, b) 1% w/w, c) 1.5% w/w, d) 2% w/w, e) 3% w/w, f) 5% w/w, g) 8% w/w, h) 10% w/w, i) 12.5% w/w, j) 15% w/w, l) 20% w/w, l) 30% w/w

EVOO B with soybean oil

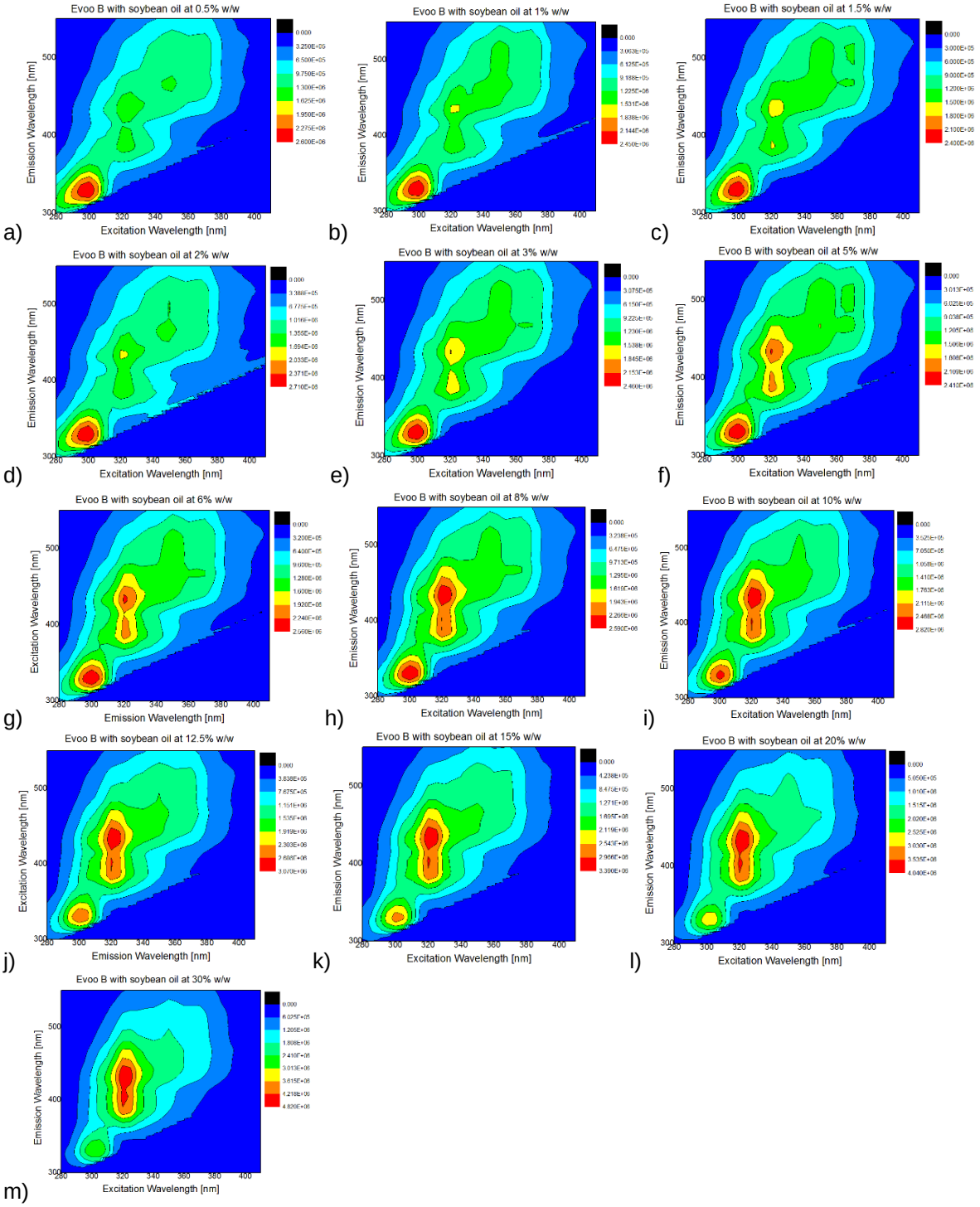

Figure A7. Fluorescence Excitation-Emission Matrices (EEMs) of EVOO B with soybean oil in different concentrations at: a) 0.5% w/w, b) 1% w/w, c) 1.5% w/w, d) 2% w/w, e) 3% w/w, f) 5% w/w, g) 6% w/w, h) 8% w/w, i) 10% w/w, j) 12.5% w/w, k) 15% w/w, l) 20% w/w, m) 30% w/w

EVOO C with Corn oil

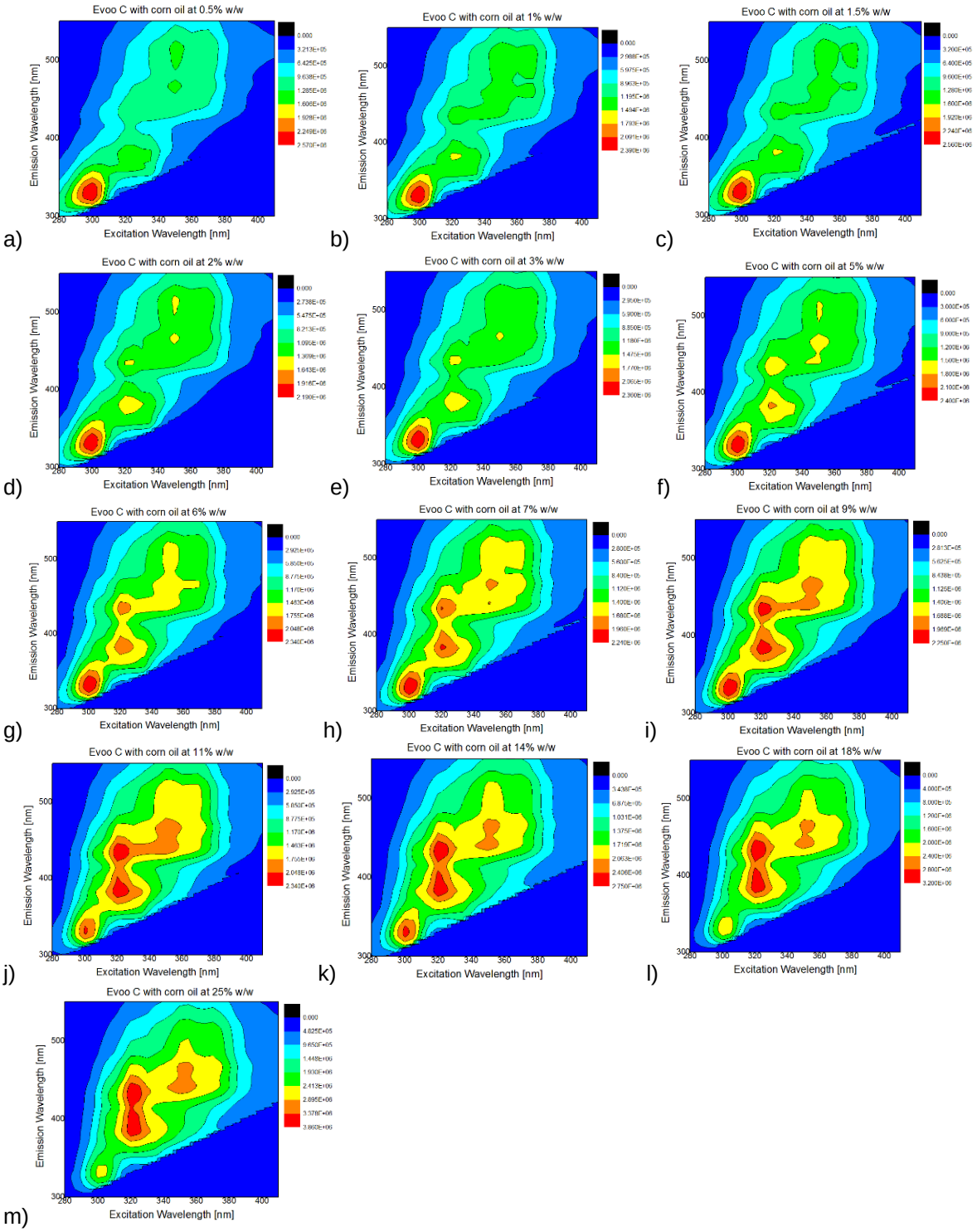

Figure A8. Fluorescence Excitation-Emission Matrices (EEMs) of EVOO C with corn oil in different concentrations at a) 0.5% w/w, b) 1% w/w, c) 1.5% w/w, d) 2% w/w, e) 3% w/w, f) 5% w/w, g) 6% w/w, h) 7% w/w, i) 9% w/w, j) 11% w/w, k) 14% w/w, l) 18% w/w, m) 25% w/w

EVOO C with sunflower

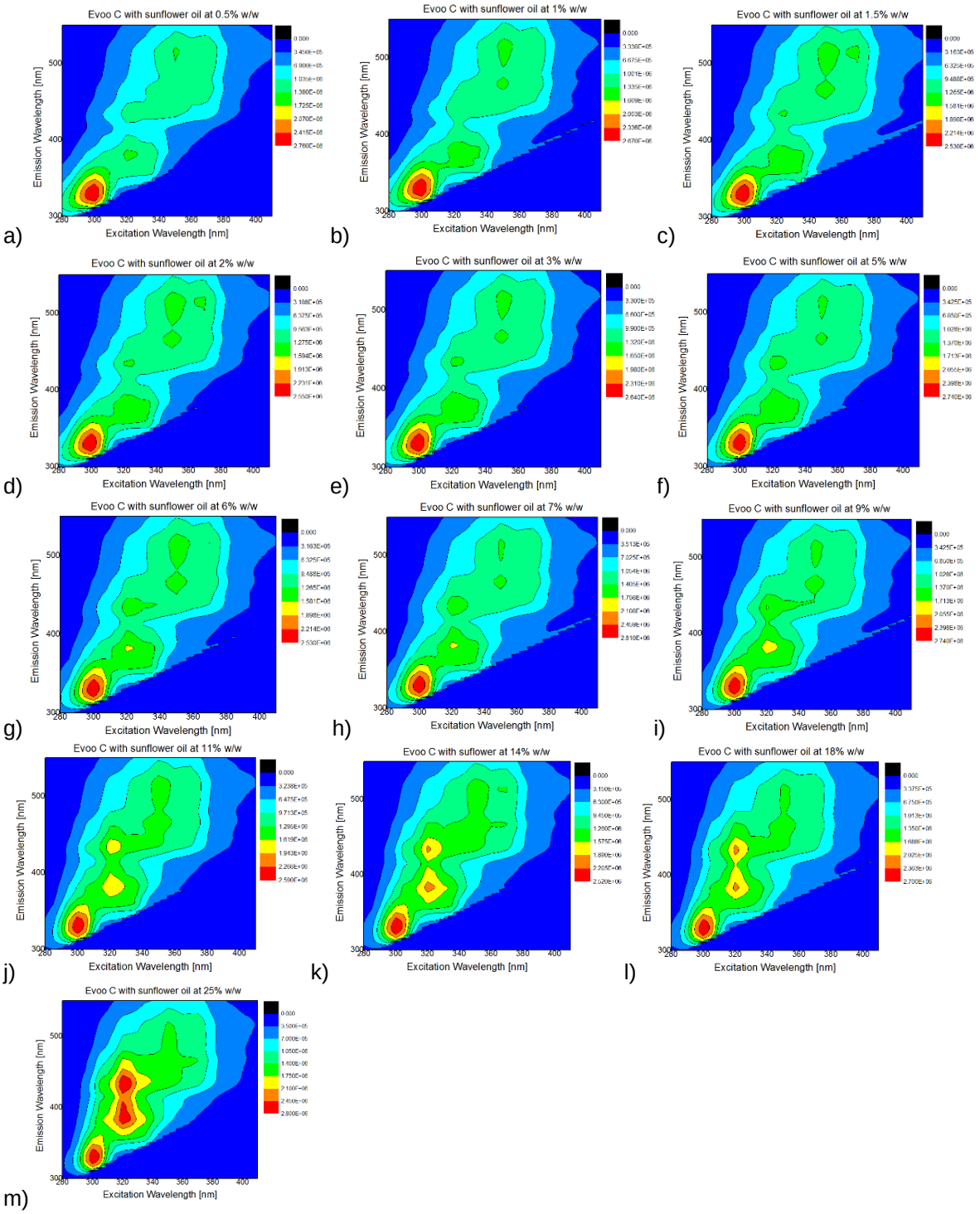

Figure A9. Fluorescence Excitation-Emission Matrices (EEMs) of EVOO C with sunflower oil in different concentrations at a) 0.5% w/w, b) 1% w/w, c) 1.5% w/w, d) 2% w/w, e) 3% w/w, f) 5% w/w, g) 6% w/w, h) 7% w/w, i) 9% w/w, j) 11% w/w, k) 14% w/w, l) 18% w/w, m) 25% w/w

EVOO C with pomace

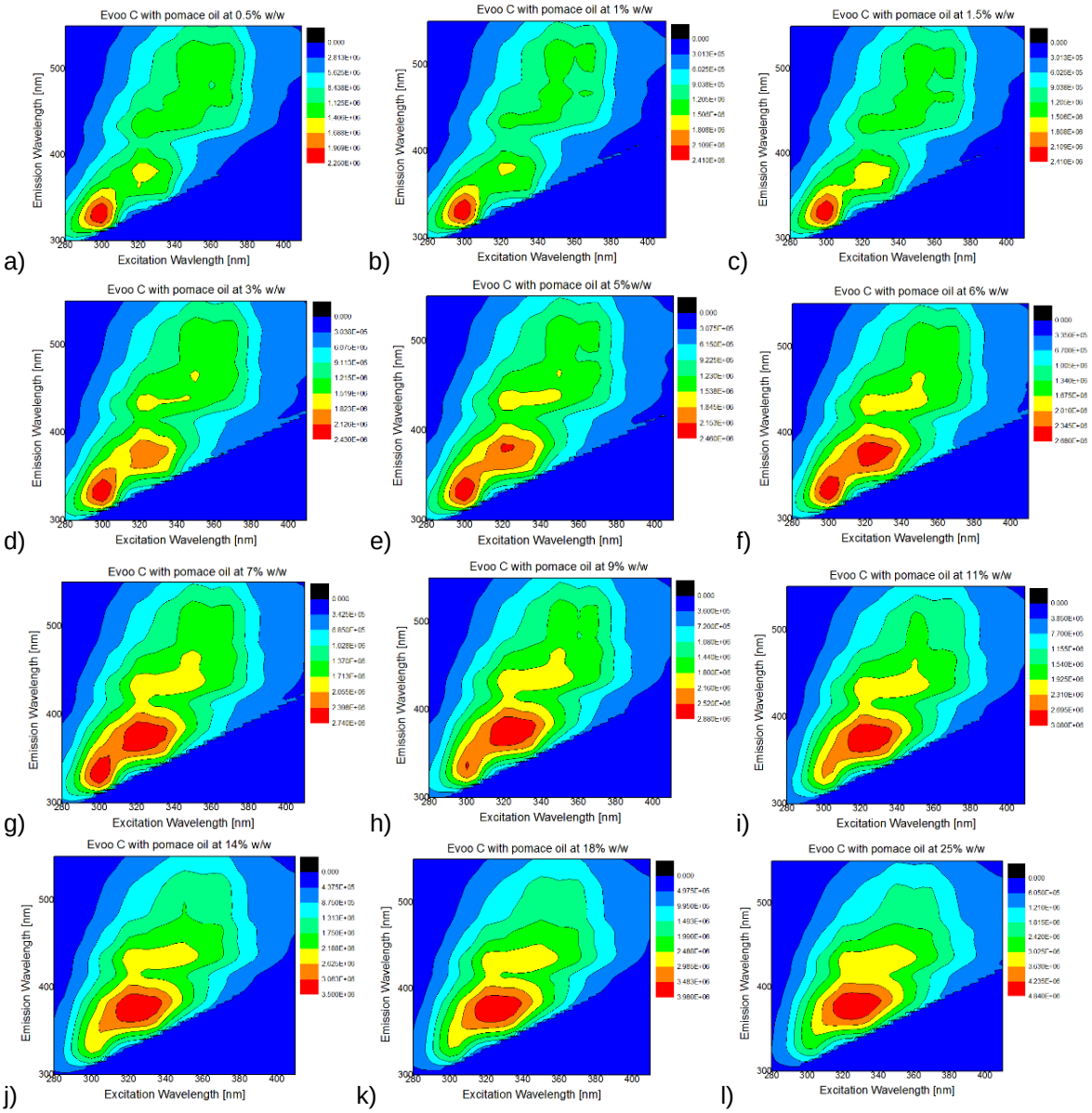

Figure A10. Fluorescence Excitation-Emission Matrices (EEMs) of EVOO C with pomace oil in different concentrations at: a) 0.5% w/w, b) 1% w/w, c) 1.5% w/w, d) 3% w/w, e) 5% w/w, f) 6% w/w, g) 7% w/w, h) 9% w/w, i) 11% w/w, j) 14% w/w, k) 18% w/w, l) 25% w/w

EVOO C with soybean oil

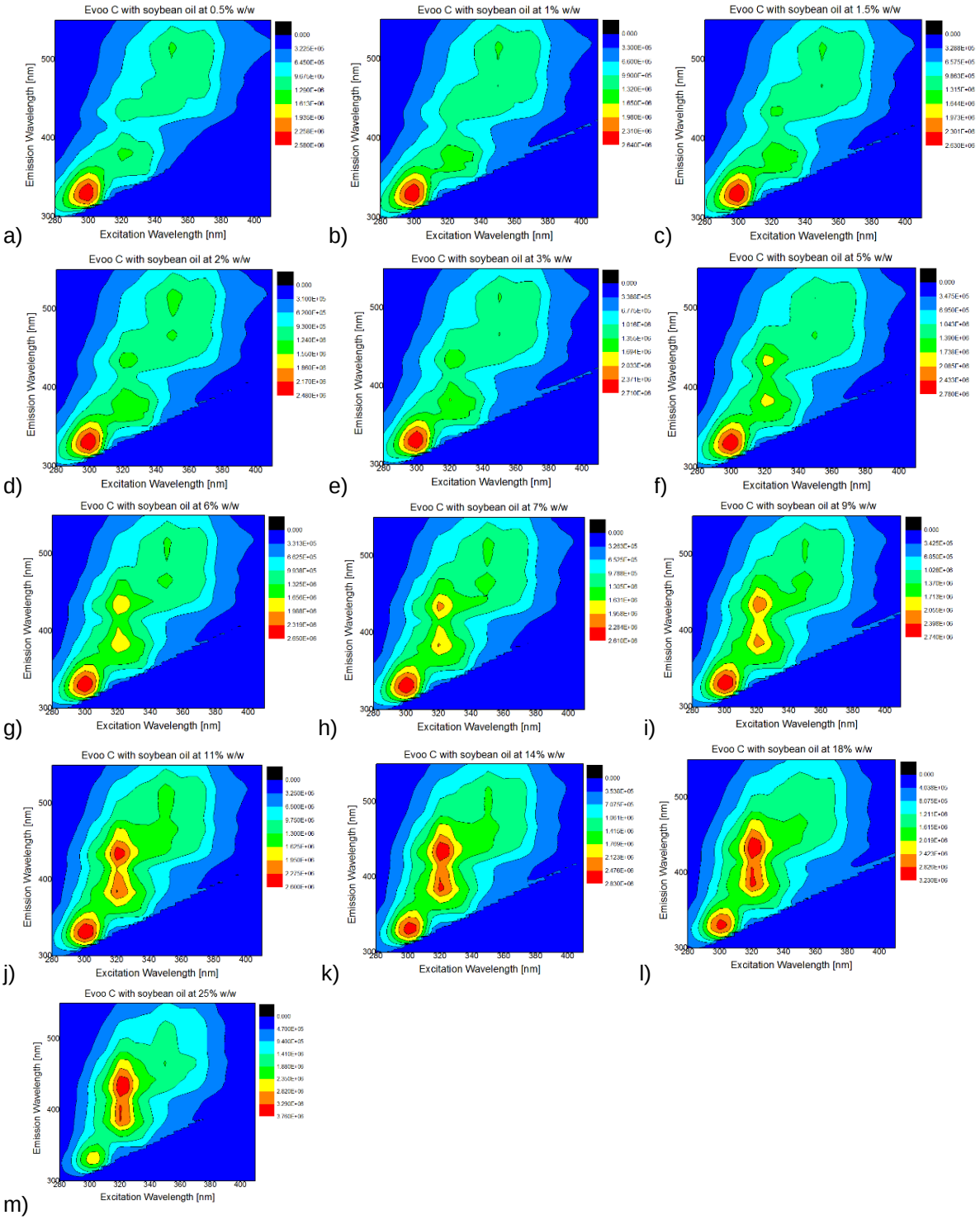

Figure A11. Fluorescence Excitation-Emission Matrices (EEMs) of EVOO D with soybean oil in different concentrations at: a) 0.5% w/w, b) 1% w/w, c) 1.5% w/w, d) 2% w/w, e) 3% w/w, f) 5% w/w, g) 6% w/w, h) 7% w/w, i) 9% w/w, j) 11% w/w, k) 14% w/w, l) 18% w/w, m) 25% w/w

EVOO D with corn oil

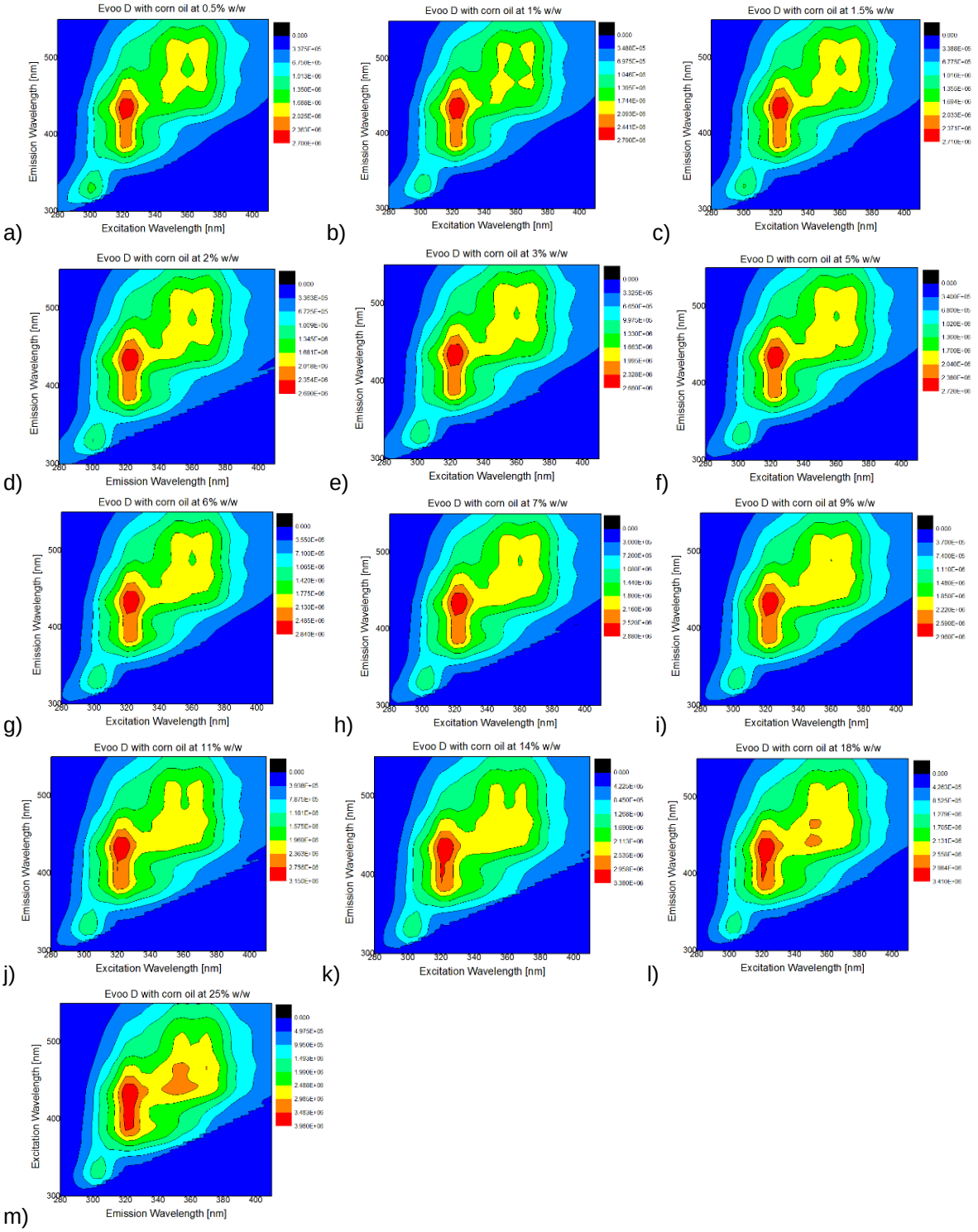

Figure A12. Fluorescence Excitation-Emission Matrices (EEMs) of EVOO D with corn oil in different concentrations at a) 0.5% w/w, b) 1% w/w, c) 1.5% w/w, d) 2% w/w, e) 3% w/w, f) 5% w/w, g) 6% w/w, h) 7% w/w, i) 9% w/w, j) 11% w/w, k) 14% w/w, l) 18% w/w, m) 25% w/w

EVOO D with sunflower oil

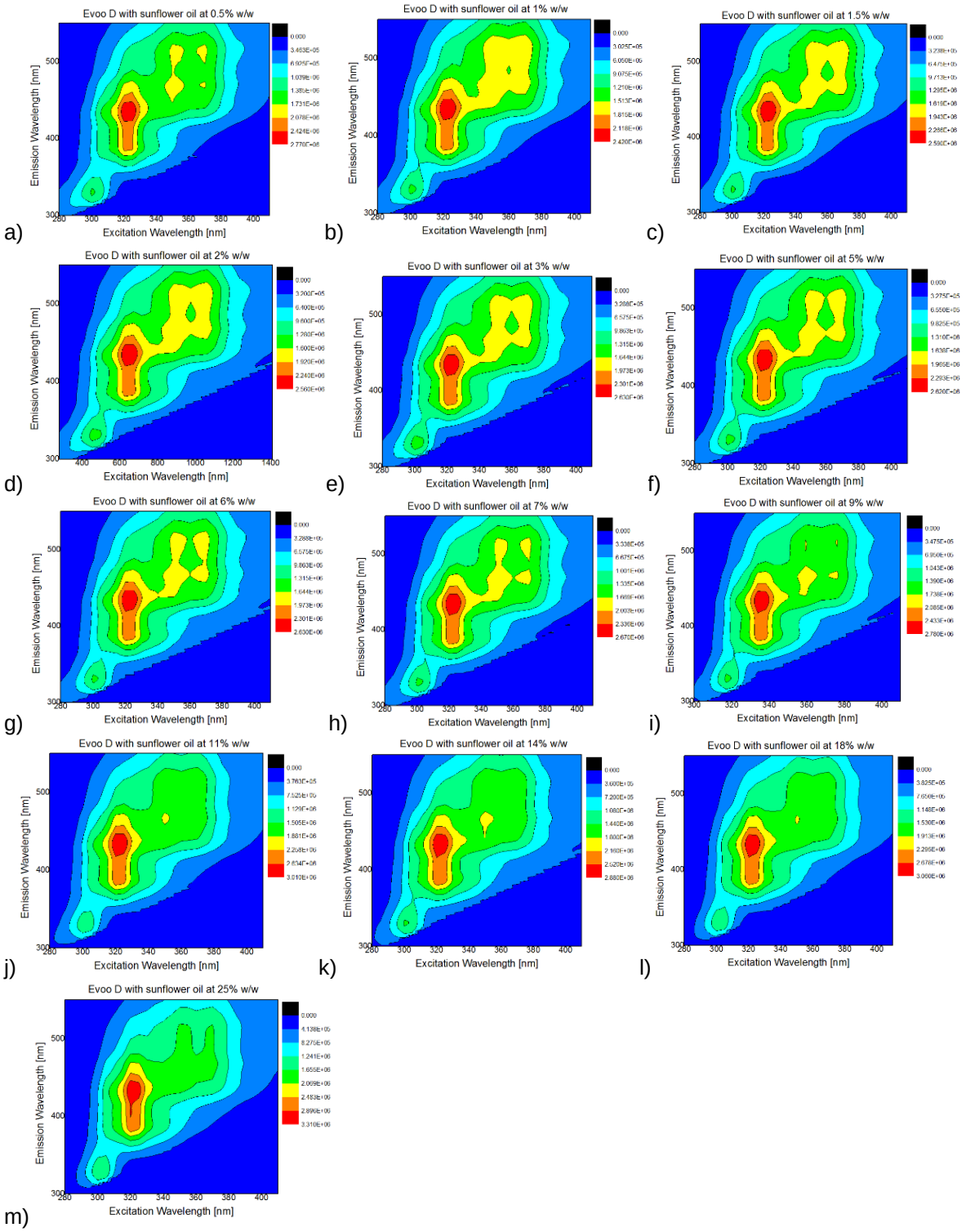

Figure A13. Fluorescence Excitation-Emission Matrices (EEMs) of EVOO D with sunflower oil in different concentrations at a) 0.5% w/w, b) 1% w/w, c) 1.5% w/w, d) 2% w/w, e) 3% w/w, f) 5% w/w, g) 6% w/w, h) 7% w/w, i) 9% w/w, j) 11% w/w, k) 14% w/w, l) 18% w/w, m) 25% w/w

EVOO D pomace oil

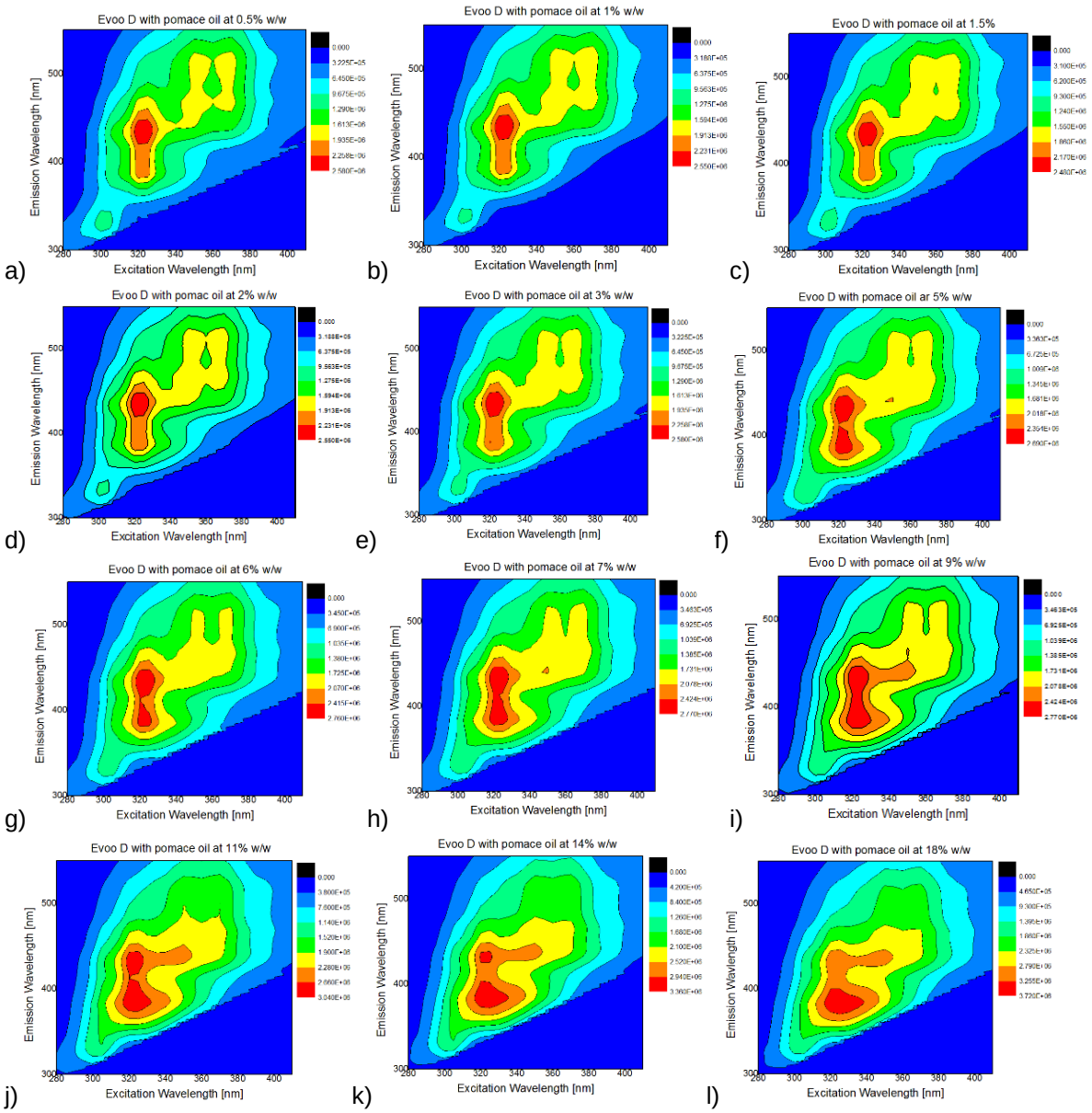

Figure A14. Fluorescence Excitation-Emission Matrices (EEMs) of EVOO D with pomace oil in different concentrations at a) 0.5% w/w, b) 1% w/w, c) 1.5% w/w, d) 2% w/w, e) 3% w/w, f) 5% w/w, g) 6% w/w, h) 7% w/w, i) 9% w/w, j) 11% w/w, k) 14% w/w, l) 18% w/w

EVOO D soybean oil

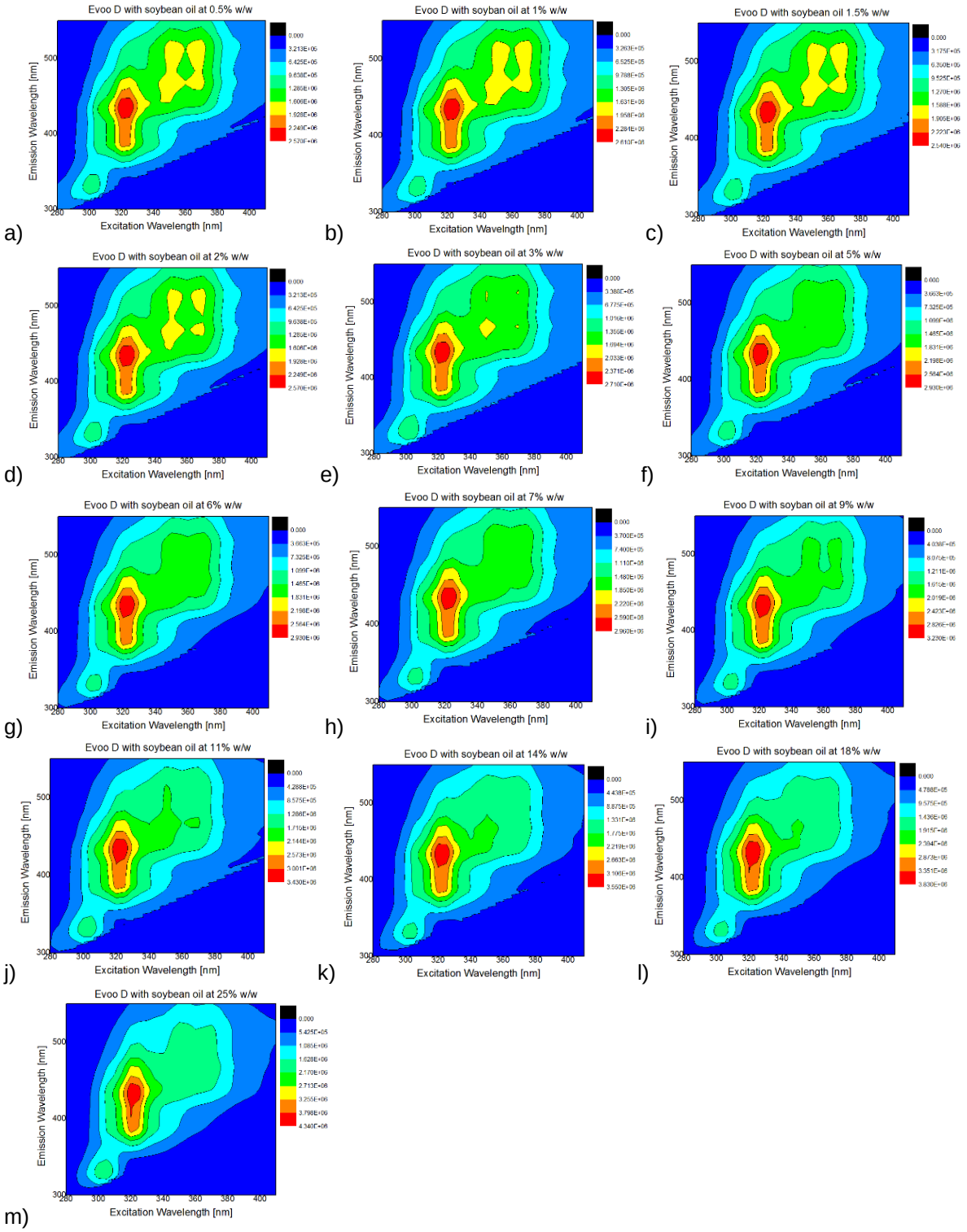

Figure A15. Fluorescence Excitation-Emission Matrices (EEMs) of EVOO D with soybean oil in different concentrations at: a) 0.5% w/w, b) 1% w/w, c) 1.5% w/w, d) 2% w/w, e) 3% w/w, f) 5% w/w, g) 6% w/w, h) 7% w/w, i) 9% w/w, j) 11% w/w, k) 14% w/w, l) 18% w/w, m) 25% w/w

EVOO E with corn oil

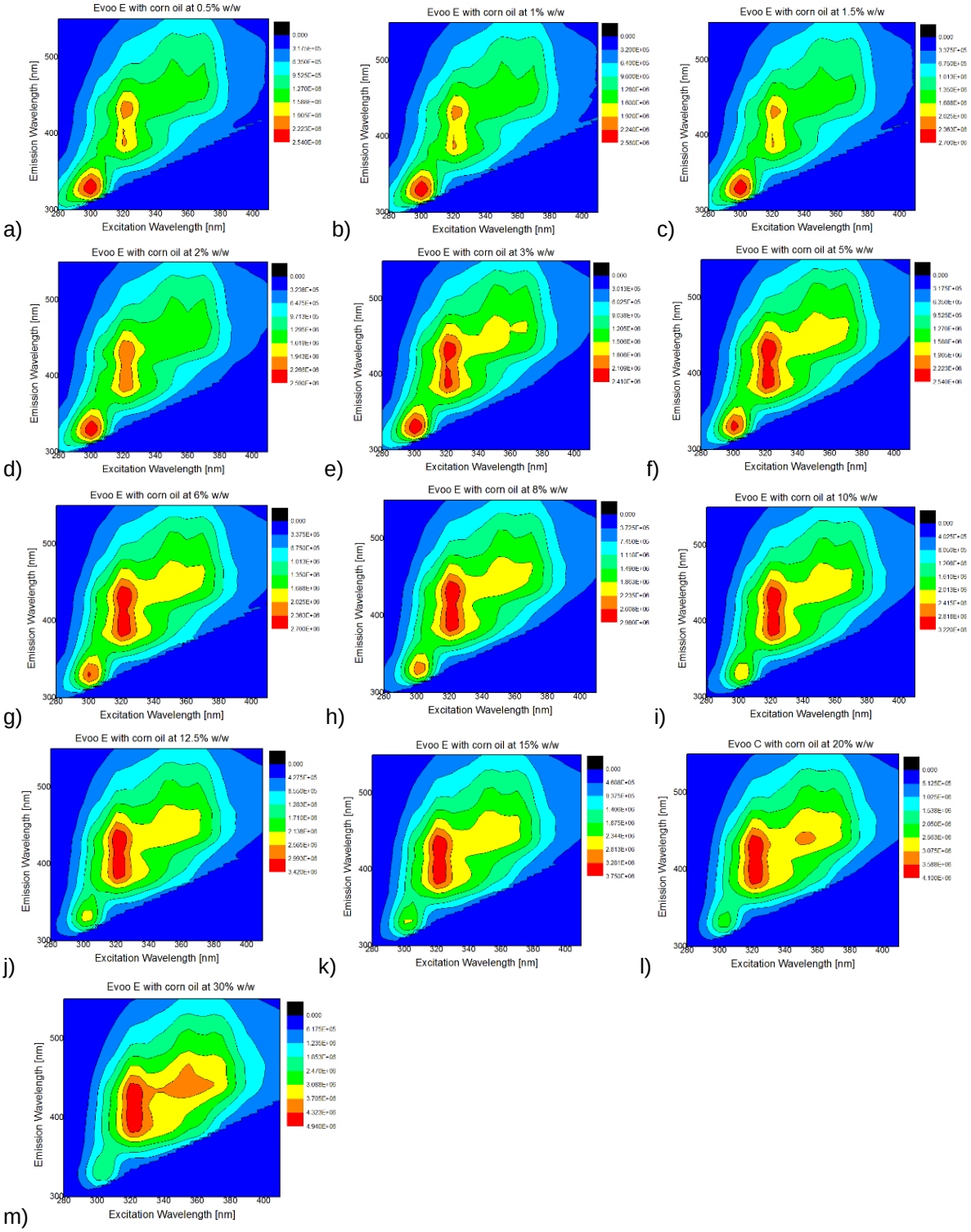

Figure A16. Fluorescence Excitation-Emission Matrices (EEMs) of EVOO E with corn oil in different concentrations at a) 0.5% w/w, b) 1% w/w, c) 1.5% w/w, d) 2% w/w, e) 3% w/w, f) 5% w/w, g) 6% w/w, h) 8% w/w, i) 10% w/w, j) 12.5% w/w, k) 15% w/w, l) 20% w/w, m) 30% w/w

EVOO E with sunflower oil

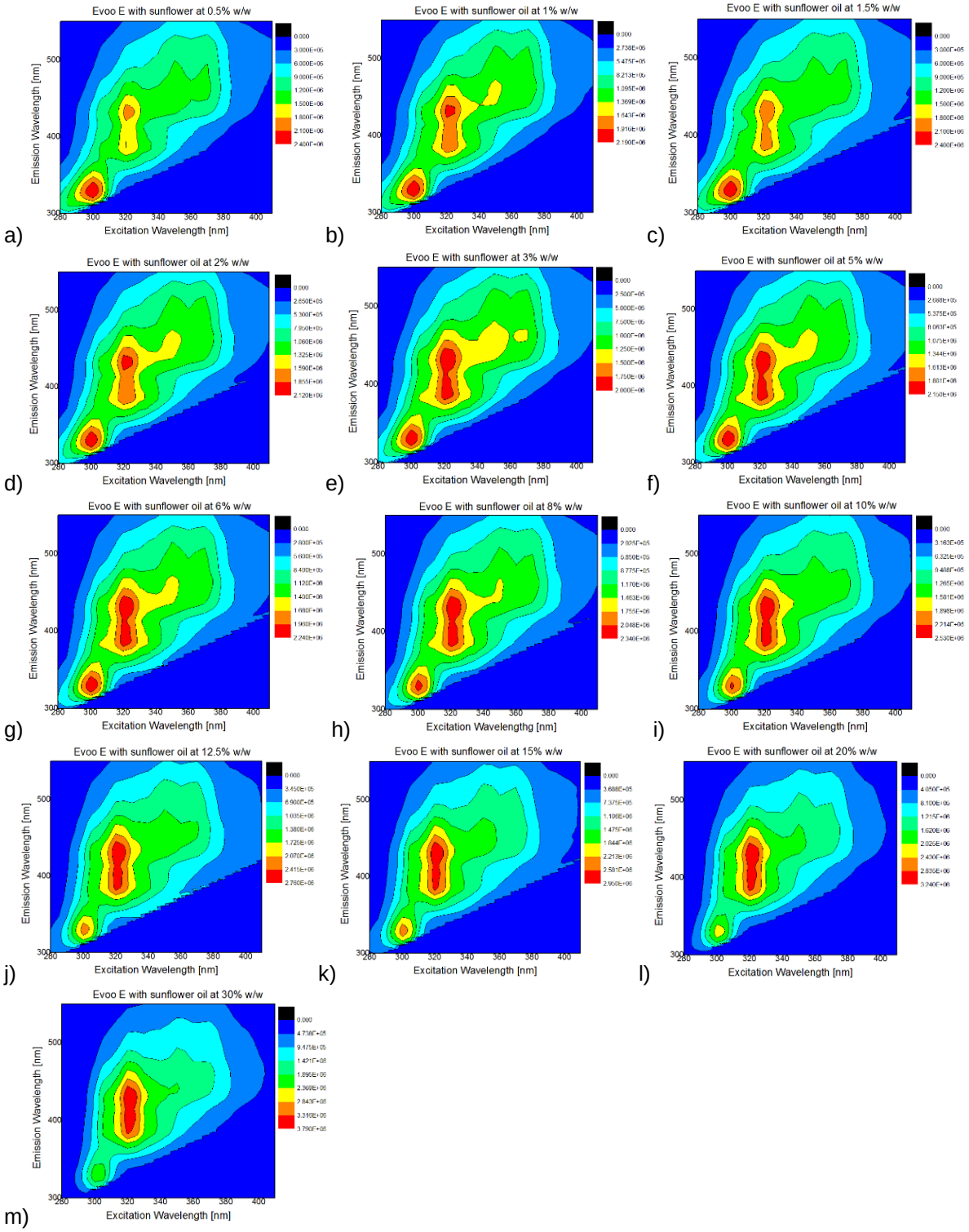

Figure A17. Fluorescence Excitation-Emission Matrices (EEMs) of EVOO E with sunflower oil in different concentrations at: a) 0.5% w/w, b) 1% w/w, c) 1.5% w/w, d) 2% w/w, e) 3% w/w, f) 5% w/w, g) 6% w/w, h) 8% w/w, i) 10% w/w, j) 12.5% w/w, k) 15% w/w, l) 20% w/w, m) 30% w/w

EVOO E with pomace oil

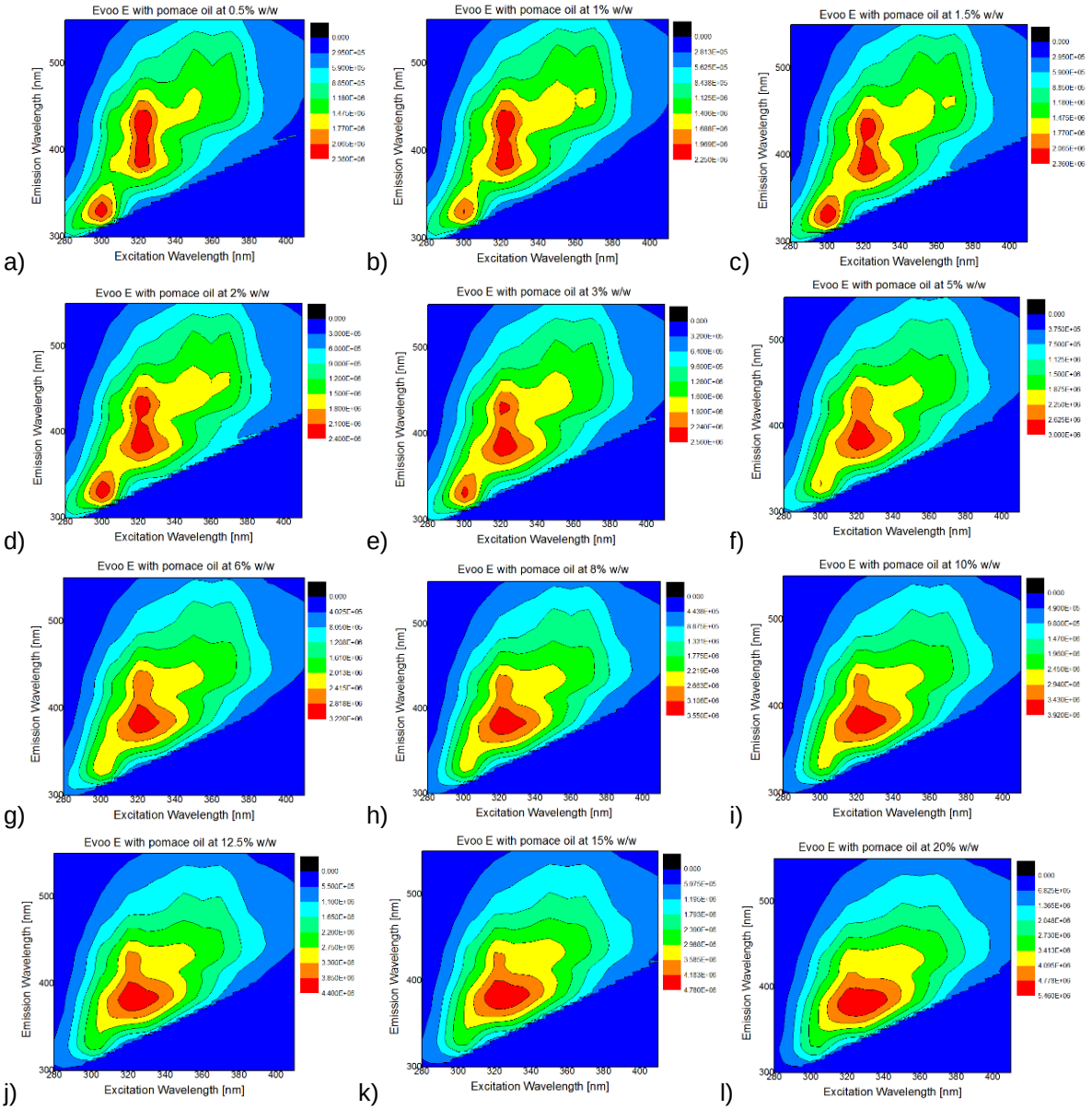

Figure A18. Fluorescence Excitation-Emission Matrices (EEMs) of EVOO E with pomace oil in different concentrations at: a) 0.5% w/w, b) 1% w/w, c) 1.5% w/w, d) 2% w/w, e) 3% w/w, f) 5% w/w, g) 6% w/w, h) 8% w/w, i) 10% w/w, j) 12.5% w/w, k) 15% w/w, l) 20% w/w

EVOO E with soybean oil

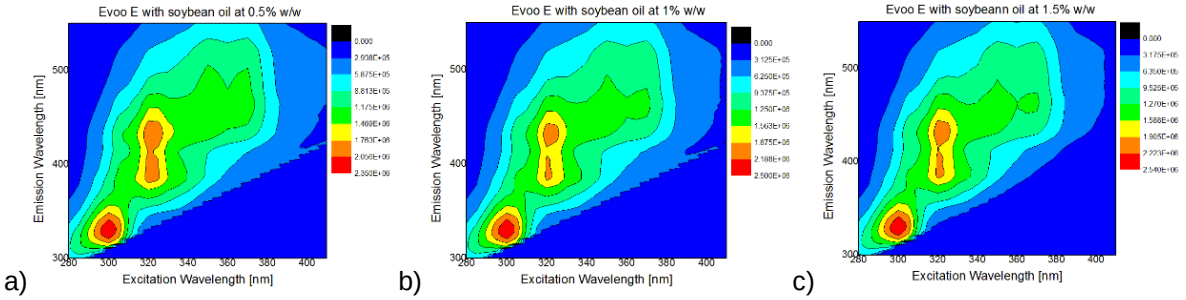

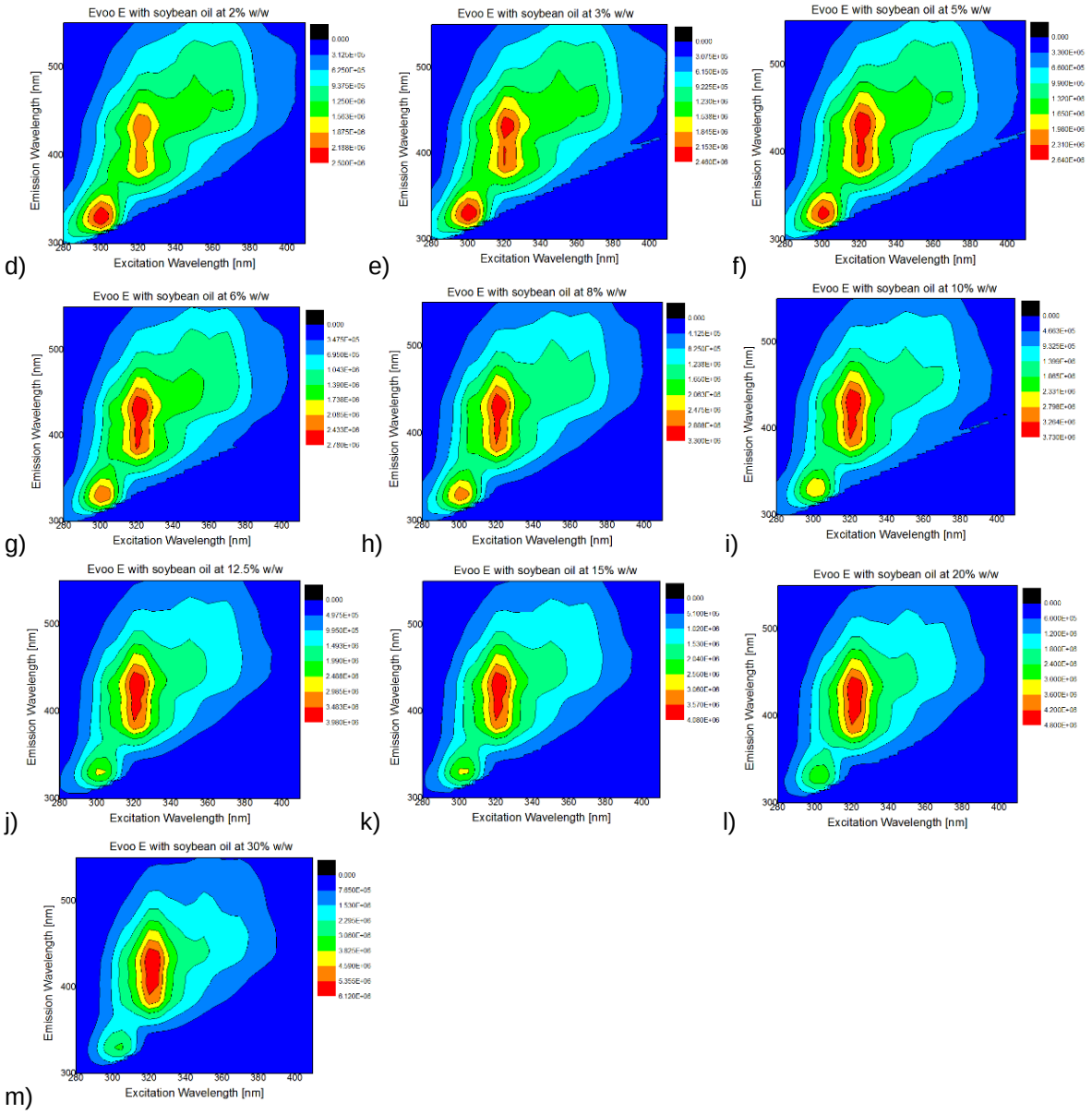

Figure A19. Fluorescence Excitation-Emission Matrices (EEMs) of EVOO E with soybean oil in different concentrations at: a) 0.5% w/w, b) 1% w/w, c) 1.5% w/w, d) 2% w/w, e) 3% w/w, f) 5% w/w, g) 6% w/w, h) 8% w/w, i) 10% w/w, j) 12.5% w/w, k) 15% w/w, l) 20% w/w, m) 30% w/w

Appendix B of Spiked Extra Virgin Olive Oil with Mineral Oil

Pure Extra Virgin Olive Oil

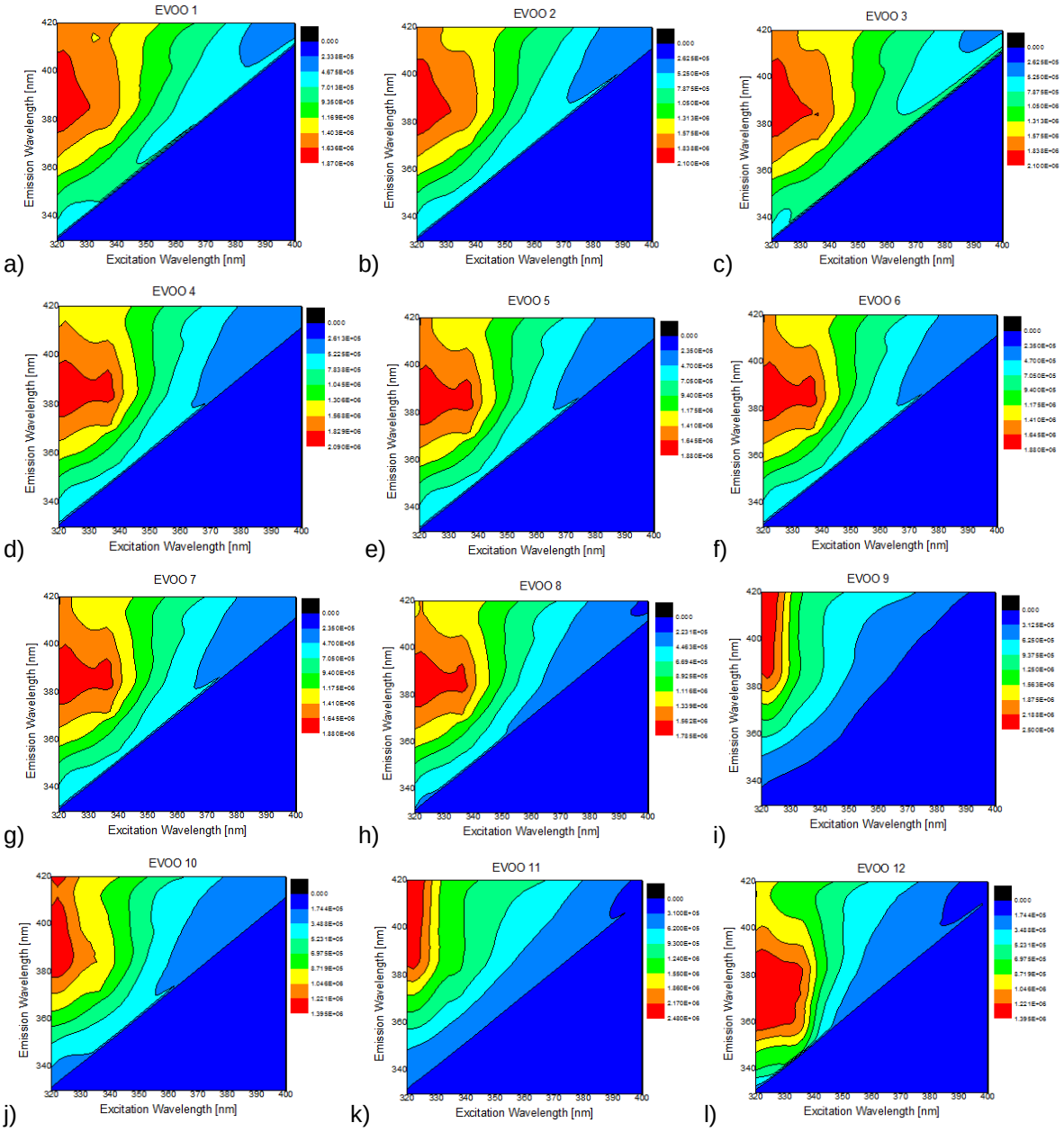

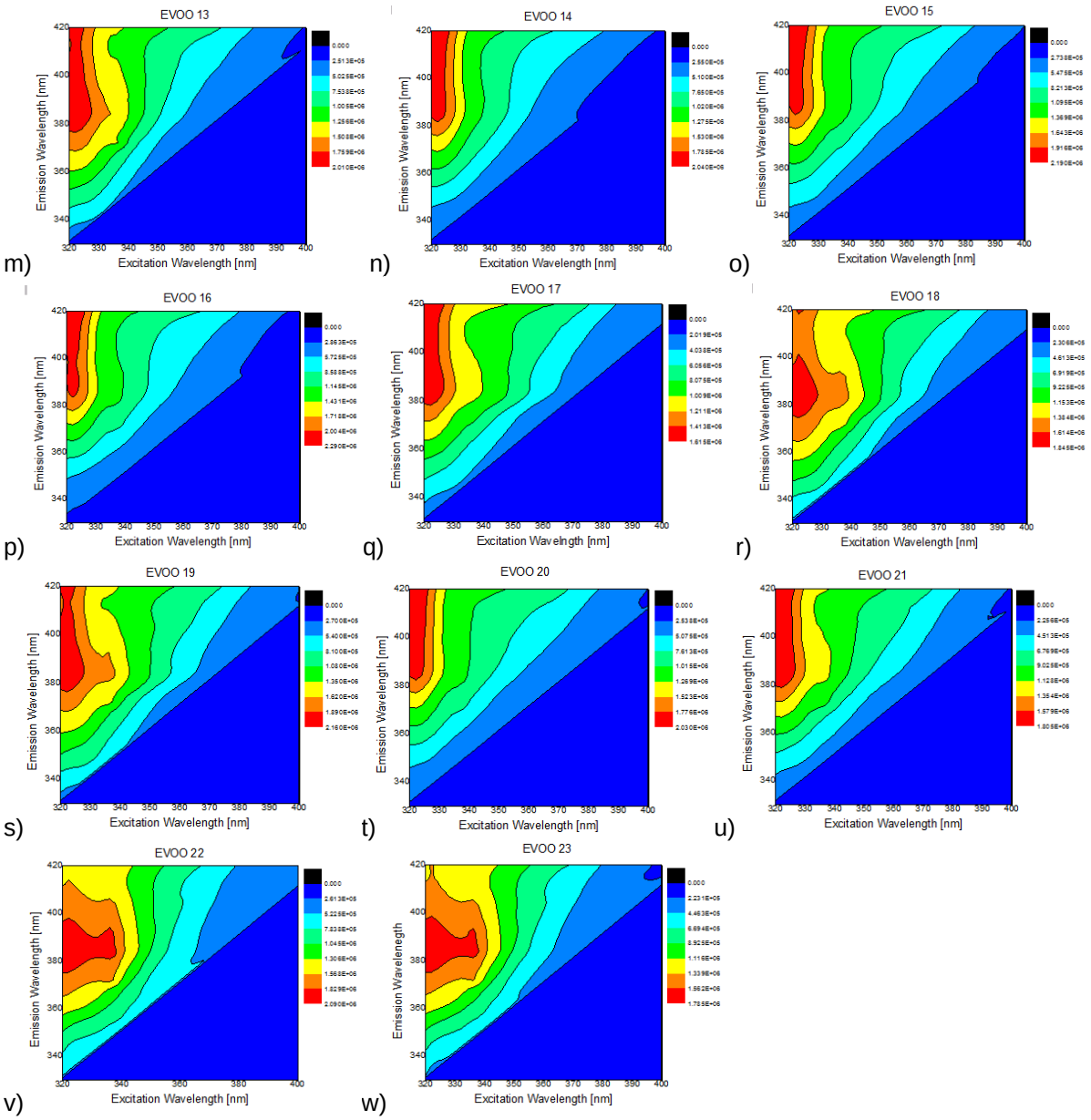

Figure B1. Fluorescence Excitation-Emission Matrices (EEMs) of 23 different pure EVOOs

Sample A

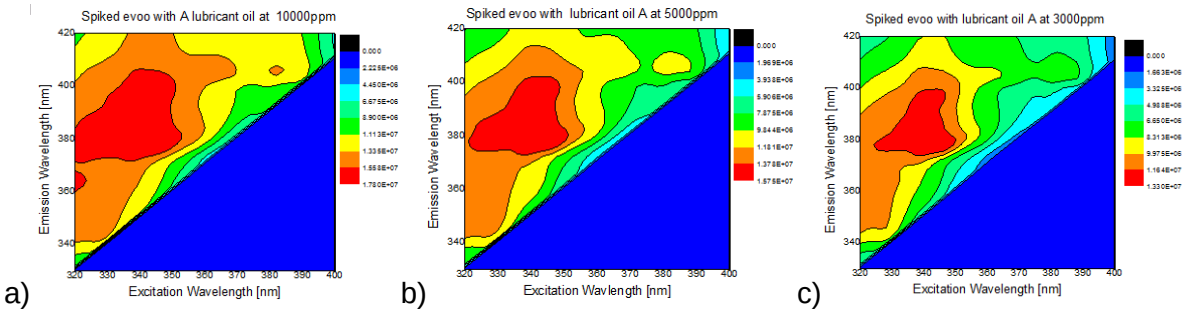

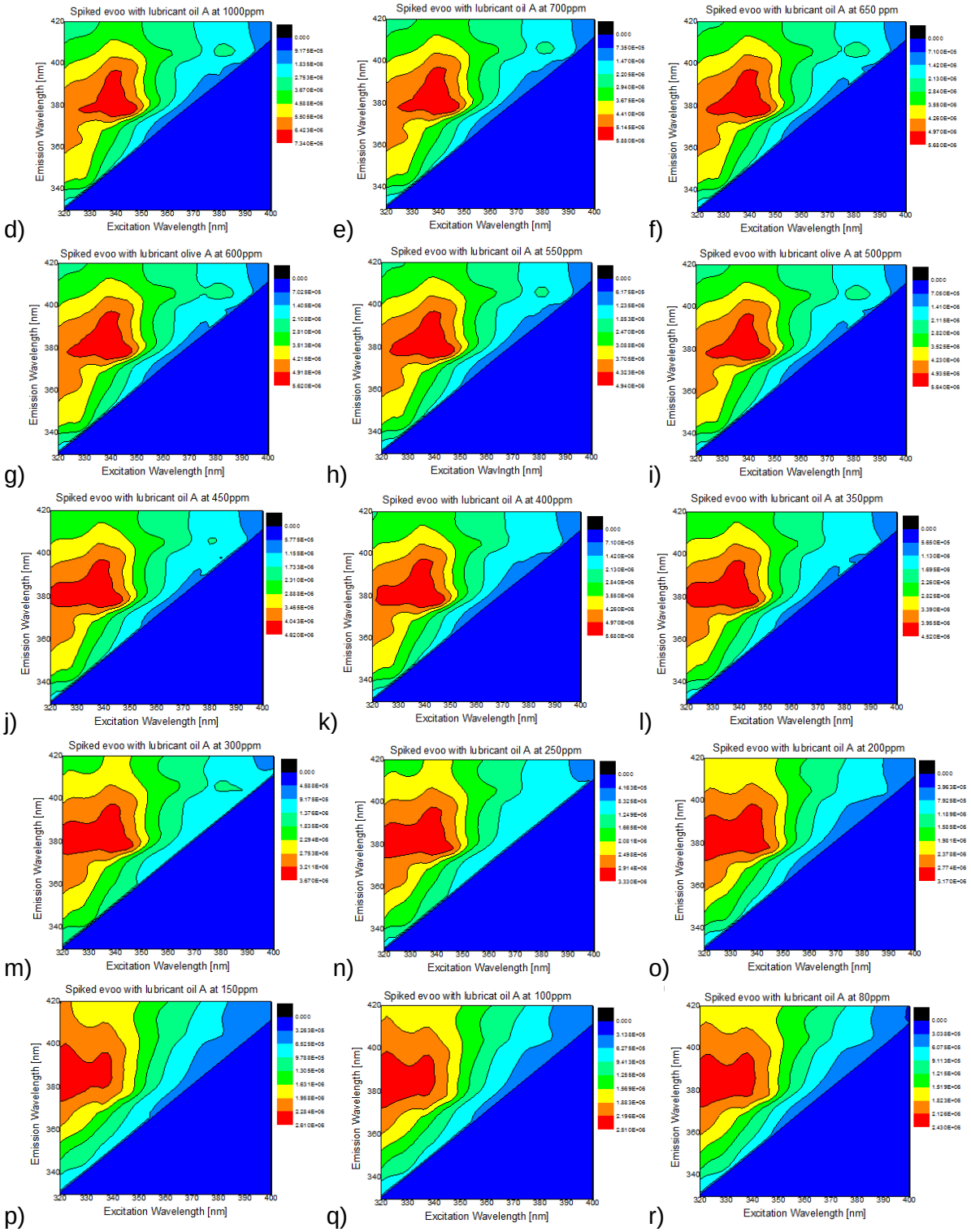
Spiked evoo with lubricant oil A at 1000ppm
Emission Wavelength [nm]
Excitation Wavelength [nm]
d)
Spiked evoo with lubricant oil A at 700ppm
Emission Wavelength [nm]
Excitation Wavelength [nm]
e)
Spiked evoo with lubricant oil A at 650 ppm
Emission Wavelength [nm]
Excitation Wavelength [nm]
f)
Spiked evoo with lubricant olive A at 600ppm
Emission Wavelength [nm]
Excitation Wavelength [nm]
g)
Spiked evoo with lubricant oil A at 550ppm
Emission Wavelength [nm]
Excitation Wavlngth [nm]
h)
Spiked evoo with lubricant olive A at 500ppm
Emission Wavelength [nm]
Excitation Wavelength [nm]
i)
Spiked evoo with lubricant oil A at 450ppm
Emission Wavelength [nm]
Excitation Wavelength [nm]
j)
Spiked evoo with lubricant oil A at 400ppm
Emission Wavelength [nm]
Excitation Wavelength [nm]
k)
Spiked evoo with lubricant oil A at 350ppm
Emission Wavelength [nm]
Excitation Wavelength [nm]
l)
Spiked evoo with lubricant oil A at 300ppm
Emission Wavelength [nm]
Excitation Wavelength [nm]
m)
Spiked evoo with lubricant oil A at 250ppm
Emission Wavelength [nm]
Excitation Wavelength [nm]
n)
Spiked evoo with lubricant oil A at 200ppm
Emission Wavelength [nm]
Excitation Wavelength [nm]
o)
Spiked evoo with lubricant oil A at 150ppm
Emission Wavelength [nm]
Excitation Wavelength [nm]
p)
Spiked evoo with lubricat oil A at 100ppm
Emission Wavelength [nm]
Excitation Wavelength [nm]
q)
Spiked evoo with lubricant oil A at 80ppm
Emission Wavelength [nm]
Excitation Wavelength [nm]
r)

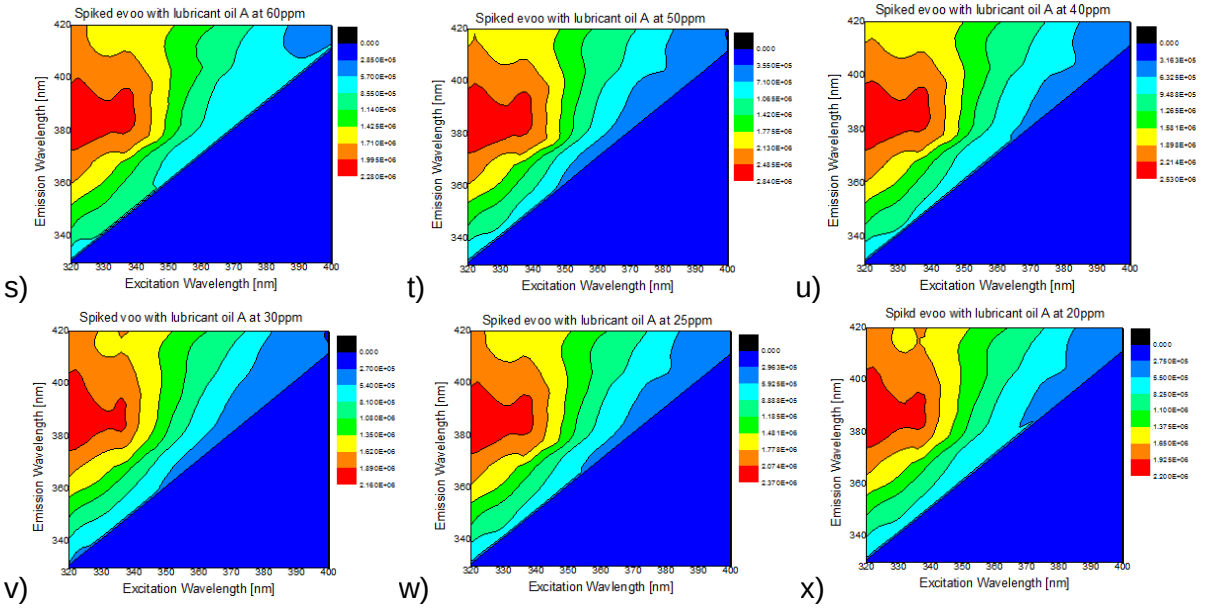

Figure B2. Fluorescence Excitation-Emission Matrices (EEMs) of the spiked EVOO with mineral oil A in different concentrations at a) 10000 ppm, b) 5000 ppm, c) 3000 ppm, d) 1000 ppm, e) 700 ppm, f) 650 ppm, g) 600 ppm, h) 550 ppm, i) 500 ppm, j) 450 ppm, k) 400 ppm, l) 350 ppm, m) 300 ppm, n) 250 ppm, o) 200 ppm, p) 150 ppm, q)100 ppm, r) 80 ppm, s) 60 ppm, t) 50 ppm, u) 40 ppm, v) 30 ppm, w) 25 ppm, x) 20 ppm

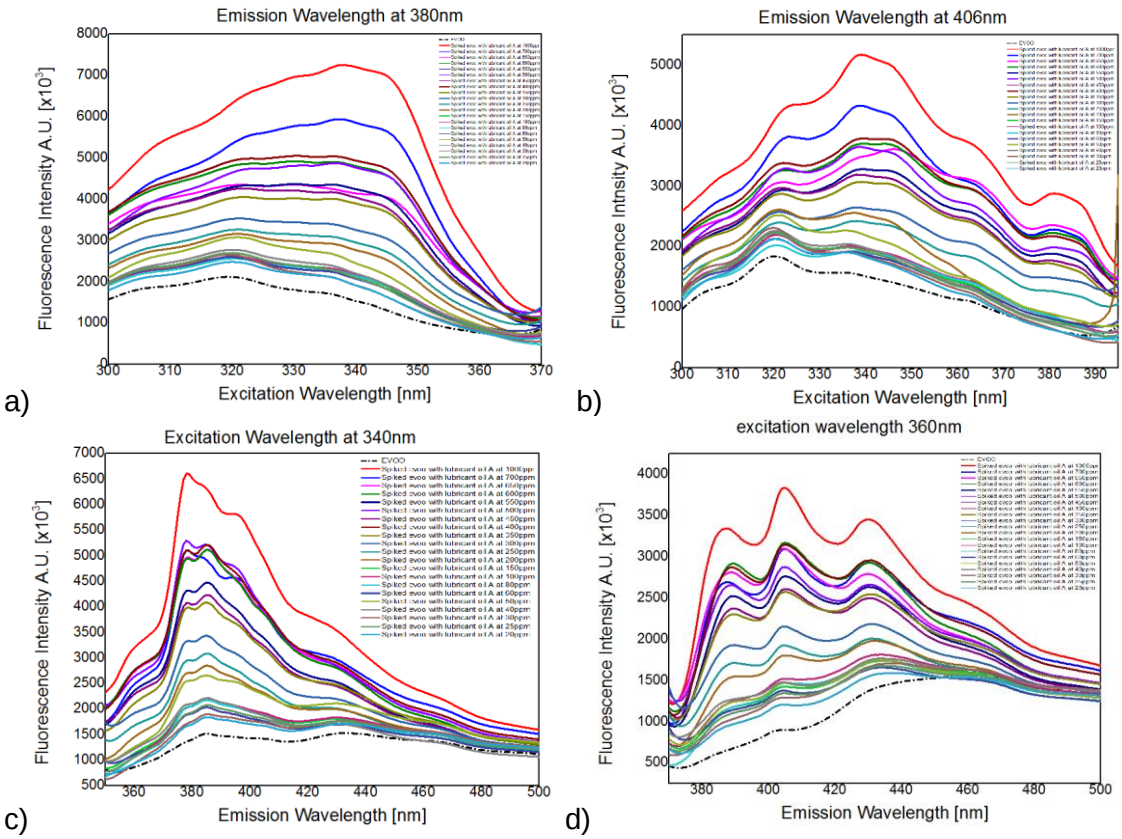

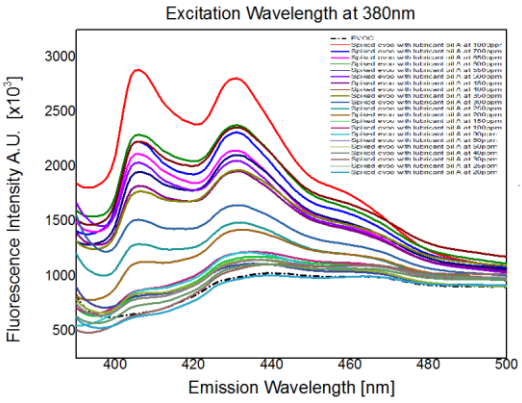

e)

Figure B3. Fluorescence intensity at constant wavelength of the spiked EVOO with mineral oil A in different concentrations: a) Emission Wavelength at 380nm, b) Emission Wavelength at 406nm, c) Excitation Wavelength at 340nm, d) Excitation Wavelength at 360nm, e) Excitation Wavelength at 380nm

Sample B

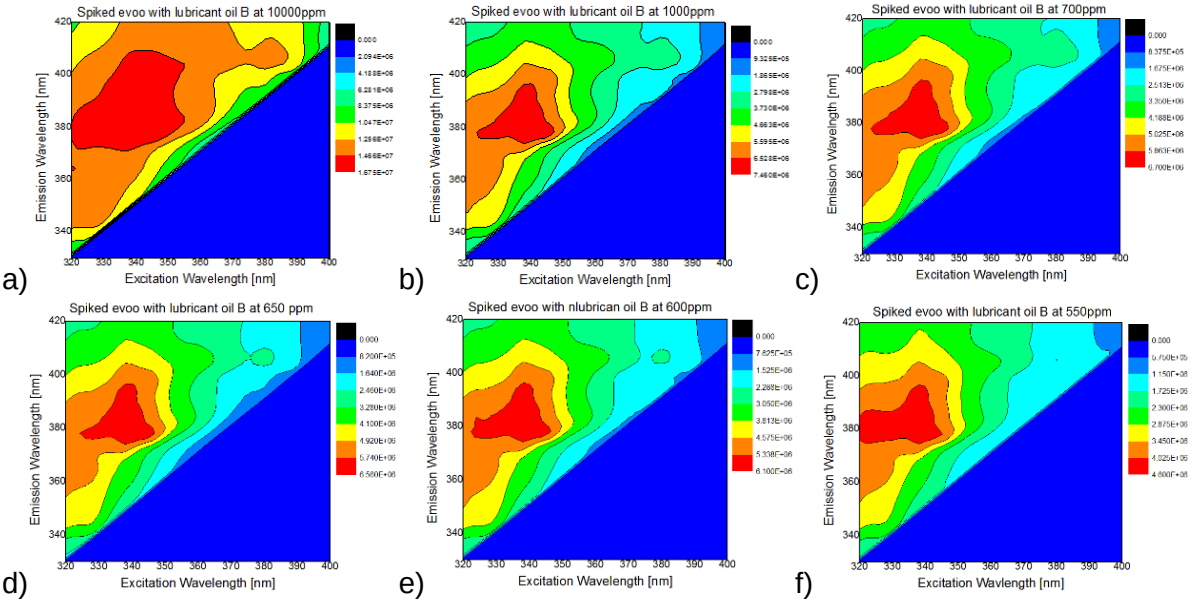

a) b) c)

d) e) f)

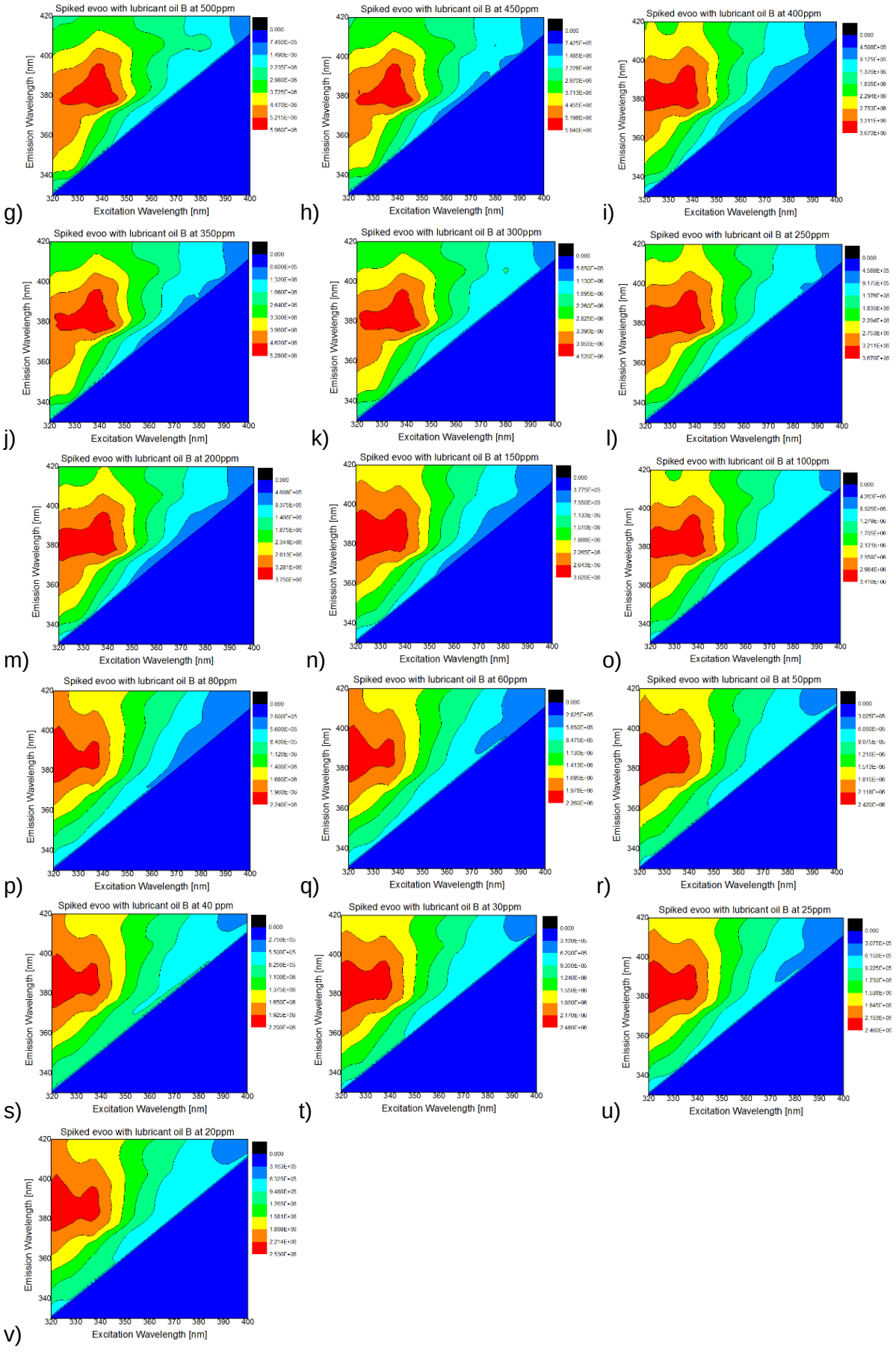
Spiked evoo with lubricant oil B at 500ppm
Spiked evoo with lubricant oil B at 450ppm
Spiked evoo with lubricant oil B at 400ppm
Spiked evoo with lubricant oil B at 350ppm
Spiked evoo with lubricant oil B at 300ppm
Spiked evoo with lubricant oil B at 250ppm
Spiked evoo with lubricant oil B at 200ppm
Spiked evoo with lubricant oil B at 150ppm
Spiked evoo with lubricant oil B at 100ppm
Spiked evoo with lubricant oil B at 80ppm
Spiked evoo with lubricant oil B at 60ppm
Spiked evoo with lubricant oil B at 50ppm
Spiked evoo with lubricant oil B at 40 ppm
Spiked evoo with lubricant oil B at 30ppm
Spiked evoo with lubricant oil B at 25ppm
Spiked evoo with lubricant oil B at 20ppm
Emission Wavelength [nm]
Excitation Wavelength [nm]
g)
h)
i)
j)
k)
l)
m)
n)
o)
p)
q)
r)
s)
t)
u)
v)

Figure B4. Fluorescence Excitation-Emission Matrices (EEMs) of the spiked EVOO with mineral oil B in different concentrations at a) 10000ppm, b) 1000ppm, c) 700ppm, d) 650ppm, e) 600ppm, f) 550ppm, g) 500ppm, h) 450ppm, i) 400ppm, j) 350ppm, k) 300ppm, l) 250ppm, m) 200ppm, n) 150ppm, o) 100ppm, p) 80ppm, q) 60ppm, r) 50ppm, s) 40ppm, t) 30ppm, u) 25ppm, v) 20ppm

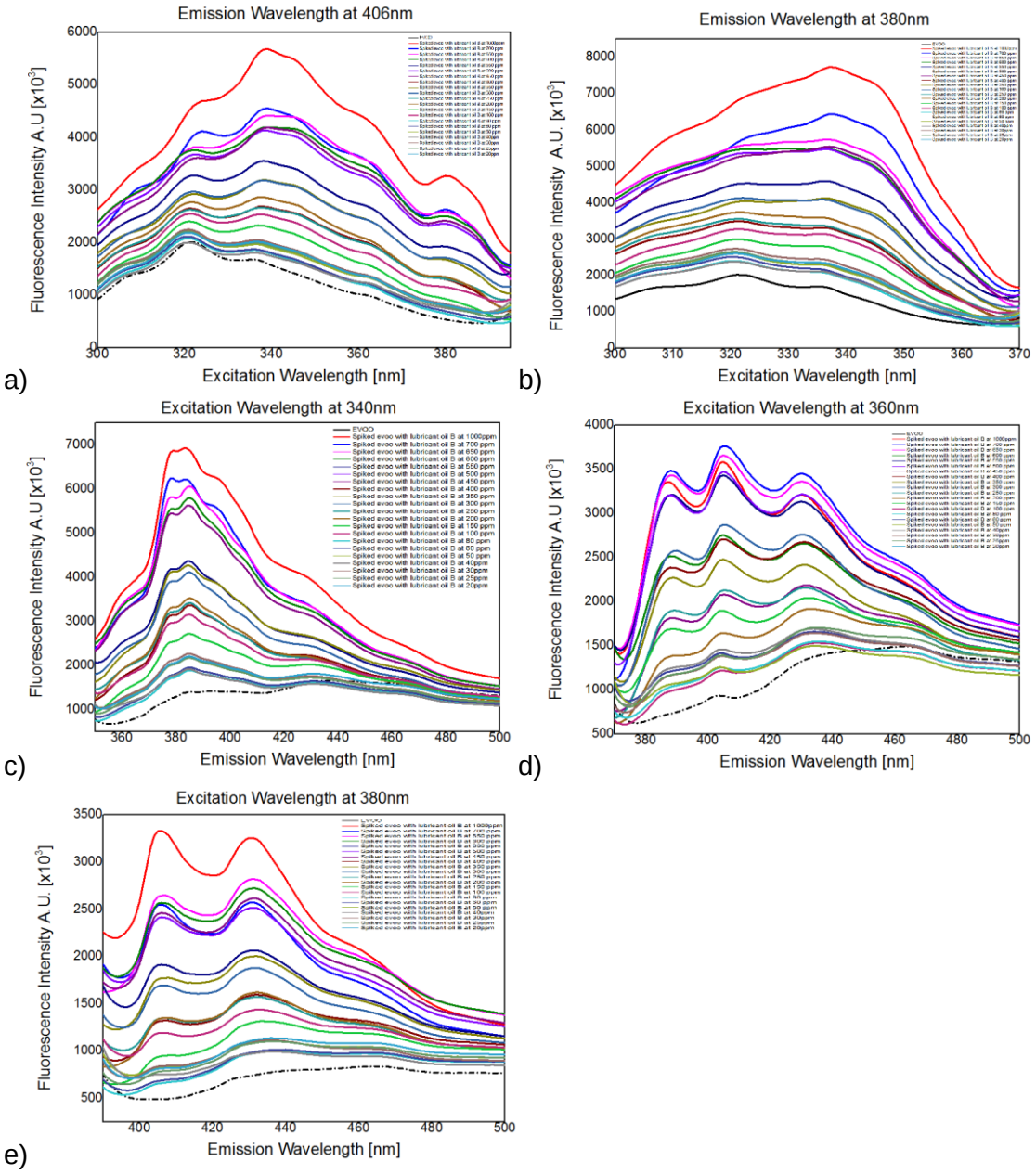

Figure B5. Fluorescence intensity at a constant wavelength of the spiked EVOO with mineral oil B in different concentrations: a) Emission Wavelength at 406nm, b) Emission Wavelength at 380nm, c) Excitation Wavelength at 340nm, d) Excitation Wavelength at 360nm, e) Excitation Wavelength at 380nm

Sample C

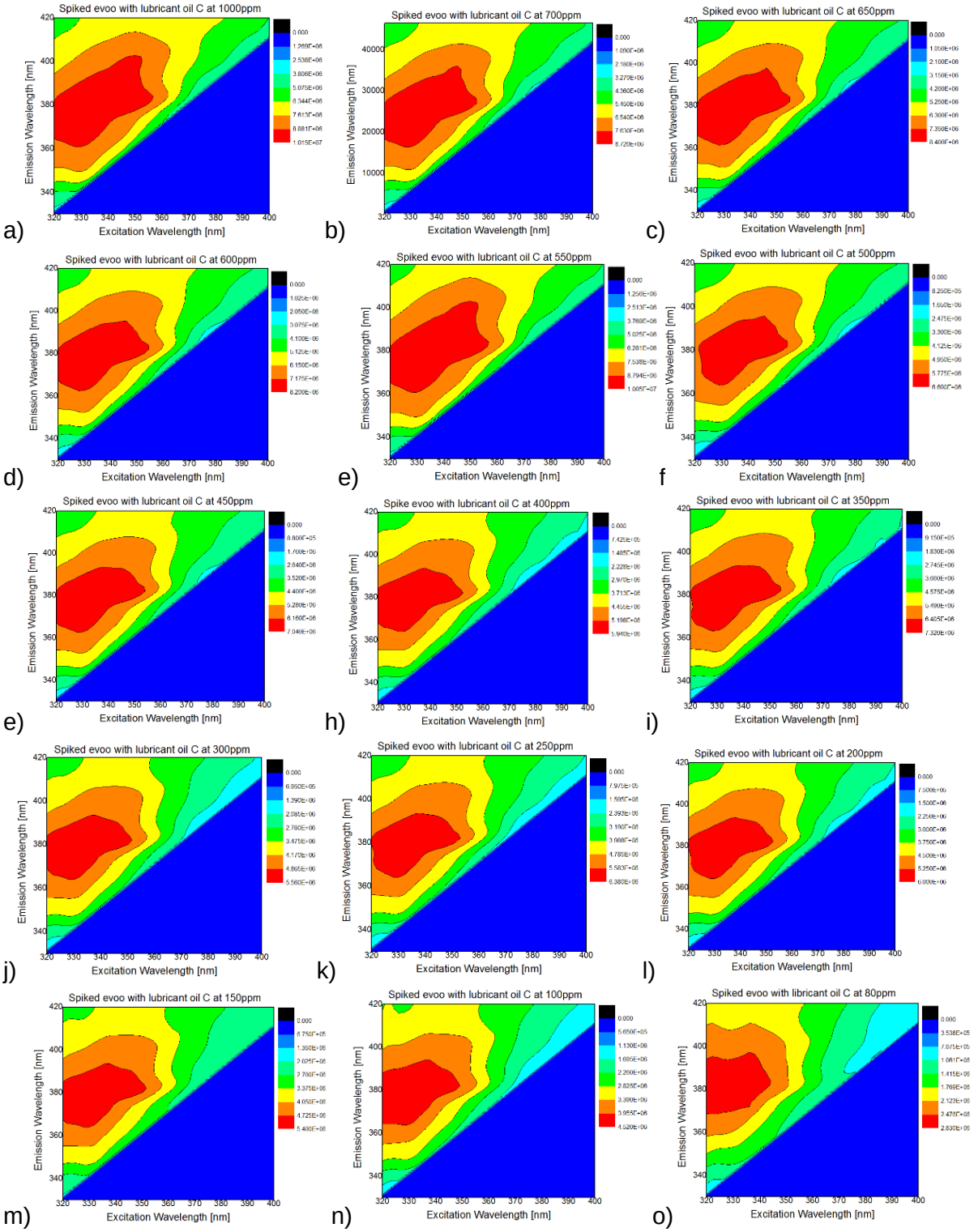
Spiked evoo with lubricant oil C at 1000ppm
Emission Wavelength [nm]
Excitation Wavelength [nm]
a)
Spiked evoo with lubricant oil C at 700ppm
b)
Spiked evoo with lubricant oil C at 650ppm
c)
Spiked evoo with lubricant oil C at 600ppm
d)
Spiked evoo with lubricant oil C at 550ppm
e)
Spiked evoo with lubricant oil C at 500ppm
f
Spiked evoo with lubricant oil C at 450ppm
e)
Spike evoo with lubricant oil C at 400ppm
h)
Spiked evoo with lubricant oil C at 350ppm
i)
Spiked evoo with lubricant oil C at 300ppm
j)
Spiked evoo with lubricant oil C at 250ppm
k)
Spiked evoo with lubricant oil C at 200ppm
l)
Spiked evoo with lubricant oil C at 150ppm
m)
Spiked evoo with lubricant oil C at 100ppm
n)
Spiked evoo with libricant oil C at 80ppm
o)

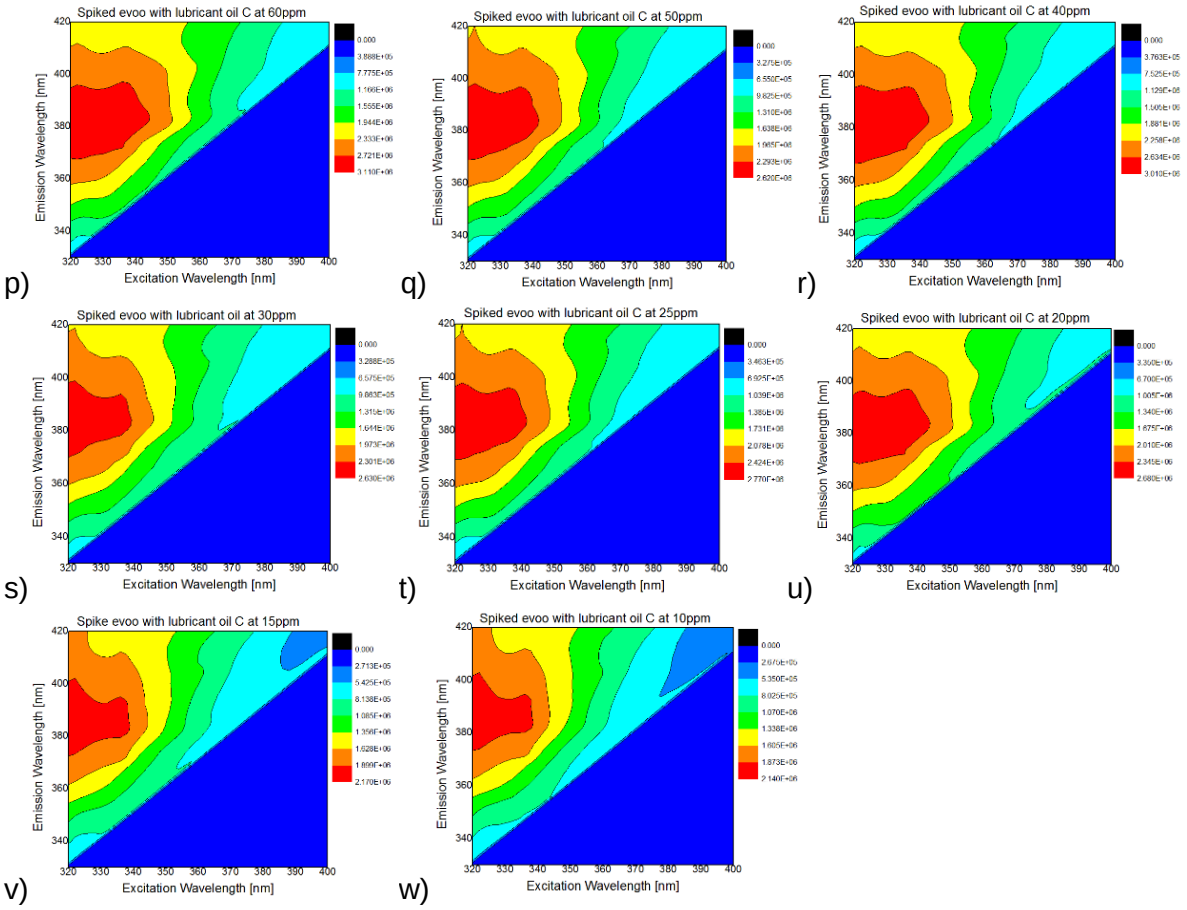

Figure B6. Fluorescence Excitation-Emission Matrices (EEMs) of the spiked EVOO with mineral oil C in different concentrations at a) 1000ppm, b) 700ppm, c) 650ppm, d) 600ppm, e) 550ppm, f) 500ppm, g) 450ppm, h) 400ppm, i) 350ppm, j) 300ppm, k) 250ppm, l) 200ppm, m) 150ppm, n) 100ppm, o) 80ppm, p) 60ppm, q) 50ppm, r) 40ppm, s) 30ppm, t) 25ppm, u) 20ppm, v) 15ppm, w) 10ppm

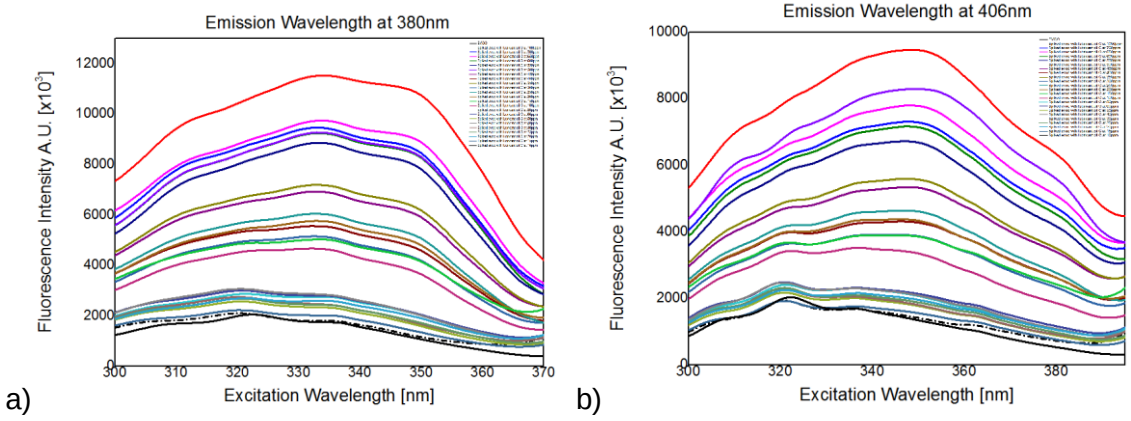

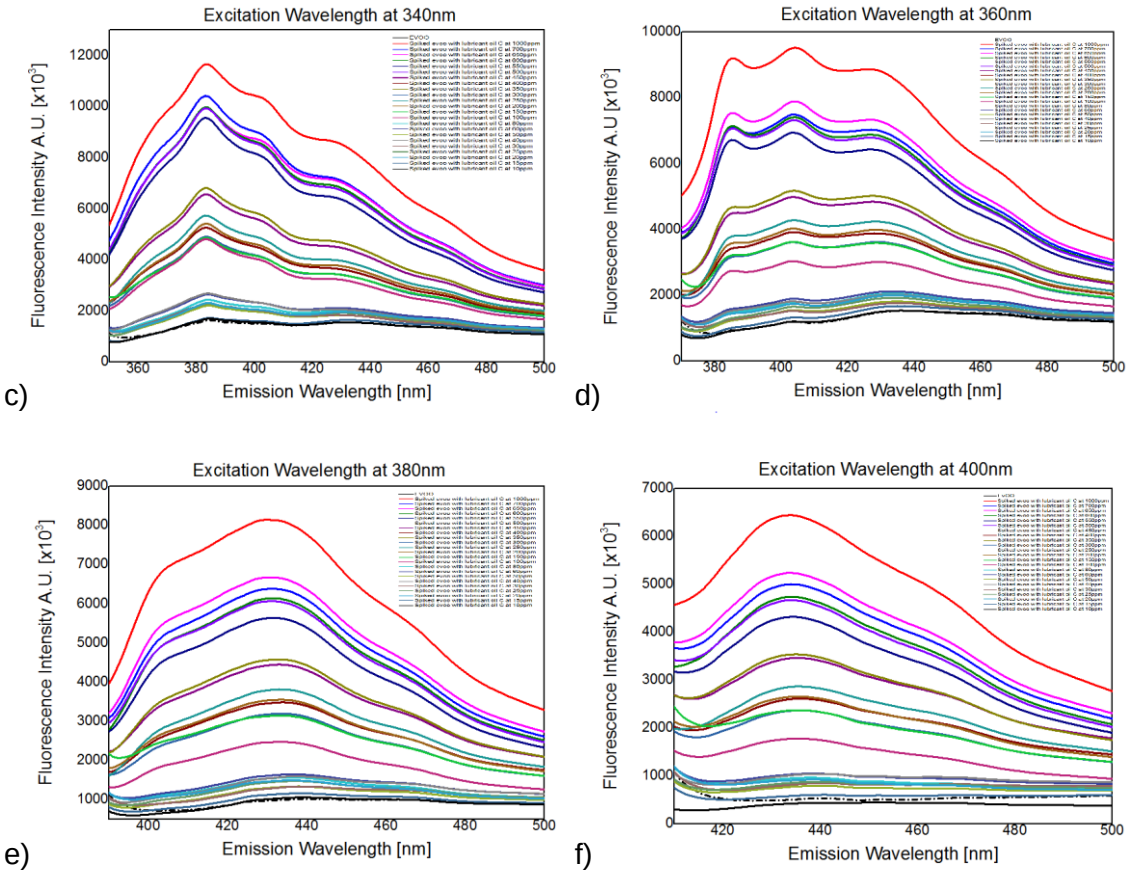

Figure B7. Fluorescence intensity at a constant wavelength of the spiked EVOO with mineral oil C in different concentrations: a) Emission Wavelength at 406nm, b) Emission Wavelength at 380nm, c) Excitation Wavelength at 340nm, d) Excitation Wavelength at 360nm, e) Excitation Wavelength at 380nm

Sample D

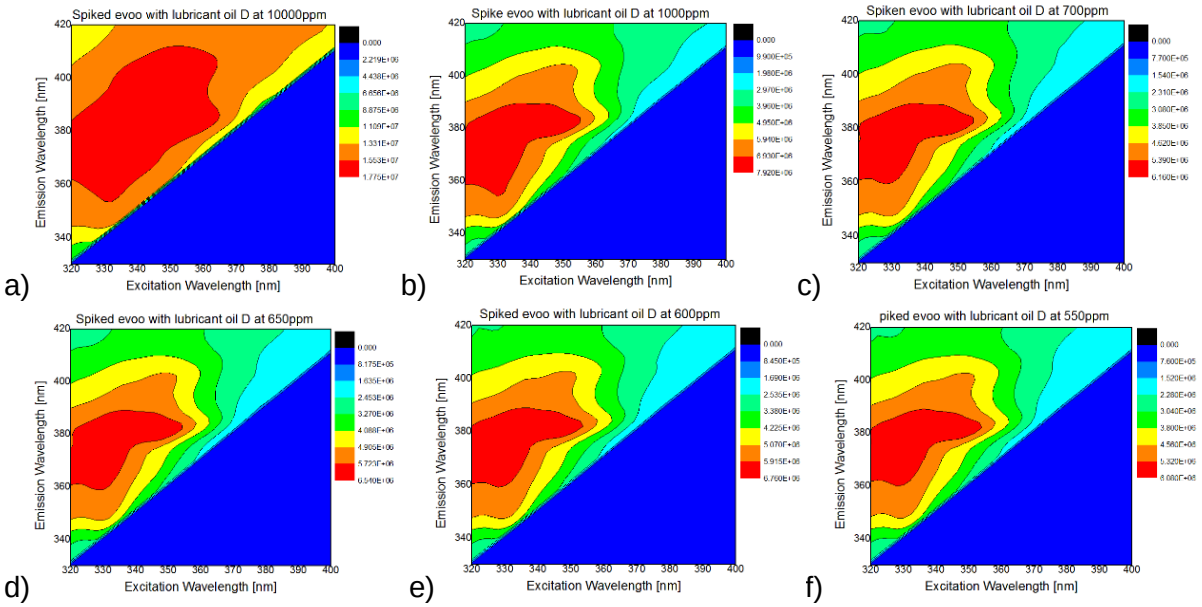

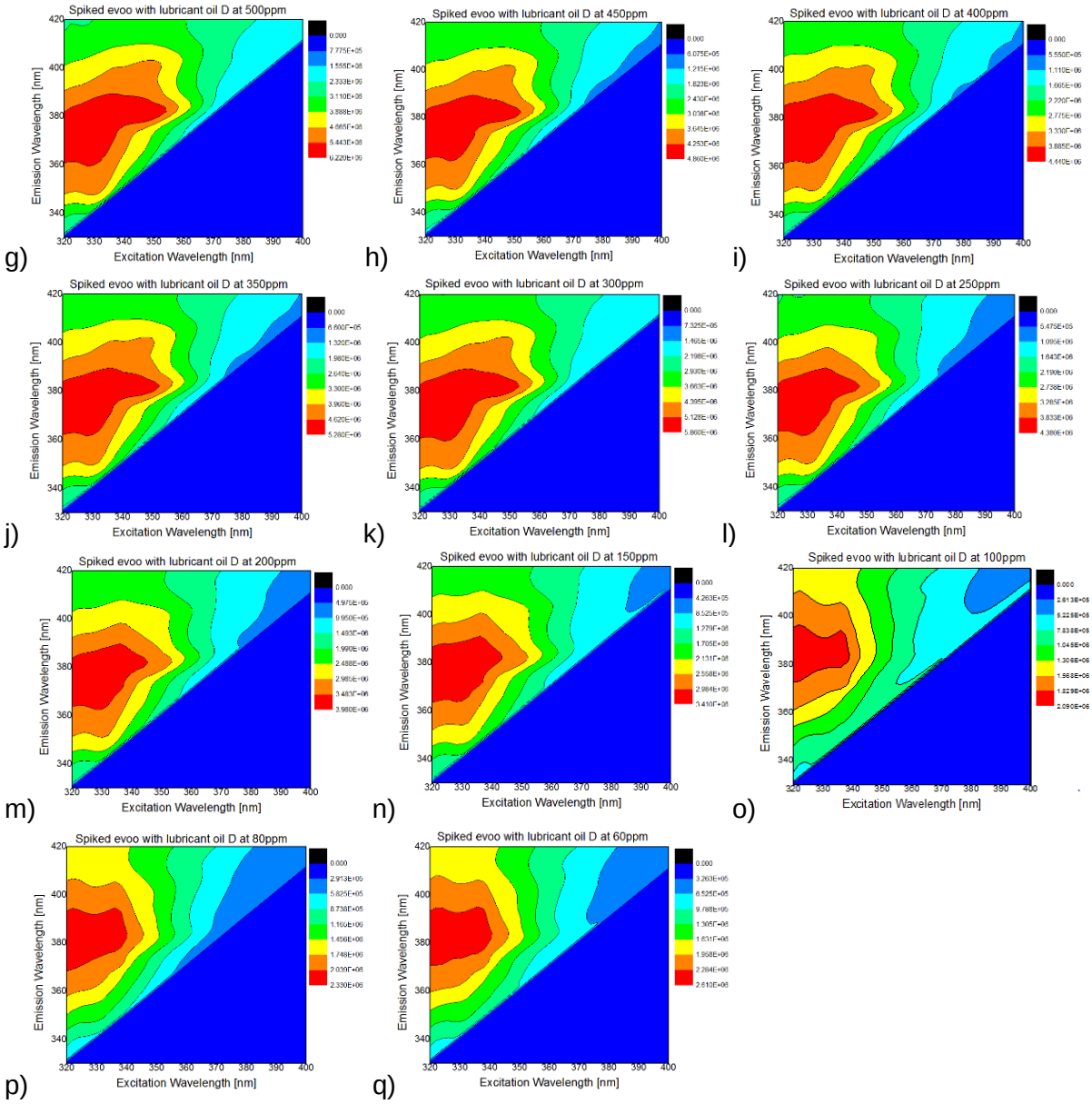

Figure B8. Fluorescence Excitation-Emission Matrices (EEMs) of the spiked EVOO with mineral oil in different concentrations at a) 10000ppm, b) 10000ppm, c) 700ppm, d) 650ppm, e) 600ppm, f) 550ppm, g) 500ppm, h) 450ppm, i) 400ppm, j) 350ppm, k) 300ppm, l) 250ppm, m) 200ppm, n) 150ppm, o) 100ppm, p) 80ppm, q) 60ppm

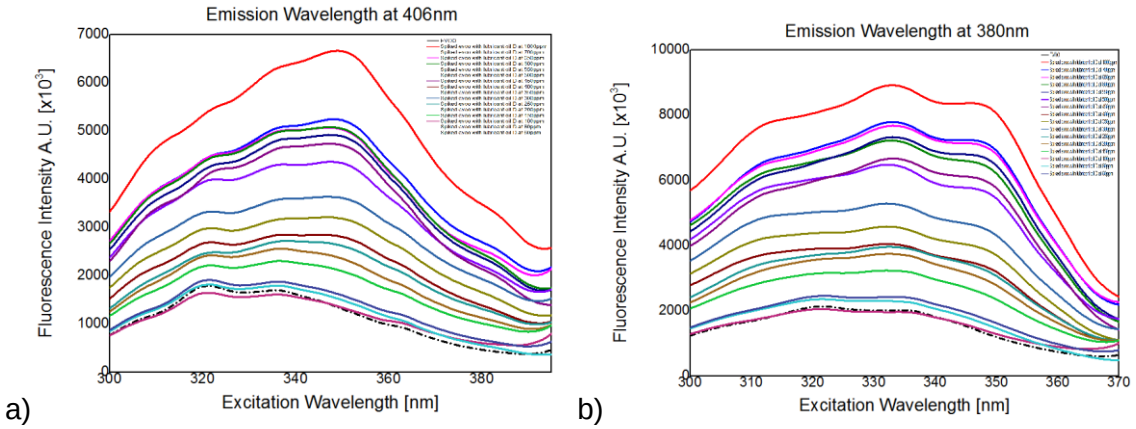

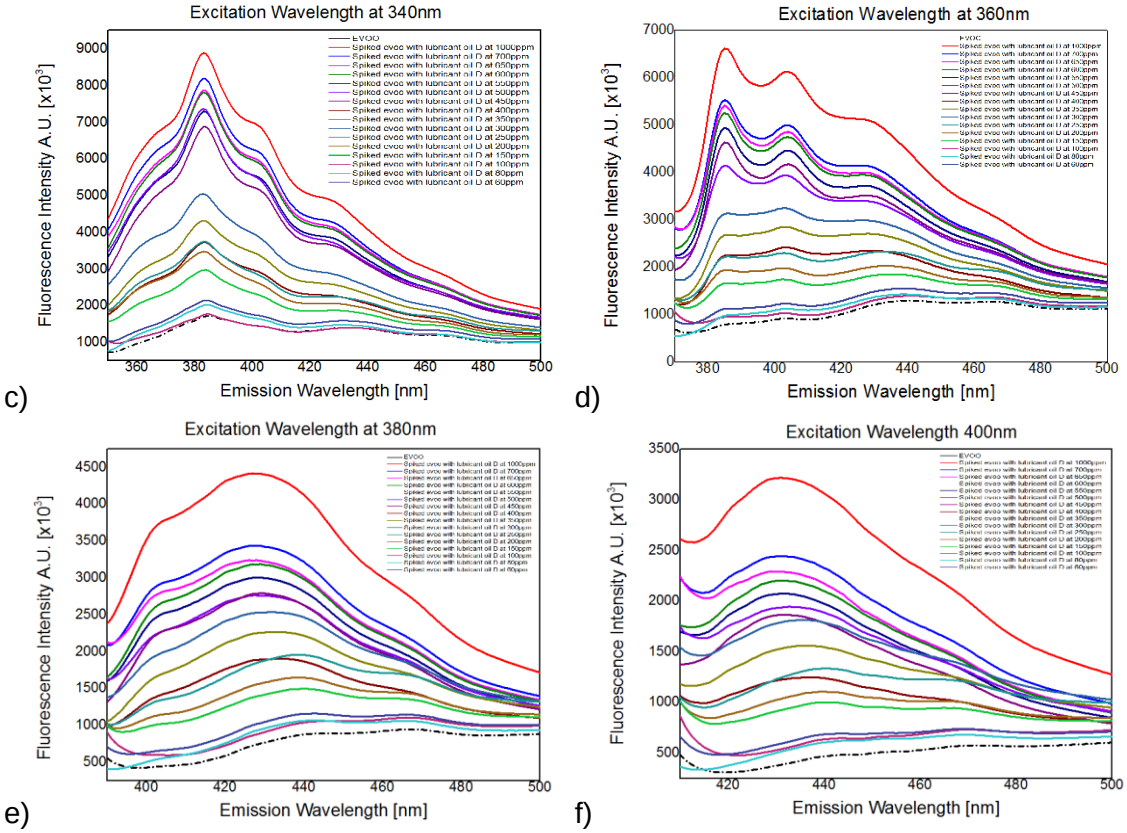

Figure B9. Fluorescence intensity at a constant wavelength of the spiked EVOO with mineral oil D in different concentrations: a) Emission Wavelength at 406nm, b) Emission Wavelength at 380nm, c) Excitation Wavelength at 340nm, d) Excitation Wavelength at 360nm, e) Excitation Wavelength at 380nm, f) Excitation Wavelength at 400nm

Sample E

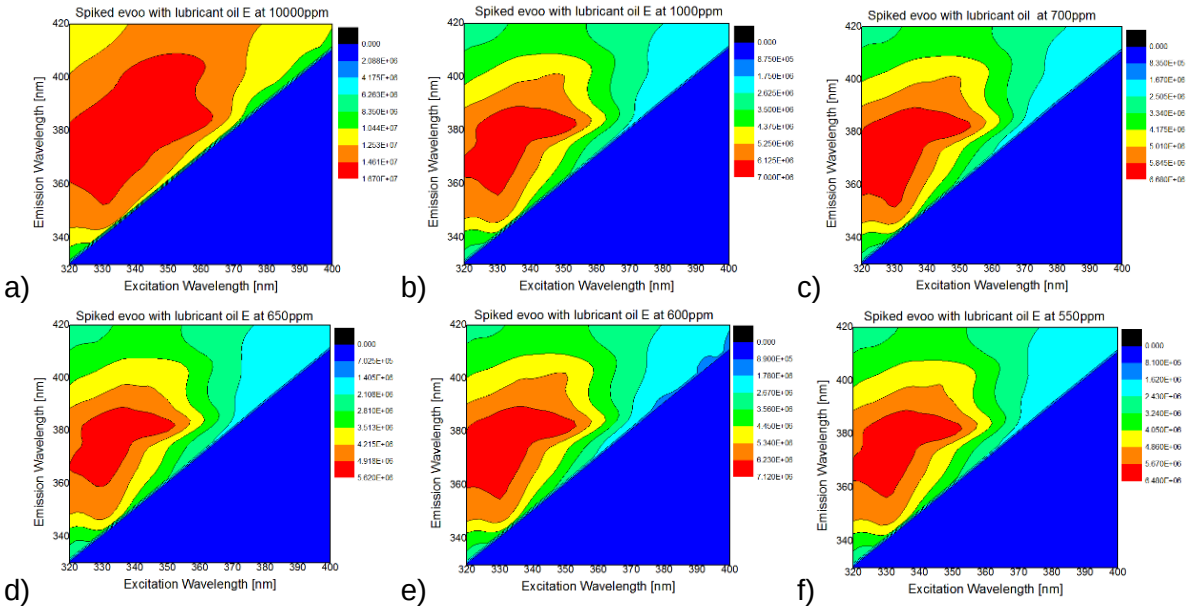

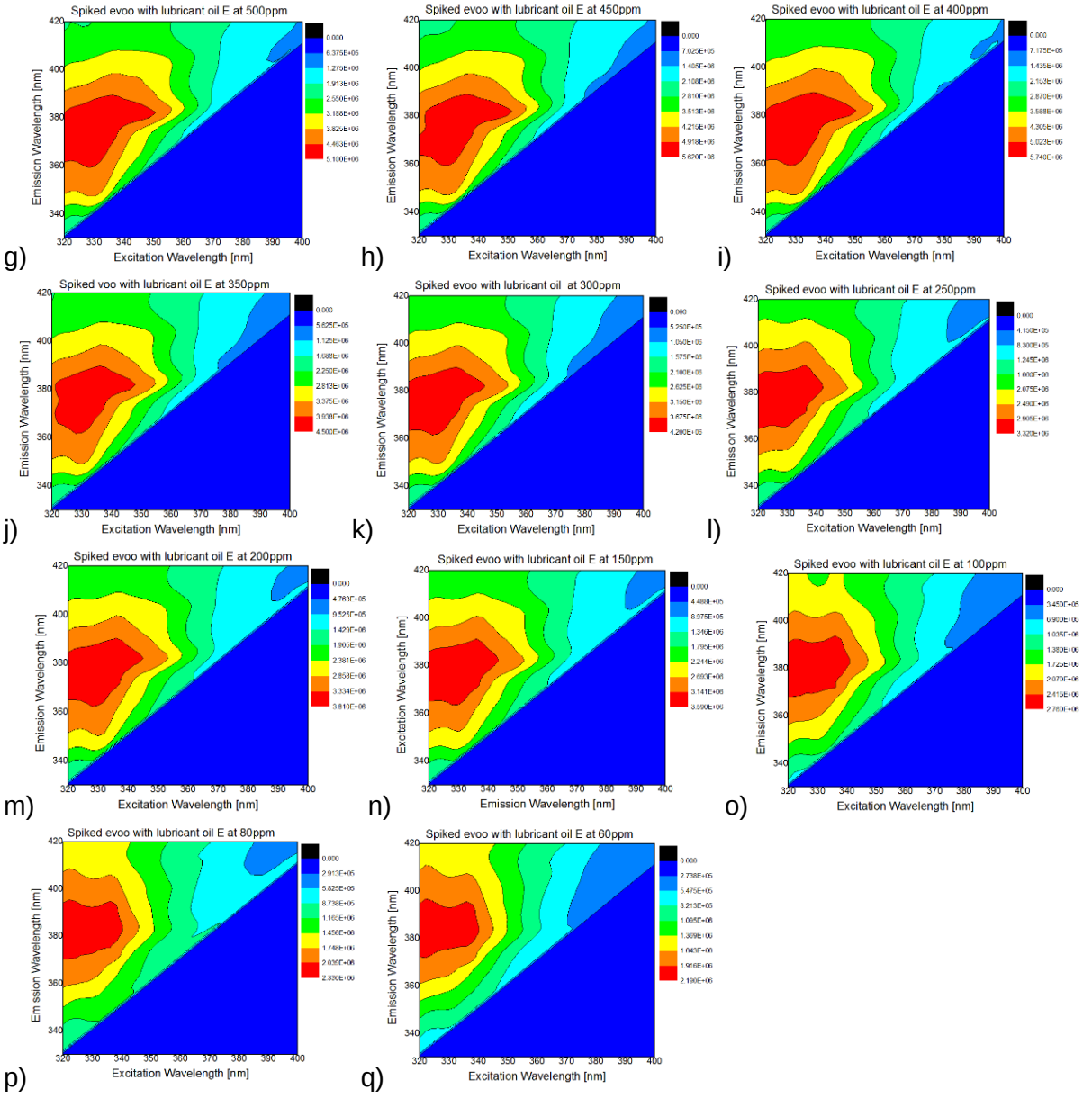

Figure B10. Fluorescence Excitation-Emission Matrices (EEMs) of the spiked EVOO with mineral oil E in different concentrations at a) 10000ppm, b) 10000ppm, c) 700ppm, d) 650ppm, e) 600ppm, f) 550ppm, g) 500ppm, h) 450ppm, i) 400ppm, j) 350ppm, k) 300ppm, l) 250ppm, m) 200ppm, n) 150ppm, o) 100ppm, p) 80ppm, q) 60ppm

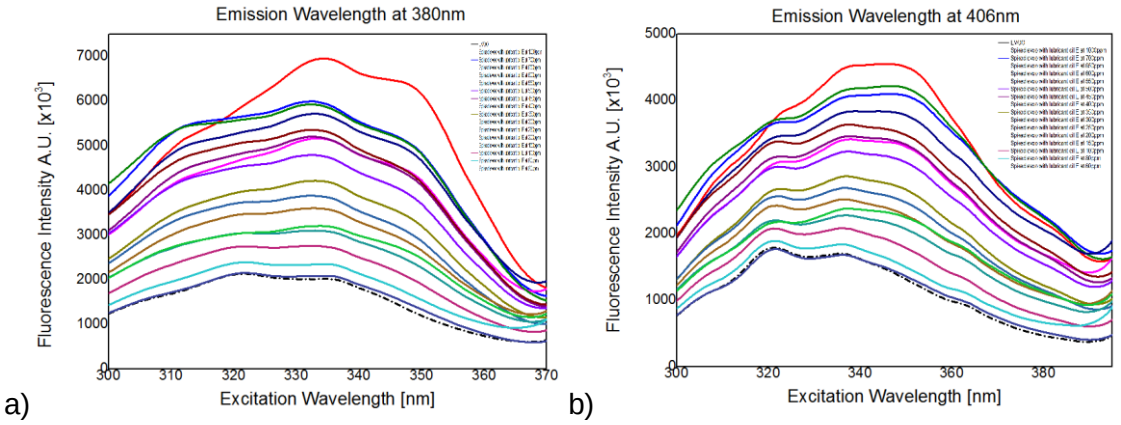

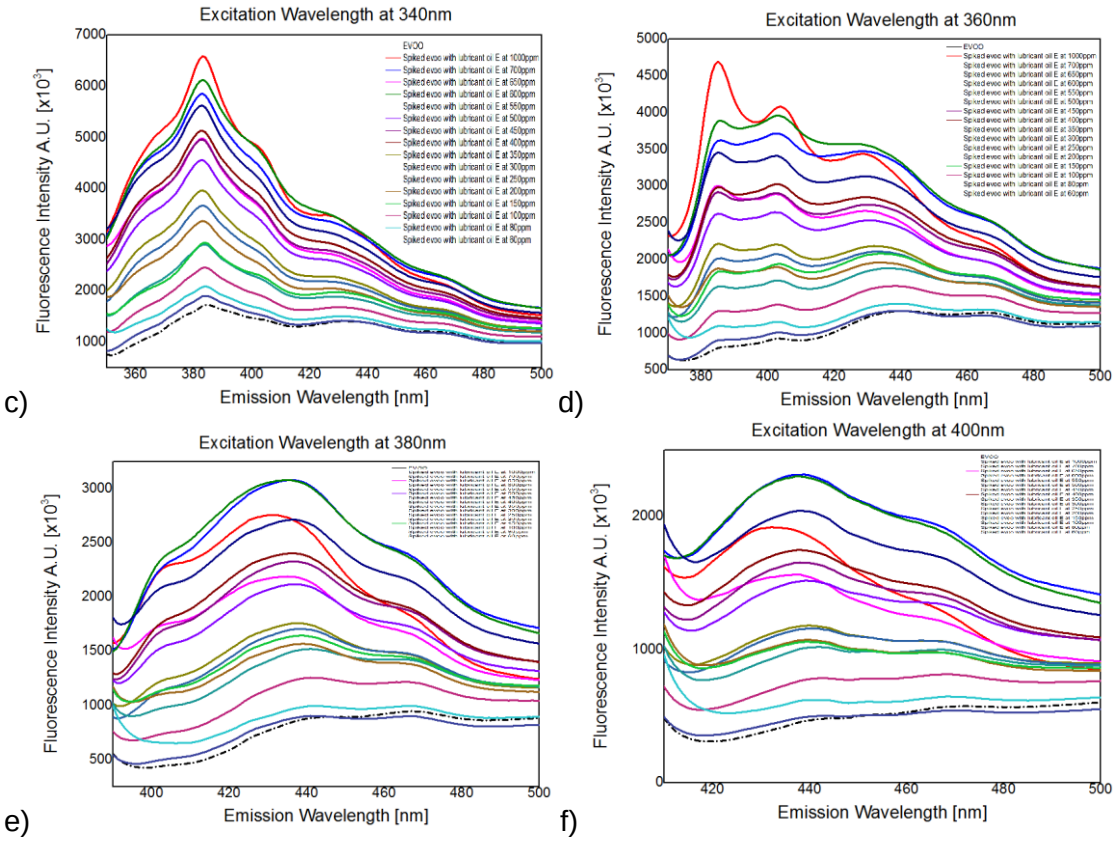

Figure B11. Fluorescence intensity at the constant wavelength of the spiked EVOO with mineral oil E in different concentrations: a) Emission Wavelength at 406nm, b) Emission Wavelength at 380nm, c) Excitation Wavelength at 340nm, d) Excitation Wavelength at 360nm, e) Excitation Wavelength at 380nm, f) Excitation Wavelength at 400nm

Sample F

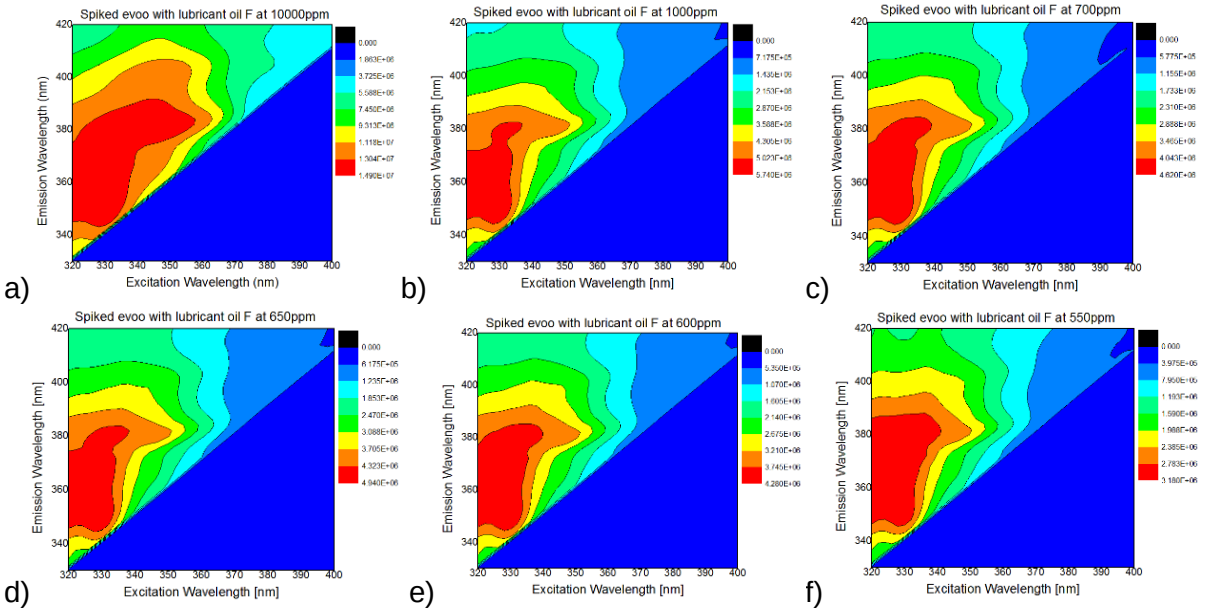

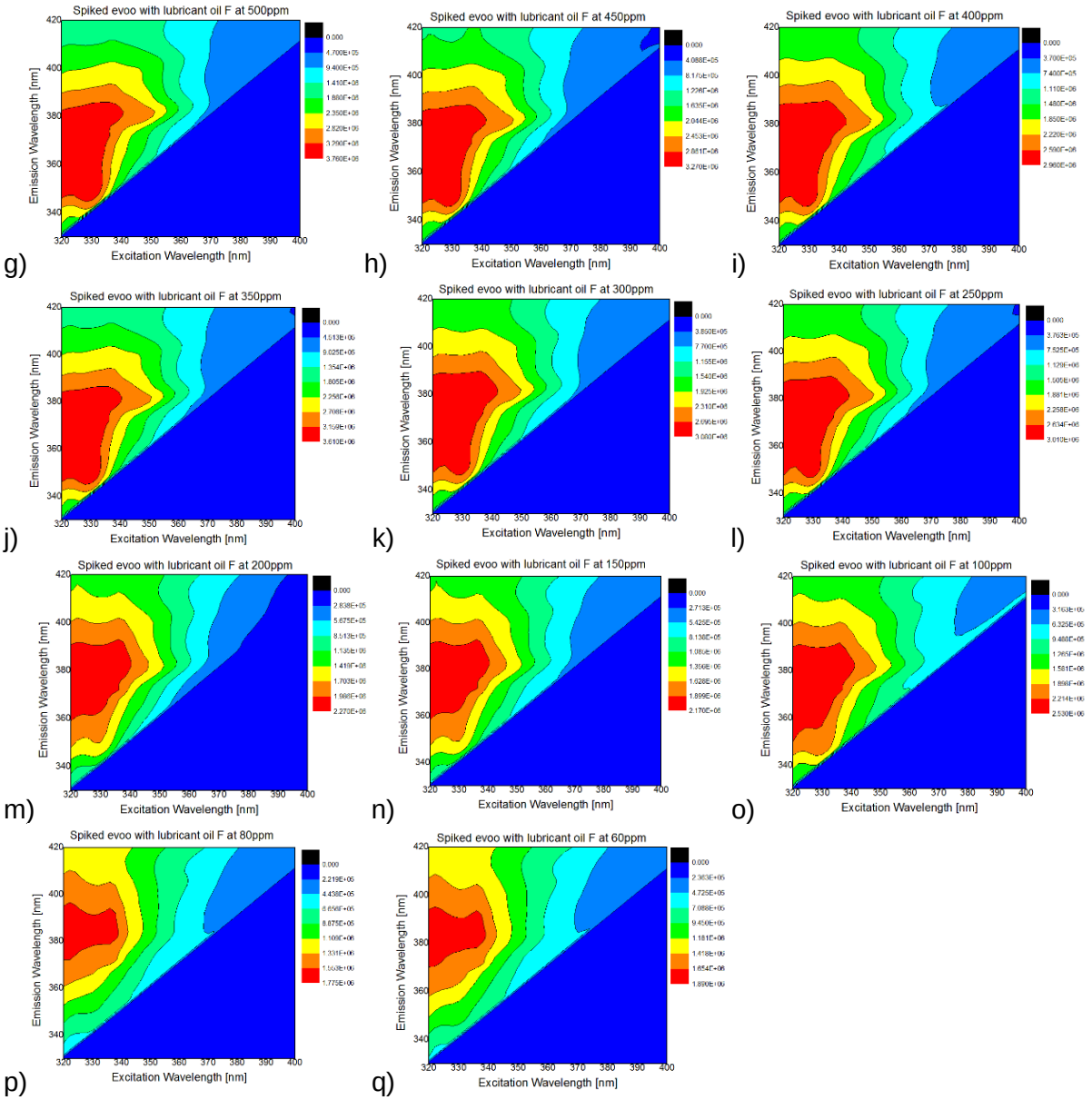

Figure B12. Fluorescence Excitation-Emission Matrices (EEMs) of the spiked EVOO with mineral oil 7 in different concentrations at a) 10000ppm, b) 10000ppm, c) 700ppm, d) 650ppm, e) 600ppm, f) 550ppm, g) 500ppm, h) 450ppm, i) 400ppm, j) 350ppm, k) 300ppm, l) 250ppm, m) 200ppm, n) 150ppm, o) 100ppm, p) 80ppm, q) 60ppm

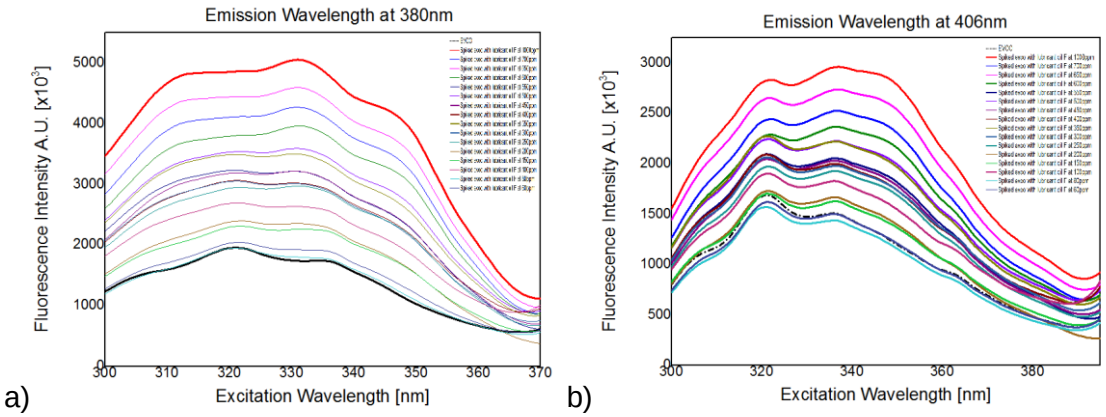

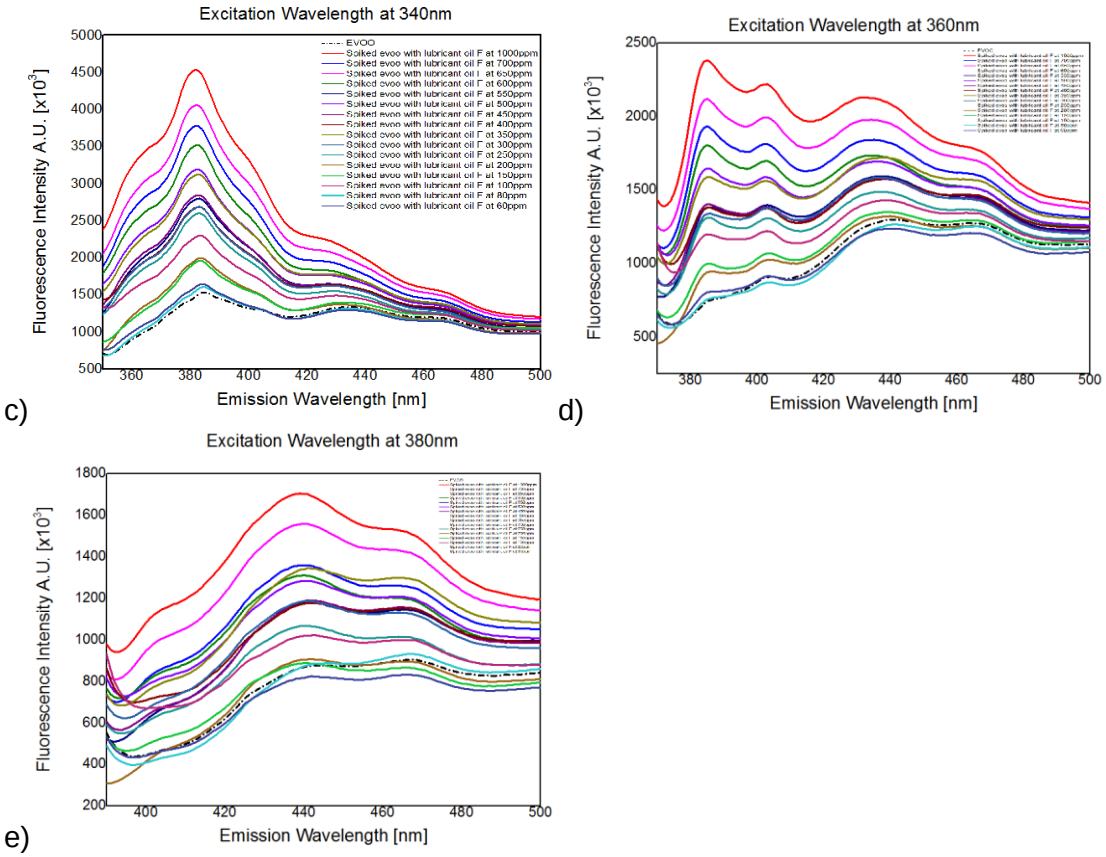

Figure B13. Fluorescence intensity at a constant wavelength of the spiked EVOO with mineral oil F in different concentrations: a) Emission Wavelength at 406nm, b) Emission Wavelength at 380nm, c) Excitation Wavelength at 340nm, d) Excitation Wavelength at 360nm, e) Excitation Wavelength at 380nm

Sample G

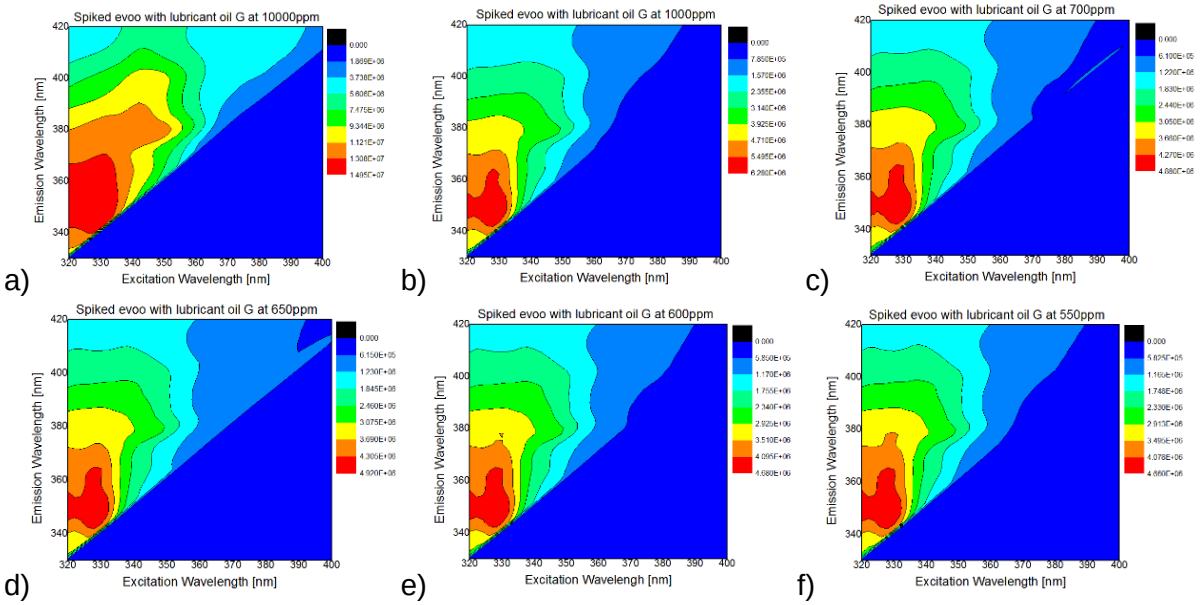

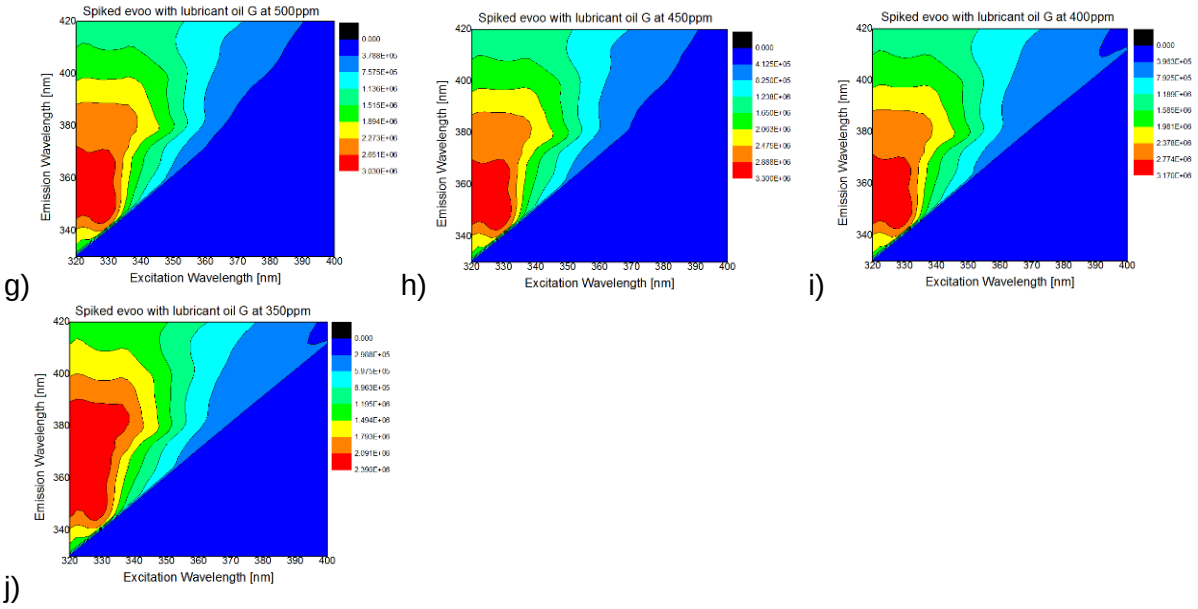

Figure B14. Fluorescence Excitation-Emission Matrices (EEMs) of the spiked EVOO with mineral oil G in different concentrations at a) 10000ppm, b) 10000ppm, c) 700ppm, d) 650ppm, e) 600ppm, f) 550ppm, g) 500ppm, h) 450ppm, i) 400ppm, j) 350ppm

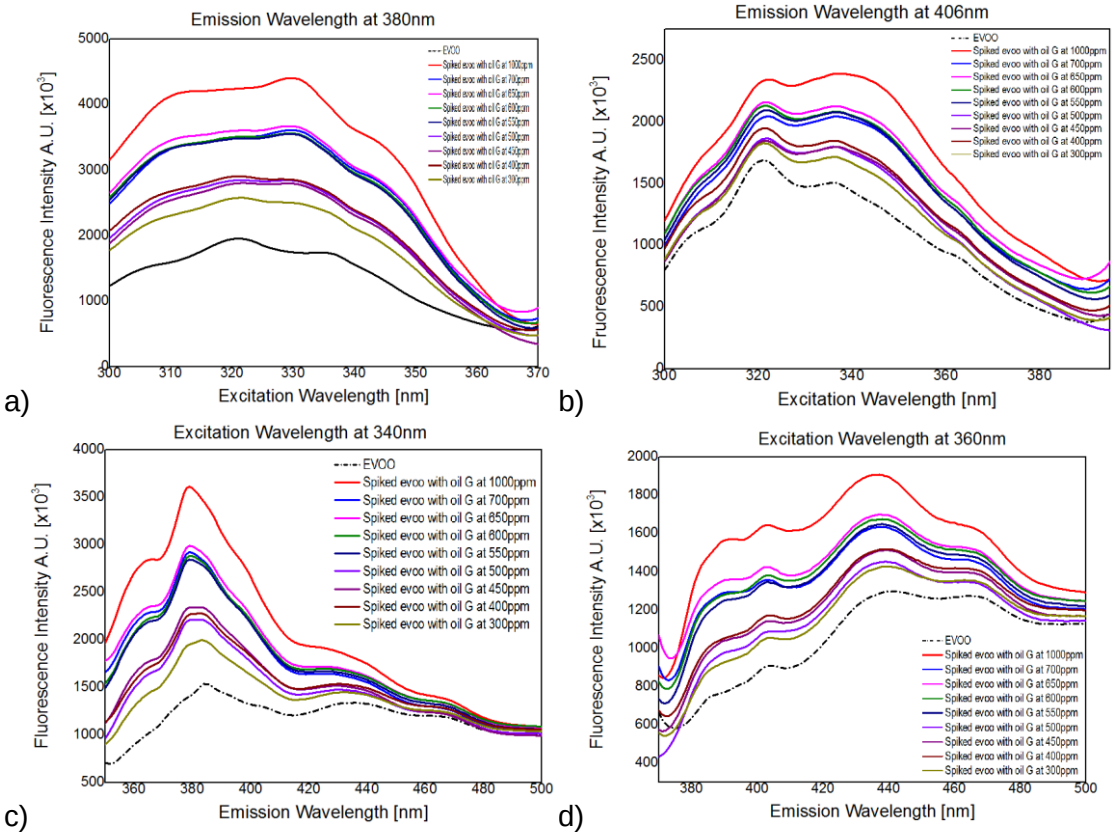

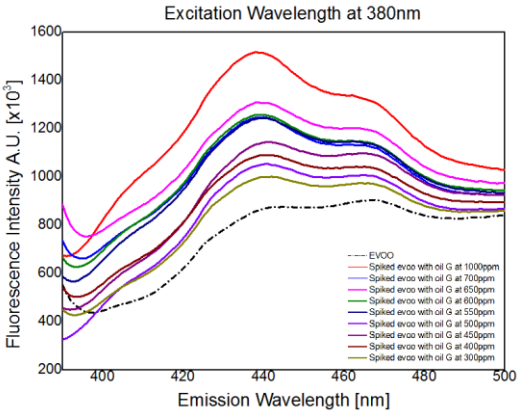

e)

Figure B15. Fluorescence intensity at constant wavelength of the spiked EVOO with mineral oil G in different concentrations: a) Emission Wavelength at 406nm, b) Emission Wavelength at 380nm, c) Excitation Wavelength at 340nm, d) Excitation Wavelength at 360nm, e) Excitation Wavelength at 380nm

Sample H

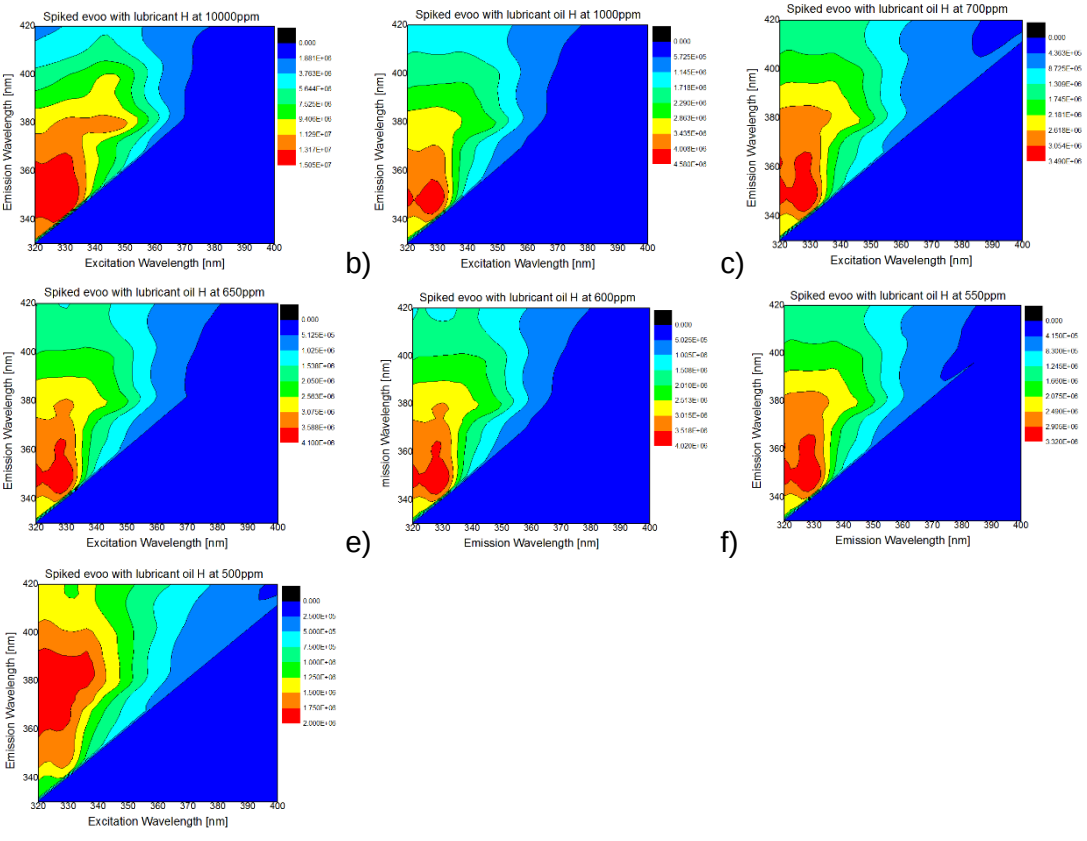

a) b) c) d) e) f) g)

Figure B16. Fluorescence Excitation-Emission Matrices (EEMs) of the spiked EVOO with mineral oil H in different concentrations at a) 10000ppm, b) 10000ppm, c) 700ppm, d) 650ppm, e) 600ppm, f) 550ppm, g) 500ppm

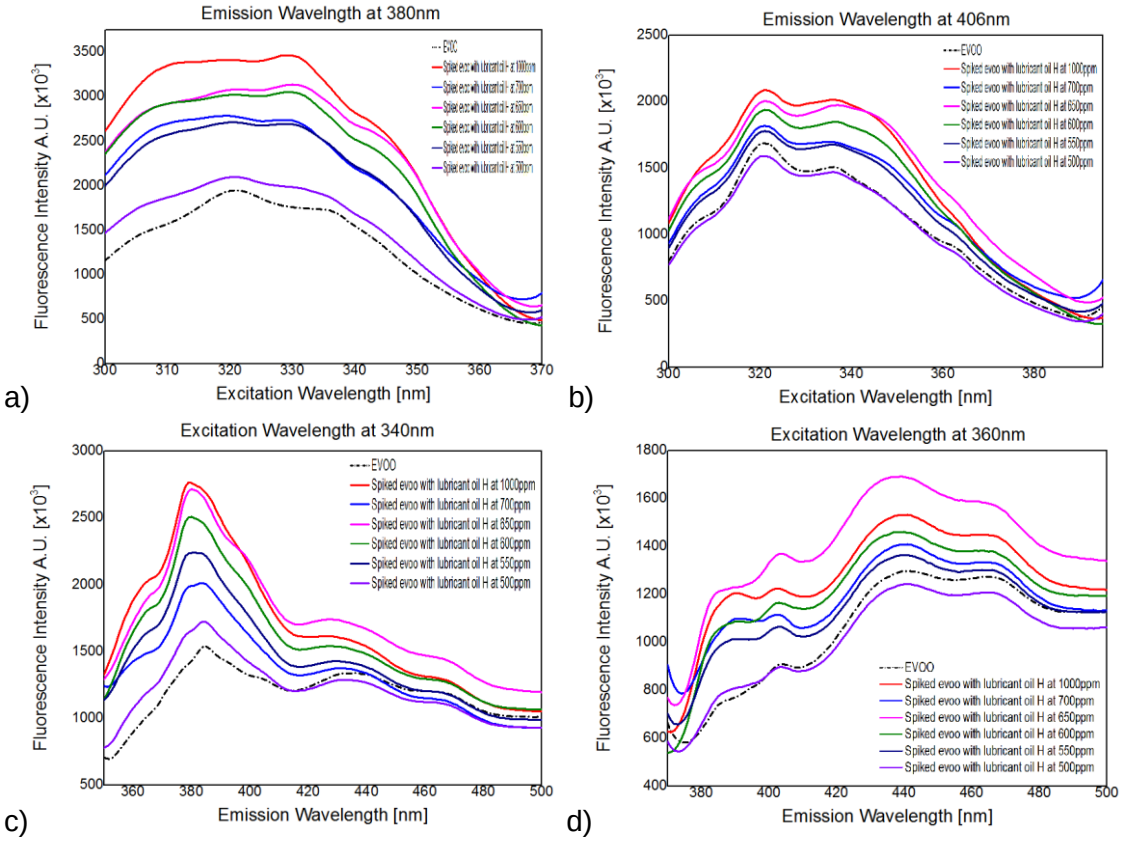

Figure B17. Fluorescence intensity at constant wavelength of the spiked EVOO with mineral oil H in different concentrations: a) Emission Wavelength at 406nm, b) Emission Wavelength at 380nm, c) Excitation Wavelength at 340nm, d) Excitation Wavelength at 360nm

Spiked EVOO with mineral oil I

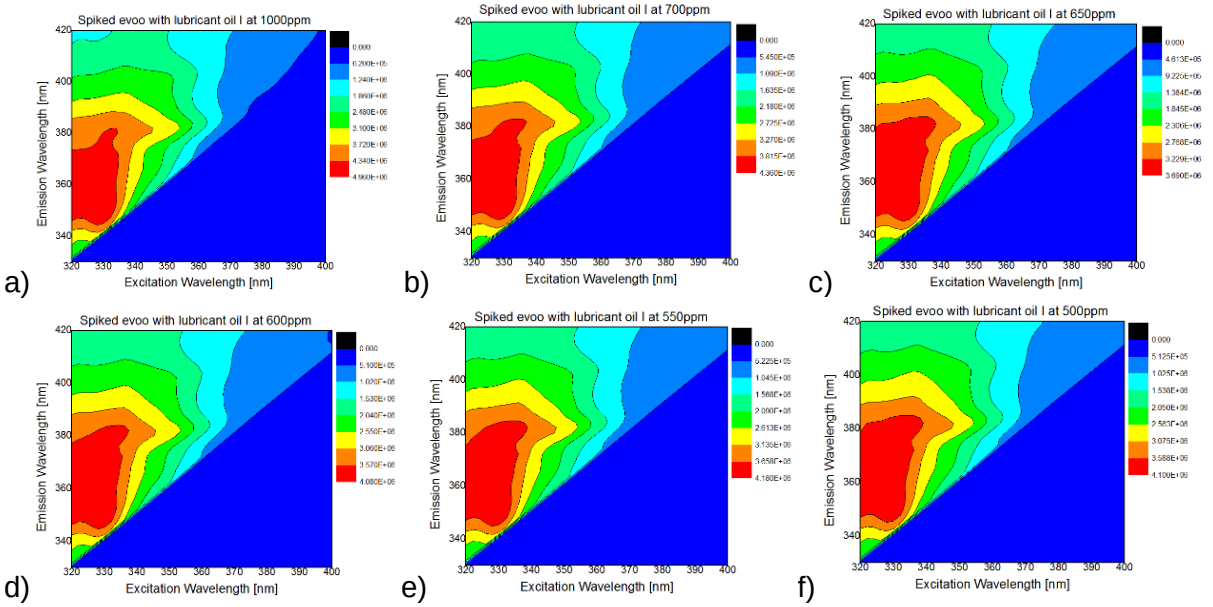

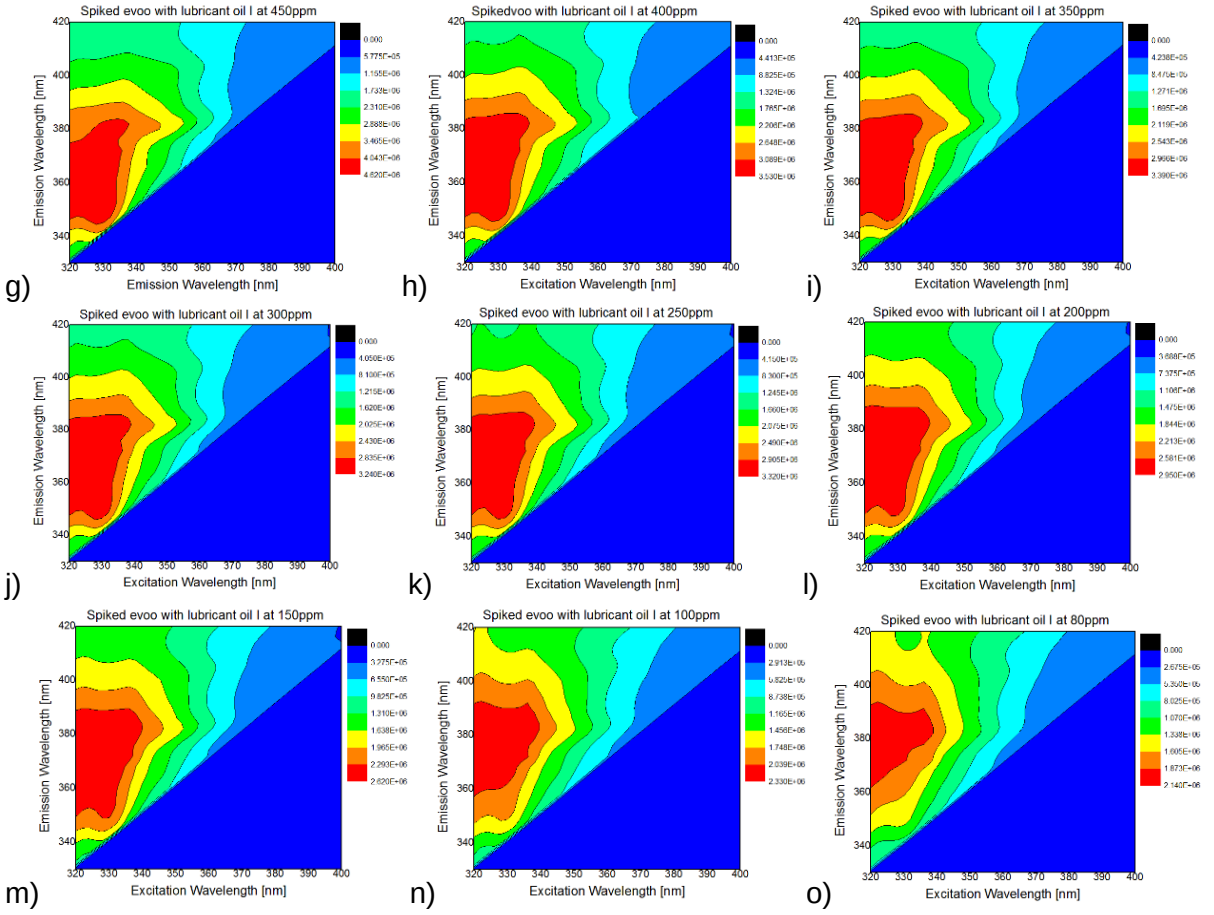

Figure B18. Fluorescence Excitation-Emission Matrices (EEMs) of the spiked EVOO with mineral oil I in different concentrations at a) 1000ppm, b) 700ppm, c) 650ppm, d) 600ppm, e) 550ppm, f) 500ppm, g) 450ppm, h) 400ppm, i) 350ppm, j) 300ppm, k) 250ppm, l) 200ppm, m) 150ppm, n) 100ppm, o) 80ppm

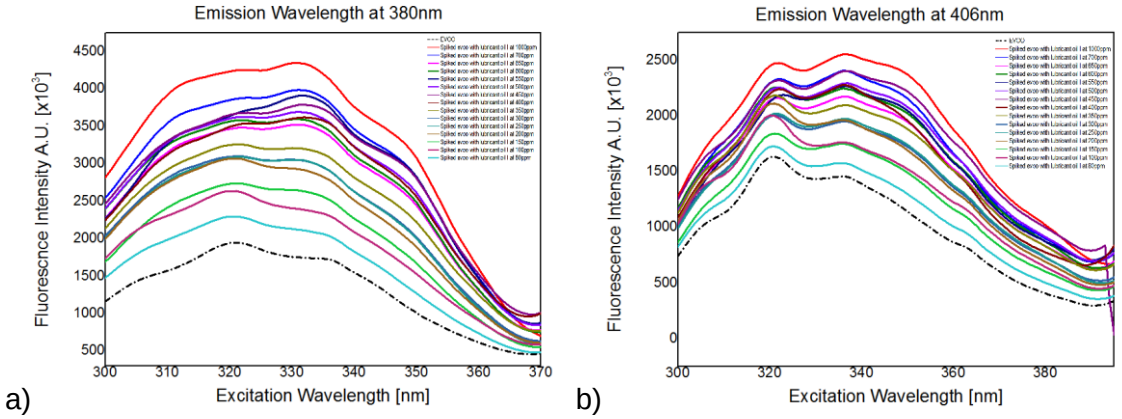

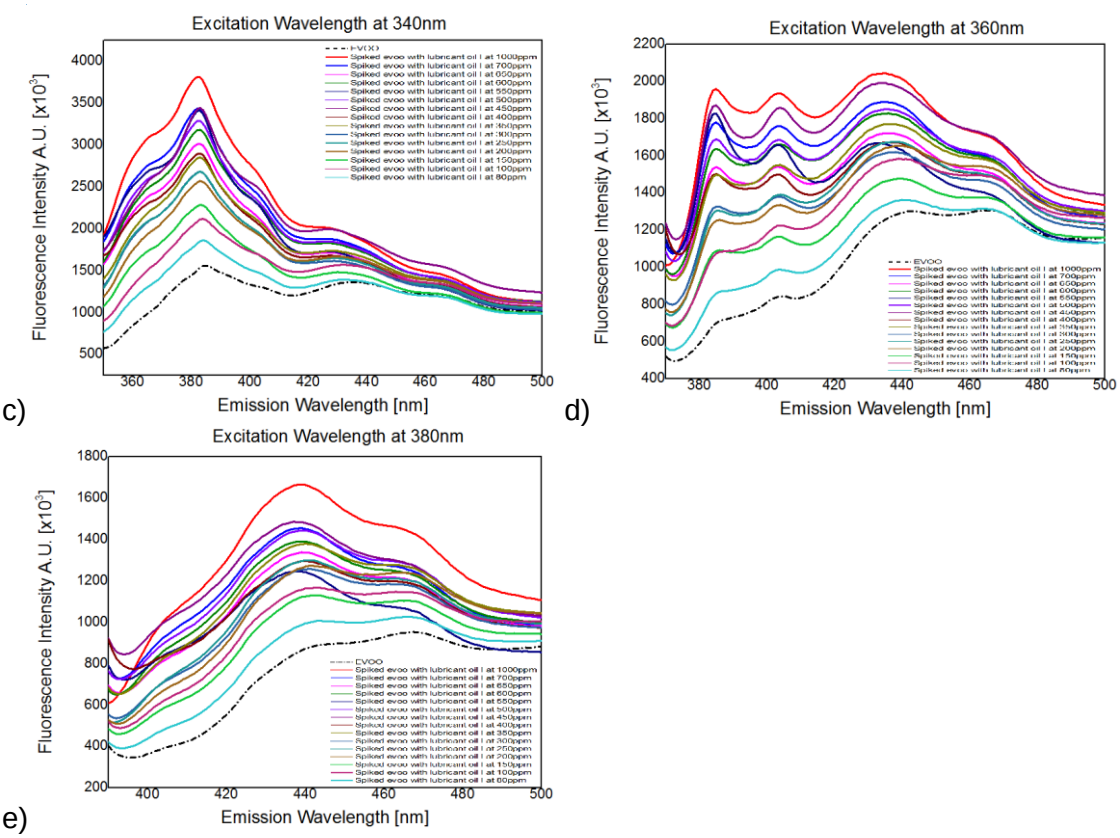

Figure B19. Fluorescence intensity at constant wavelength of the spiked EVOO with mineral oil I in different concentrations: a) Emission Wavelength at 406nm, b) Emission Wavelength at 380nm, c) Excitation Wavelength at 340nm, d) Excitation Wavelength at 360nm, e) Excitation Wavelength at 380nm

Sample J

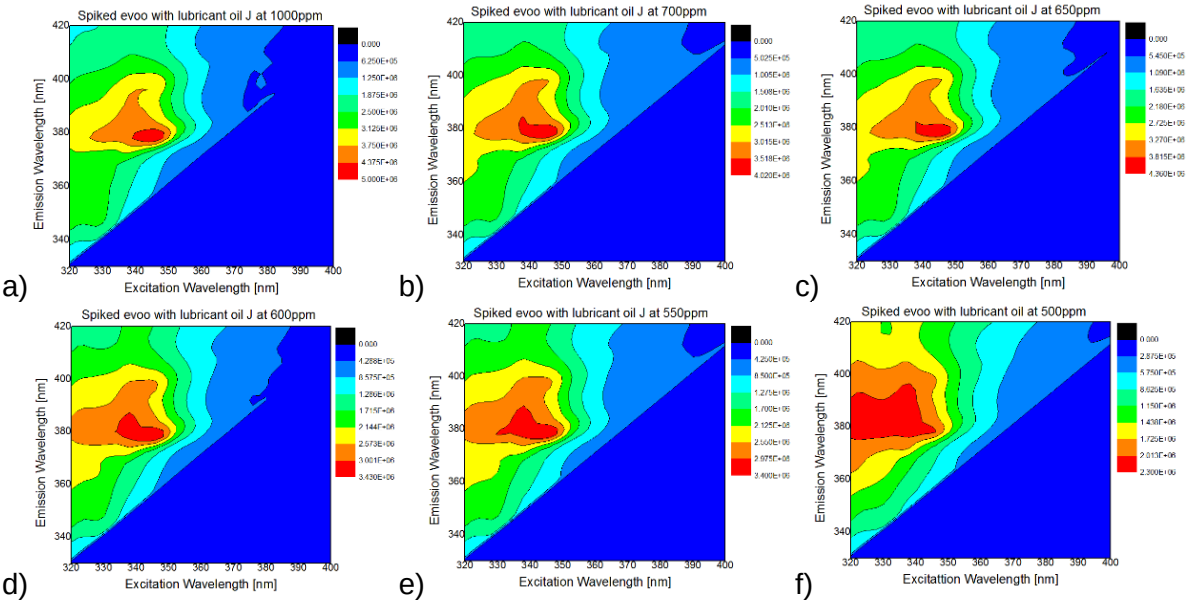

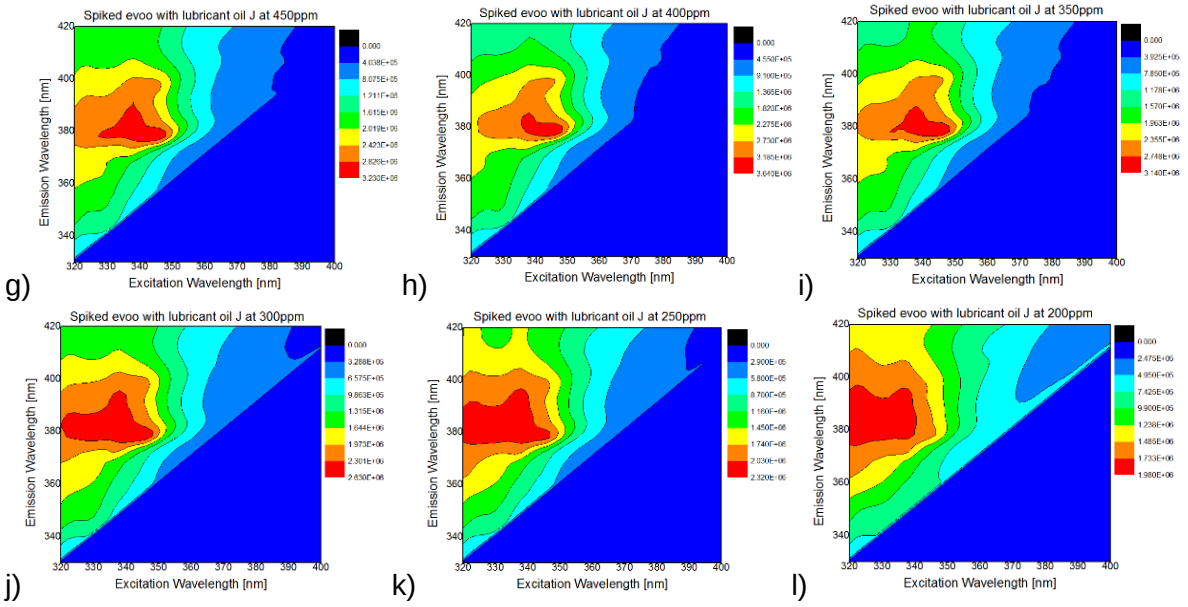

Figure B20. Fluorescence Excitation-Emission Matrices (EEMs) of the spiked EVOO with mineral oil J in different concentrations at a) 1000ppm, b) 700ppm, c) 650ppm, d) 600ppm, e) 550ppm, f) 500ppm, g) 450ppm, h) 400ppm, i) 350ppm, j)300ppm, k)250ppm, l)200ppm

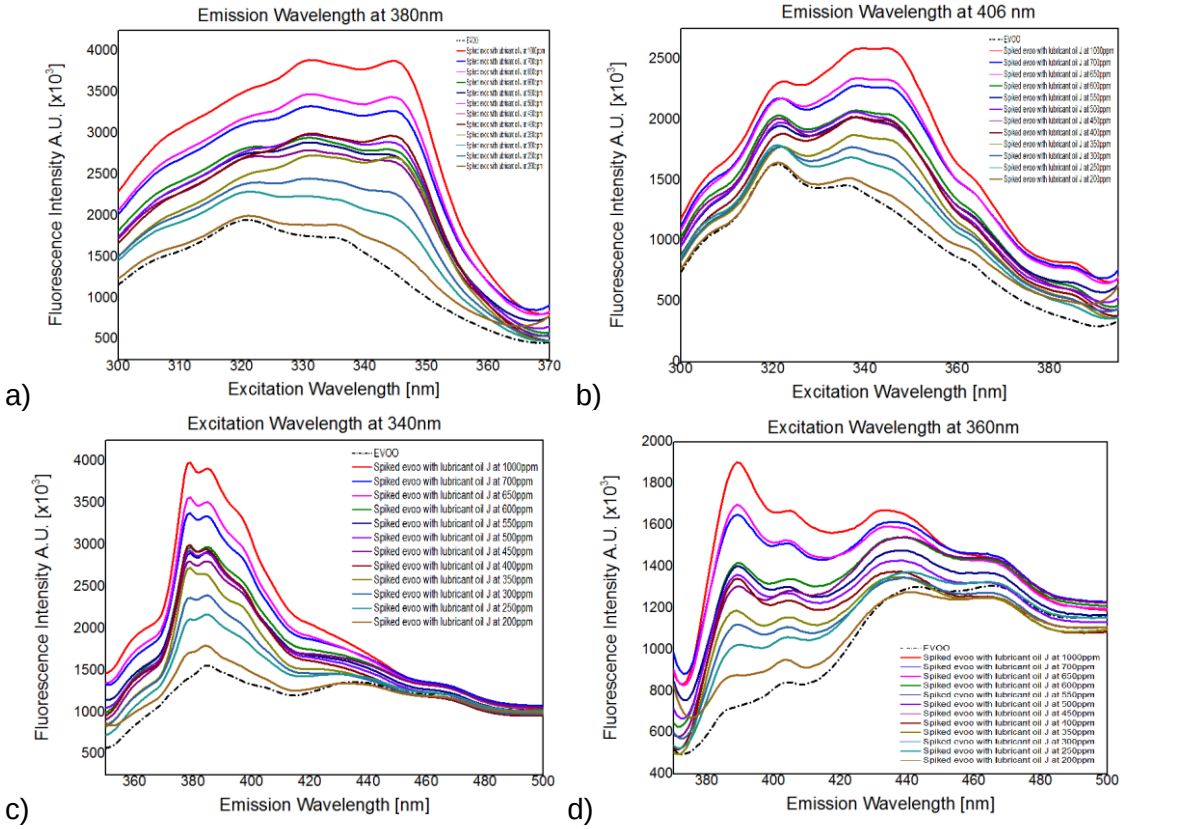

Figure B21. Fluorescence intensity at a constant wavelength of the spiked EVOO with mineral oil J in different concentrations: a) Emission Wavelength at 380nm, b) Emission Wavelength at 406nm, c) Excitation Wavelength at 340nm, d) Excitation Wavelength at 360nm

Literature

(1) Vlasiadi M. 'Application of spectroscopy for the quantitative determination of sugars in honey and for the detection of adulteration in olive oil' University of Crete 2023

(2) Stavrakakis, Giorgos, Aggelos Philippidis, and Michalis Velegrakis. 'Application of Optical Spectroscopic Techniques and Multivariate Statistical Analysis as a Method of Determining the Percentage and Type of Adulteration of Extra Virgin Olive Oil'. *Food Analytical Methods* 15, no. 2 (February 2022): 285–93. https://doi.org/10.1007/s12161-021-02055-8.

(3) Grazia, Anna, Leonardo Ciaccheri, Andrea Azelio, and Antonio Cimato. 'Optical Absorption Spectroscopy for Quality Assessment of Extra Virgin Olive Oil.' In *Olive Oil - Constituents, Quality, Health Properties and Bioconversions*, edited by Dimitrios Boskou. InTech, 2012. https://doi.org/10.5772/30275.

(4) Sauer, Markus, Johan Hofkens, and J. Enderlein. *Handbook of Fluorescence Spectroscopy and Imaging: From Single Molecules to Ensembles*. Weinheim: Wiley-VCH, 2011.

(5) Zwinkels, Joanne. 'Light, Electromagnetic Spectrum'. In *Encyclopedia of Color Science and Technology*, edited by Ronnier Luo, 1–8. Berlin, Heidelberg: Springer Berlin Heidelberg, 2015. https://doi.org/10.1007/978-3-642-27851-8_204-1.

(6) An Introduction to Fluorescence Spectroscopy

(7) Orfanakis E. IDENTIFICATION AND STUDYOF AUTHENTICITY OF HONEY, OLIVE OIL AND WINE WITH THE USE OF OPTICAL SPECTROSCOPIC TECHNIQUES WITH THE COMBINATION OF MACHINE LEARNING METHODS. University of Crete 2019

(8) Nawrocka, Agnieszka, and Joanna Lamorsk. 'Determination of Food Quality by Using Spectroscopic Methods'. In *Advances in Agrophysical Research*, edited by Stanisaw Grundas. InTech, 2013. https://doi.org/10.5772/52722.

(9) 'Physics of Fluorescence-the Jablonski Diagramm', n.d. https://nightsea.com/articles/jablonski-diagram-for-fluorescence/.

(10) Dong, Chen Y. 'Fluorescence Spectrophotometry'. *ENCYCLOPEDIA OF LIFE SCIENCES*, 2002.

(11) Sikorska, Ewa, Igor Khmelinskii, and Marek Sikorski. 'Analysis of Olive Oils by Fluorescence Spectroscopy: Methods and Applications'. In *Olive Oil - Constituents, Quality, Health Properties and Bioconversions*, edited by Dimitrios Boskou. InTech, 2012. https://doi.org/10.5772/30676.

(12) Saccenti, Edoardo, Huub C. J. Hoefsloot, Age K. Smilde, Johan A. Westerhuis, and Margriet M. W. B. Hendriks. 'Reflections on Univariate and Multivariate Analysis of Metabolomics Data'. *Metabolomics* 10, no. 3 (June 2014): 361–74. https://doi.org/10.1007/s11306-013-0598-6.

(13) Chen, Kani. 'Multivariate Statistical Analysis', n.d.

(14) Miller, James N., and Jane Charlotte Miller. *Statistics and Chemometrics for Analytical Chemistry*. 6th ed. Harlow: Prentice Hall/Pearson, 2010.

(15) Dos Santos, Felipe Rodrigues, José Francirlei De Oliveira, Evandro Bona, Graziela M.C. Barbosa, and Fábio Luiz Melquiades. 'Evaluation of Pre-Processing and Variable Selection on Energy Dispersive X-Ray Fluorescence Spectral Data with Partial Least Square Regression: A Case of Study for Soil Organic Carbon Prediction'. *Spectrochimica Acta Part B: Atomic Spectroscopy* 175 (January 2021): 106016. https://doi.org/10.1016/j.sab.2020.106016.

(16) Philippidis, Aggelos, Emmanouil Poulakis, Renate Kontzedaki, Emmanouil Orfanakis, Aikaterini Symianaki, Aikaterini Zoumi, and Michalis Velegrakis. 'Application of Ultraviolet-Visible Absorption Spectroscopy with Machine Learning Techniques for the Classification of Cretan Wines'. *Foods* 10, no. 1 (22 December 2020): 9. https://doi.org/10.3390/foods10010009.

(17) Ballabio, Davide, and Viviana Consonni. ‘Classification Tools in Chemistry. Part 1: Linear Models. PLS-DA’. *Analytical Methods* 5, no. 16 (2013): 3790. https://doi.org/10.1039/c3ay40582f.
(18) Wold, Svante, Michael Sjöström, and Lennart Eriksson. ‘PLS-Regression: A Basic Tool of Chemometrics’. *Chemometrics and Intelligent Laboratory Systems* 58, no. 2 (October 2001): 109–30. https://doi.org/10.1016/S0169-7439(01)00155-1.
(19) Rinnan, Åsmund, Frans Van Den Berg, and Søren Balling Engelsen. ‘Review of the Most Common Pre-Processing Techniques for near-Infrared Spectra’. *TrAC Trends in Analytical Chemistry* 28, no. 10 (November 2009): 1201–22. https://doi.org/10.1016/j.trac.2009.07.007.
(20) Lu, Cong-Hui, Bao-Qiong Li, Quan Jing, Dong Pei, and Xin-Yi Huang. ‘A Classification and Identification Model of Extra Virgin Olive Oil Adulterated with Other Edible Oils Based on Pigment Compositions and Support Vector Machine’. *Food Chemistry* 420 (September 2023): 136161. https://doi.org/10.1016/j.foodchem.2023.136161.
(21) Drakopoulou, Sofia, Emmanouil Orfanakis, Ioulia Karagiannaki, Fragiskos Gaitis, Stavroula Skoulika, Andreas Papaioannou, George Boukouvalas, et al. ‘Comparative Evaluation of Different Targeted and Untargeted Analytical Approaches to Assess Greek Extra Virgin Olive Oil Quality and Authentication.’ *Molecules* 27, no. 4 (16 February 2022): 1350. https://doi.org/10.3390/molecules27041350.
(22) Jimenez-Lopez, Cecilia, Maria Carpena, Catarina Lourenço-Lopes, Maria Gallardo-Gomez, Jose M. Lorenzo, Francisco J. Barba, Miguel A. Prieto, and Jesus Simal-Gandara. ‘Bioactive Compounds and Quality of Extra Virgin Olive Oil’. *Foods* 9, no. 8 (28 July 2020): 1014. https://doi.org/10.3390/foods9081014.
(23) European Commission. 'Facts in Olive Oil'
(24) Gasparrini, Massimiliano, Francesca Giampieri, Josè M. Alvarez Suarez, Luca Mazzoni, Tamara Y. Forbes Hernandez, Josè L. Quiles, Pedro Bullon, and Maurizio Battino. ‘AMPK as a New Attractive Therapeutic Target for Disease Prevention: The Role of Dietary Compounds AMPK and Disease Prevention’. *Current Drug Targets* 17, no. 8 (4 May 2016): 865–89. https://doi.org/10.2174/1573399811666150615150235.
(25) Zou, Xiaobo, and Jiewen Zhao. *Nondestructive Measurement in Food and Agro-Products*. Dordrecht: Springer Netherlands, 2015. https://doi.org/10.1007/978-94-017-9676-7.
(26) Chavez-Angel, Emigdio, Blanca Puertas, Martin Kreuzer, Robert Soliva Fortuny, Ryan C. Ng, Alejandro Castro-Alvarez, and Clivia M. Sotomayor Torres. ‘Spectroscopic and Thermal Characterization of Extra Virgin Olive Oil Adulterated with Edible Oils’. *Foods* 11, no. 9 (29 April 2022): 1304. https://doi.org/10.3390/foods11091304.
(27) Xie, Yaoqing, Bingning Li, Lingling Liu, Jie Ouyang, and Yanwen Wu. ‘Rapid Screening of Mineral Oil Aromatic Hydrocarbons (MOAH) in Grains by Fluorescence Spectroscopy’. *Food Chemistry* 294 (October 2019): 458–67. https://doi.org/10.1016/j.foodchem.2019.05.057.
(28) Xia, Qing, Zhaolin Du, Dasong Lin, Lili Huo, Li Qin, Wei Wang, Liwen Qiang, Yanpo Yao, and Yi An. ‘Review on Contaminants in Edible Oils and Analytical Technologies.’ *Oil Crop Science* 6, no. 1 (March 2021): 23–27. https://doi.org/10.1016/j.ocsci.2021.02.001.
(29) Morassuti, Claudio Yamamoto, Sandro Marcio Lima, Fabio Alencar Dos Santos, and Luis Humberto Da Cunha Andrade. ‘Fluorescence Spectroscopy Applied in Lubricant Oils’. *Orbital: The Electronic Journal of Chemistry* 10, no. 1 (31 January 2018): 42–46. https://doi.org/10.17807/orbital.v10i1.1032.
(30) 'Scientific Opinion on Mineral Oil Hydrocarbons in Food'. EFSA Journal 2012
(31) Mbogning Feudjio, William, Gilbert Yvon Mbesse Kongbonga, Sagesse Bel Christ Kogniwali-Gredibert, Hassen Ghalila, Pale Wang-Yang, Youssef Majdi, Cyril Kenfack Assongo, and Mama Nsangou. ‘Characterization of Engine Lubricants by Fluorescence Spectroscopy and Chemometrics’. *Spectrochimica Acta Part A: Molecular and Biomolecular Spectroscopy* 252 (May 2021): 119539. https://doi.org/10.1016/j.saa.2021.119539.